

ANALYTICAL MODELING FOR TRANSIENT  
PROBE RESPONSE IN EDDY CURRENT TESTING

MODÉLISATION ANALYTIQUE DE RÉPONSE  
TRANSITOIRE EN CONTRÔLE PAR COURANT DE  
FOUCAULT

By

Daniel Desjardins

A thesis submitted to the Graduate Program in Physics, Engineering Physics & Astronomy  
in conformity with the requirements for the  
Doctor of Philosophy

Queen's University  
Kingston, Ontario, Canada

June 2015

Copyright © Daniel Desjardins, 2015

## ABSTRACT

Analytical models that describe the electromagnetic field interactions arising between field generating and sensing coils in close proximity to conducting structures can be used to enhance analysis and information extracted from signals obtained using electromagnetic non-destructive evaluation technologies. A novel strategy, which enables the derivation of exact solutions describing all electromagnetic interactions arising in inductively coupled circuits due to a voltage excitation, is developed in this work. Differential circuit equations are formulated in terms of an arbitrary voltage excitation and of the magnetic fields arising in inductive systems, using Faraday's law and convolution, and solved using the Fourier transform. The approach is valid for systems containing any number of driving and receiving coils, and include nearby conducting and ferromagnetic structures. In particular, the solutions account for feedback between a ferromagnetic conducting test piece and the driving and sensing coils, providing correct voltage response of the coils. Also arising from the theory are analytical expressions for complex inductances in a circuit, which account for real (inductive) and imaginary (loss) elements associated with conducting and ferromagnetic structures. A novel model-based method for simultaneous characterization of material parameters, which includes magnetic permeability, electrical conductivity, wall thickness and liftoff, is subsequently developed from the forward solutions. Furthermore, arbitrary excitation waveforms, such as a sinusoid or a square wave, for applications in conventional and transient eddy current, respectively, may be considered. Experimental results, obtained for a square wave excitation, are found to be in excellent agreement with the analytical predictions.

## **CO-AUTHORSHIP**

Student: Daniel Desjardins

Supervisor: Dr. Thomas Krause

Supervisor: Dr. Lynann Clapham

## ACKNOWLEDGEMENTS

I am most indebted towards Dr. Thomas Krause, Royal Military College, for the tremendous amount of support and advice he has provided me over the duration of this endeavour. He provided countless ideas and corrections that have led to the completion of this professional product. I cannot understate how fortunate I was to have him as a supervisor; he is a true professional, passionate about his field, and truly dedicates himself to his students.

I would also like to thank Dr. Lynann Clapham, Queen's University, who has helped me every step of the way. She was most helpful in coordinating all the necessary administration. I am especially grateful towards Mrs. Loanne Meldrum for her help and support in all matters relating to courses and program requirements. She was essential in facilitating timely progress and coordinating administrative affairs.

Dr. Ross Underhill, Royal Military College, provided ample insight into eddy current phenomena, technical training in the laboratory, and was instrumental in helping me acquire the experimental data which validated the theoretical work performed in this thesis.

I would like to thank my loving parents, Normand and Judy Desjardins, and dear sisters Amelia and Leandra Desjardins, for their continued encouragement, love and support. Knowledge is acquired and may sometimes be forgotten, but family is forever.

Finally, to Ashley Parr, the most amazing woman on this Earth, I wish to thank you for being the best part of my life. You inspire me with your intellect and your passion, and I am forever yours.

# TABLE OF CONTENTS

ABSTRACT.....	ii
ACKNOWLEDGEMENTS.....	iv
TABLE OF CONTENTS.....	v
LIST OF TABLES.....	ix
LIST OF FIGURES.....	x
LIST OF ABBREVIATIONS.....	xii
LIST OF SYMBOLS.....	xiii
CHAPTER 1 – INTRODUCTION.....	1
1.1. Eddy current testing.....	2
1.2. Research survey.....	6
1.3. Objective.....	9
1.4. Scope and methodology.....	9
1.5. Structure.....	10
CHAPTER 2 – THEORY.....	13
2.1. Electrodynamics.....	13
1.6. Magnetic Permeability.....	16
2.2. Material interface.....	17
2.3. Integral transforms.....	19
2.4. Fourier series.....	22

2.5. Convolution.....	24
2.6. Kirchhoff's voltage law .....	26
2.7. Computation of results .....	32
CHAPTER 3 – EXPERIMENT.....	33
3.1. Pulser systems.....	33
3.2. Electromagnetic coils .....	40
3.3. Rods and Tubes .....	42
3.4. Linear permeability .....	44
3.5. Experimental results .....	47
CHAPTER 4 – MANUSCRIPTS .....	50
Concerning the derivation of exact solutions to inductive circuit problems for eddy current testing .....	51
I. Introduction.....	52
II. Theoretical Development.....	54
III. Experimental Results.....	64
IV. Conclusion .....	68
V. References.....	68
Transient response of a driver coil in transient eddy current testing .....	72
I. Introduction.....	72
II. Theory .....	74

III. Experimental Results.....	83
IV. Discussion.....	86
V. Summary.....	88
VI. References.....	88
Transient response of a driver-pickup coil probe in transient eddy current testing .....	93
I. Introduction.....	93
II. Theory .....	95
III. Experimental Results.....	105
IV. Discussion.....	109
V. Summary.....	112
VI. References.....	113
Transient response of a driver-pickup probe encircling a ferromagnetic conducting tube .....	117
I. Introduction.....	117
II. Forward Problem.....	119
III. Experimental Results.....	123
IV. Discussion & Future Work .....	127
V. Summary.....	128
VI. References.....	129
Simultaneous Evaluation of Material Parameters Using Analytical Transient Eddy Current Models .....	132

I. Introduction.....	132
II. Forward problem.....	134
III. Inverse Problem.....	136
IV. Array computation.....	139
V. Example application.....	141
VI. Discussion.....	143
VII. Conclusion.....	144
VIII. References.....	144
CHAPTER 5 – DISCUSSION .....	148
CHAPTER 6 – CONCLUSION .....	151
CHAPTER 7 – FUTURE WORK.....	153
REFERENCES.....	155
ANNEX A.....	160
ANNEX B.....	161

# LIST OF TABLES

Table 1: Useful Fourier transform rules. ....	20
Table 2: Useful Fourier cosine transform rules. ....	21
Table 3: Useful first-order Hankel transform rules. ....	21
Table 4: Gain $G$ and internal resistance $R_{int}$ of the battery pulser calculated from linearized data sets. .....	36
Table 5: Tandem probe characteristics. ....	41
Table 6: Encircling probe characteristics. ....	41
Table 7: Rod characteristics. ....	43
Table 8: Tube specifications. ....	43
Table 9: Areas under the transient leading and trailing edge signals shown in Figure 18. ....	46

## LIST OF FIGURES

Figure 1: A time-varying magnetic field (blue) induces eddy currents (red) in a nearby conducting structure, which generate an opposing magnetic field (yellow). .....	2
Figure 2: Magnetization curve of commercial iron. Permeability is given by the ratio $B/H$ . (Redrawn from [41]) .....	16
Figure 3: Cross-sectional view of a coil encircling a rod depicting a vertical boundary. ....	18
Figure 4: Cross-sectional view of a coil above a plate depicting a horizontal boundary. ....	19
Figure 5: Fourier representation of a square wave with amplitude $v_0$ pulse length $P$ . ....	23
Figure 6: Input arising at time $\tau$ and its response $A(t - \tau)$ . ....	24
Figure 7: Response of a Dirac impulse from an arbitrary input. ....	24
Figure 8: Total response to an arbitrary input is the sum of the component responses. ....	25
Figure 9: RLC series circuit. ....	27
Figure 10: Plots of exact solutions (47) and (49), describing overdamped and underdamped systems, respectively, compared to an equivalent Fourier series representation (59). ....	31
Figure 11: Driver (a) and driver-pickup (b) circuit diagrams for the battery pulser. ....	34
Figure 12: Battery pulser calibration plots. ....	36
Figure 13: Leading edge of the square pulse generated by the battery pulser. ....	37
Figure 14: Driver (a) and driver-pickup (b) circuit diagrams for the conventional power supply pulser. ....	38
Figure 15: Leading edge of the square pulse generated by the conventional power supply pulser. ....	39
Figure 16: Tandem driver-pickup tube probe (left) and encircling driver-pickup rod probe (right). .....	40

Figure 17: Assorted aluminum, stainless steel, brass and carbon steel tubes with  $\frac{3}{4}$ " outer diameter.  
.....43

Figure 18: Transient responses to the leading and trailing edges of a square wave excitation. ....46

Figure 19: Areas under transient response signals for various tubes at various input voltages.....47

Figure 20: Air (blue) and brass tube (orange) pickup signals; 1x (left axis) and 500x (right axis) zoom.  
.....48

Figure 21: Formatted experimental data.....49

Figure 22: Experimental and theoretical results; graphical overlay format. ....49

## LIST OF ABBREVIATIONS

AC	Alternating current
AWG	American wire gauge
EMF	Electromotive force
CPU	Central processing unit
DAQ	Digital Acquisition
DC	Direct current
FEM	Finite Element Method
LHS	Left-hand-side
MQS	Magnetoquasistatic
NAG	Numerical algorithms group
NDE	Non-destructive evaluation
NDT	Non-destructive testing
Op-Amp	Operational amplifier
PDE	Partial differential equation
RHS	Right-hand-side
RLC	Resistor-Inductor-Capacitor
TEC	Transient eddy current
TREE	Truncated-region eigenfunction expansion
USB	Universal serial bus

## LIST OF SYMBOLS

$\nabla$	Gradient	$J_\nu(r)$	Bessel function of the 1 <sup>st</sup> kind
$\nabla^2$	Vector Laplacian	$I_\nu(r)$	Modified Bessel fn. of 1 <sup>st</sup> kind
$\times$	Vector cross product	$K_\nu(r)$	Modified Bessel fn. of 2 <sup>nd</sup> kind
$\cdot$	Vector dot product	$u(t)$	Heaviside, or step, function
$*$	Convolution	$\delta(t)$	Dirac delta, or impulse, function
$\hat{\mathbf{n}}$	Unit normal vector	$v(t)$	Applied time-dependent voltage
$\mathbf{E}$	Electric field	$V(\omega)$	Fourier transform of $v(t)$
$\mathbf{B}$	Magnetic flux density	$v_0$	Voltage amplitude
$\mathbf{A}$	Magnetic vector potential	$G$	Gain
$\mathbf{i}$	Surface current density	$P$	Pulse length
$\mathbf{j}$	Volume current density	$N$	Number of turns
$\rho$	Charge density	$l$	Coil length
$\epsilon$	Electric permittivity	$a$	Coil inner radius
$\sigma$	Electrical conductivity	$b$	Coil outer radius
$\mu$	Magnetic permeability	$R$	Resistance
$t$	Time coordinate	$C$	Capacitance
$j$	Imaginary unit	$L$	Self-inductance
$\omega$	Angular frequency variable	$\zeta$	Dampening factor
$\varpi$	Angular frequency constant	$M$	Mutual inductance
$z$	Axial spatial coordinate	$\mathcal{L}$	Complex self-inductance
$\lambda$	Axial frequency coordinate	$\mathcal{M}$	Complex mutual inductance
$r$	Radial spatial coordinate	$\Re( )$	Real part
$\gamma$	Radial frequency coordinate	$\Im( )$	Imaginary part



# CHAPTER 1 – INTRODUCTION

There is an increasing demand for fast, reliable and economical technologies to inspect aging nuclear and petrochemical facilities, as well as aircraft and naval fleets. Electromagnetic non-destructive evaluation (NDE) technologies are candidates for addressing many of the inspection requirements. Existing and new electromagnetic NDE technologies would benefit from the development of analytical eddy current models that can accelerate development of appropriate inspection tools and methods for a given inspection application. Models can provide insights into the mechanisms of probe response and assist in the identification of parameters affecting measurement outcome, leading to improvements in flaw detection under conditions of changing material characteristics and/or sample configuration. These insights can also facilitate signal interpretation and the development of signal analysis tools. For example, Dodd and Deeds' [1] analytical closed-form solutions for sinusoidal excitations led to the formalism presently used to interpret conventional eddy current signals [2]. Forward solutions for transient voltage excitations, which are the focus of this thesis, however, are not yet available. The development of such analytical models can provide more rapid and transparent solutions to eddy current problems, which can help identify underlying physical parameters. This is in contrast to black-box type numerical approximations, often obtained using Finite Element Method (FEM) software packages, in which the problem domain is subdivided into a mesh of simpler parts and the relevant partial differential equations are solved using variational methods. Analytical modeling of driver-pickup transient eddy current testing is one such methodology that has the potential to advance present inspection capabilities.

## 1.1. Eddy current testing

Eddy current testing is based on the physical phenomenon of electromagnetic induction and is, therefore, used in inspection applications, where the target materials are electrical conductors. In conventional eddy current non-destructive testing (NDT), eddy currents are induced in a conductor by generating an alternating current (AC) through a coil that is in close proximity to the conductor, as depicted in Figure 1.

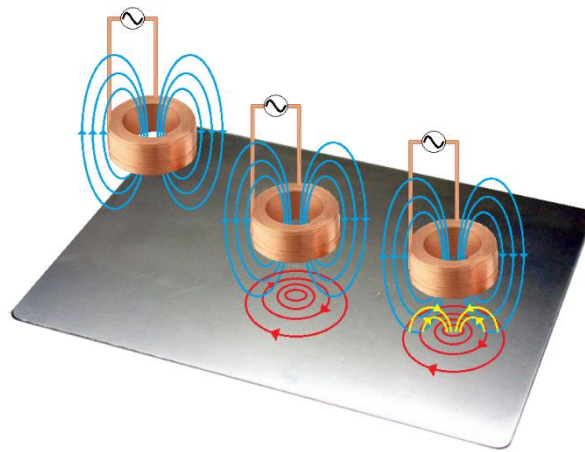


Figure 1: A time-varying magnetic field (blue) induces eddy currents (red) in a nearby conducting structure, which generate an opposing magnetic field (yellow).

AC current is time-harmonic in nature and, when applied to a coil in the proximity of a conductor, gives rise to eddy currents via Faraday's law, which are of a similar form, but with opposing direction in accordance with Lenz's law. The paths of the induced eddy currents will be modified in the presence of discontinuities, particularly those that break the sample surface, and these may be sensed as a change in the sensing coil's impedance. Detection and analysis of the signal perturbations has the potential to permit flaw identification and characterization.

In addition to flaw detection, eddy current testing can be used to perform metal thickness measurements, enabling identification of corrosion under aircraft skin and thinning of pipeline walls

for example. It may also be employed to measure conductivity, monitor the effects of heat treatment, and determine the thickness of nonconductive coatings, such as paint, over conductive substrates [3]. Eddy current testing is, therefore, widely used for safety-related and quality-related inspection requirements that arise throughout the aeronautical, nuclear and petrochemical industries [3]. Compared with ultrasonic inspection methods, eddy current NDT can examine large areas very rapidly and does not require the use of coupling liquids. However, eddy current testing is limited to metallic conductors. Furthermore, the sensitivity of conventional eddy current testing systems, depends on the depth and volume of the target discontinuity, and its reliability is reduced by other perturbing effects, such as the presence of magnetic materials or geometrical discontinuities [1].

An alternative technique to conventional AC eddy current NDT employs transient eddy currents (TEC) that are excited by means of a non-sinusoidal coil current. In most systems, a steady-state current is allowed to persist for some time before the waveform repeats. The steady state period is made sufficiently long so that all eddy currents have completely decayed away to undetectable levels. As with conventional eddy current, a nearby metallic test piece's material and geometrical properties - such as conductivity, magnetic permeability, size and shape - affect measured transient eddy current signals. However, in the Fourier sense, transient signals are far richer in information than are their conventional single-frequency counterparts, since they contain the sample's response to an infinite set of frequencies. Furthermore, transient excitations may be tailored to contain a particular distribution of frequencies with the potential of enhancing sensitivity to specific features, such as material thickness, liftoff distance and material defects. It has been determined that, in contrast to conventional eddy current signals, the presence of ferromagnetic materials may enhance flaw detection rather than impair it [4][5][6].

Unfortunately, analytical solutions for the transient case have not yet been developed, presumably due to the formidable mathematical complexity imposed by the problems inherent in feedback effects. Feedback refers to the electromagnetic coupling of the sample with the exciting coil. In this process, a current is passed through a coil and generates a time-varying magnetic field that induces eddy currents within a conducting sample. The magnetic field arising from the eddy currents induces a 'back-emf' (via Lenz's law) within the coil, thereby modifying the applied field. This circular effect, in which output affects input, has posed a mathematically intractable problem preventing the development of general solutions to transient induction phenomena. The complexity of the problem is further amplified by magnetization effects, which increase and redistribute the magnetic flux density within a ferromagnetic object [7]. In the same way that the pioneering analytical work performed by Dodd and Deeds [1] led to the advancement of the field of conventional eddy current testing [2], correct and complete transient eddy current models would enable quantitative treatment, analysis and optimization of potentially superior transient eddy current signals and systems.

Due to the unavailability of complete analytical models, however, Finite Element Method (FEM) has become an alternate means of obtaining insights into the electromagnetic interactions within inspection geometries of varying complexity and has been used for probe design [8], as well as to investigate potential methods for analysing transient signals [9]. FEM is limited due to the time models take to develop, the black-box nature of commercial software, the requirements for validation (which is also true for analytical models), the extensive computer resource requirements and the long run time for more complicated models (12 hours is not uncommon for a simple transient EC problem on a standard personal computer). FEM has the advantage, however, of being able to generate results in cases where complex geometries, in which little or no symmetry exists, that are therefore, challenging to solve analytically.

Considerable work [10][11] has been devoted to the development of analytical models, with the goal of predicting induced voltages or impedance changes in sensing coils for applications in eddy current testing. To date, these models, built upon the Dodd and Deeds formalism [1], have been fairly successful for single-coil configurations. However, in cases where two or more coils are involved, present models fail to yield results consistent with experimental observations, particularly at early times in the case of transient signals. [12] Ferromagnetic conductors, such as steel, exhibit stronger and, therefore, more complicated feedback effects between driver, pickup and sample circuit elements. These stronger feedback effects further exacerbate the disagreement between theory and experiment. A typical work-around is to convolve the pickup coil's step response with a measured or fitted driver current signal (eqn. (35) in [11], eqn. (16) in [13], section 3.6 in [14], ). While this semi-empirical approach may improve agreement between modelled and measured pick-up coil response, it does not overcome the challenges inherent in feedback, since it does not address all of the electromagnetic interactions arising within the driver-pickup eddy current circuits. Therefore, transient driver-pickup models presented in the literature offer limited experimental validation, especially for the case of ferromagnetic conductors. Since steel is a commonly encountered construction material, complete models that correctly account for these complex electromagnetic interactions are of significant interest.

It is important to note that while analytical models are faster, requiring fewer computer resources, they do require a more fundamental understanding of electromagnetic phenomena as expressed by Maxwell's equations and the associated mathematical formalisms to develop solutions. Although the development of such solutions is presently limited to simple geometries, the analytical treatment of eddy current induction problems provides a deeper understanding of the underlying physics than would be provided by finite element analysis software.

## 1.2. Research survey

A brief research survey is presented here, since an expanded review of the relevant literature is included in the introductions of the manuscripts presented in Chapter 4.

Research in transient eddy current theory had already begun by 1921 when Wwedensky [16] calculated the diffusion of magnetic fields impressed upon rigid conducting cylinders. Building upon this work, Bean [17] and Callarotti [18] developed and patented [19] eddy-current methods for measuring the resistivity of metals.

In the 1960's, Dodd and Deeds [1] used a magnetic vector potential formalism to formulate closed-form solutions that described the eddy currents produced by cylindrical coils in planar and cylindrical conductors due to a harmonic current excitation. They also proposed the volume integral method for predicting probe response to volumetric flaws. Later, these models were extended to an arbitrary number of conductive layers [20][21] using the matrix method of Cheng et al. It is stressed here that the Dodd and Deeds formalism for driver-pickup models expressed the voltage induced in an open pickup coil circuit as a function of an invariant current applied to a driver coil, rather than an applied voltage. Despite this, the well-established Dodd and Deeds models have served industry for four decades and are still widely used in eddy current non-destructive evaluation.

In 2005, Theodoulidis and Kriezis [22] recast the integral expressions for the magnetic fields, originally developed in the Dodd and Deeds models, as series expansions by truncating the solution region by imposing magnetic insulation boundaries at an appropriate distance from the source coil. As a result, computation time was considerably reduced, convergence was better controlled and computer implementation was greatly simplified. This represented a significant improvement from a computational aspect, and many authors [23]-[28] have since adopted this approach.

Recently, theoretical research efforts have focussed on extending the class of eddy current problems that could be treated analytically. Novel techniques, such as the second-order vector potential formalism [29] or a Green's dyad approach [30], have been successfully employed. Using these techniques, a broader class of eddy current problems, with various conductor geometries and coil probe configurations, could be addressed. For example, analytical models have been developed for a tilted coil above a halfspace [31], for a horizontal coil in a borehole [32] and for arbitrarily positioned and shaped coils in proximity of conductive cylinders [33]. The majority of eddy-current models, however, are formulated for single-coil configurations in impedance measurement schemes.

An analytical model for the transient current response of an absolute, air-cored coil placed next to a layered sample and excited with a step-function change in voltage was developed in [34]. This approach differs from the Dodd and Deeds formalism, which considers current as input and voltage as output. The solution correctly incorporates the effects of the layered conductor, and excellent experimental agreement is achieved. Driver-pickup models, however, are far less developed. To the knowledge of the author, an analytical model that describes the transient response of a driver-pickup probe due to a voltage excitation, and in which the pickup circuit is not an open circuit, has not been developed.

A persistent challenge to the development of transient eddy current driver-pickup models has been a lack of agreement with experimental results, particularly in cases involving ferromagnetic structures, since they exhibit stronger feedback effects. This is inopportune since steel, and many other materials commonly encountered in industry, are ferromagnetic. Most driver-pickup models found in the literature [11]-[15][23][26] are based upon the original Dodd and Deed's formulation [1], in which the voltage induced in the pickup coil is expressed as a function of a known, or prescribed,

current flowing in the driver coil. This is clearly problematic, since changing inspection conditions give rise to varying feedback effects, which continuously alter the driver current.

Analytical eddy current models are of interest since they provide a practical means of interpreting inspection data and may, ultimately, enable the quantitative evaluation of material characteristics, such as electrical conductivity, magnetic permeability and material thickness. An early method of characterising the conductivity of metallic structures, using eddy current decay times, was applied to tubes by Jardim et al. in 1987 [35]. Their model assumes a uniform field applied to a thin tube, and considers the first relaxation time of the system. Resistivity values obtained using there method and the four-terminal method agreed within approximately 2%. The model claims to provide a means to calculate the sample's magnetic permeability, however, no experimental validation is presented.

Later, in 1996, a method of characterizing the conductivity and thickness of metallic layers, using pulsed eddy current measurements, was developed by Tai et al. [34]. The method considers three signal features: signal peak height, the time of occurrence of the first peak, and a characteristic zero-crossing time. The authors of that work report an accuracy of 13% for thickness measurements, and 20-30% for conductivity measurements. As with the previous example, the authors avoid the issue of material permeability.

Recently, in 2013, Adewale and Tian [36] suggest a method of decoupling the influences of permeability and conductivity. Their approach appears to be largely empirical and relies on signal normalization in an attempt to mask/subdue the effects of permeability. Furthermore, only weak relative permeabilities are considered ( $\mu_r = 1, 1.1, 1.27$  and  $1.63$ ), whereas the relative permeability of commonly encountered carbon steel is as high as 250 [41][42]. It is doubtful that this method would

work with higher permeability materials. Clearly, further improvement in the field of material characterization involving ferromagnetic materials is required.

### **1.3. Objective**

The objective of this doctoral research is to develop a general framework for obtaining analytical solutions, which correctly address the feedback challenge, for applications in eddy current testing. The resulting solutions will incorporate all inductive coupling interactions arising in inductively coupled circuits due to a prescribed voltage, rather than a current. The proposed voltage formalism will yield novel solutions for driver-pickup transient probe response.

The development of exact mathematical models, in which feedback effects have been addressed, will facilitate the quantitative analysis and interpretation of experimental signals obtained from particular inspection geometries, thereby enhancing the potential applicability of transient eddy current non-destructive evaluation. Such models may also elucidate similarities and differences between conventional and transient eddy current techniques.

### **1.4. Scope and methodology**

In order to clearly and thoroughly establish all aspects of the theory, this thesis takes an iterative approach, beginning with the consideration of simple canonical models. Following successful experimental validation at each stage, the complexity and number of variables considered is progressively increased. This strategy ensures that the resulting theory remains self-consistent and is thoroughly validated.

The analytical descriptions examined in this thesis, however, are limited to ideal models. That is, they assume homogeneous, isotropic and linear media, and consider geometries with parallel

interfaces, such as rods, tubes and plates. Despite the relative simplicity of these models, the final solutions are equally valid for multi-layered media and structures containing corners and edges. The analytical treatment and experimental validation of such systems is deferred for future work. As an aside, electromagnetic effects of material defects are discussed, but are not included in the models.

Finally, in the development of these analytical models, emphasis has been placed on applying the relevant physics, rather than on the computational efficiency of the resulting solutions. For instance, integral expressions are computed numerically instead of being recast into rapidly calculable truncated summations. For the purpose of this work, it has not been necessary to optimize computational costs. However, should there arise a need to perform near-real-time calculations, many existing strategies can be applied to the theory presented here.

## **1.5. Structure**

This thesis, structured in accordance with the manuscript thesis format, contains six chapters and five manuscripts. Chapter 2 provides an overview of relevant concepts and equations of electromagnetic theory, introduces techniques for solving boundary value problems, defines convolution, introduces the fundamentals of circuit analysis, and discusses the computation of results.

The experimental apparatus and method are described in Chapter 3. Detailed descriptions of the pulsing system circuitry and calibration of the electromagnetic coil manufacturing process and of the conducting test pieces are provided. The experimental data post-processing and display methodology are outlined at the end of this chapter.

Five manuscripts are presented in Chapter 4. The first paper, *Concerning the Derivation of Exact Solutions to Inductive Circuit Problems for Eddy Current Testing*, develops a novel approach for the

formulation of solutions to eddy current induction problems, and applies it to the simple case of a driver-pickup probe in air. In the second paper, entitled *Transient Response of a Driver Coil in Transient Eddy Current Testing*, the theory is applied to a driver-sample system. The theory is extended, in the third paper, *Transient Response of a Driver-Pickup Coil Probe in Transient Eddy Current Testing*, to include a pickup coil. In a fourth paper, *Transient response of a driver-pickup probe encircling a ferromagnetic conducting tube*, the solutions for driver-pickup are applied to ferromagnetic conducting tubular structures. Finally, a fifth paper, entitled *Simultaneous evaluation of material parameters using analytical transient eddy current models*, develops a method to characterize a conductor's electrical, magnetic and geometric properties.

Manuscript	Journal	Status
<i>Concerning the derivation of exact solutions to inductive circuit problems for eddy current testing</i>	NDT&E Intl.	Accepted 30 Jul 2014
<i>Transient response of a driver coil in transient eddy current testing</i>	NDT&E Intl.	Accepted 1 Apr 2015
<i>Transient response of a driver-pickup coil probe in transient eddy current testing</i>	NDT&E Intl.	Accepted 28 Apr 2015
<i>Transient response of a driver-pickup probe encircling a ferromagnetic conducting tube</i>	IEEE Trans. Mag.	In preparation for submission 25 May 2015
<i>Simultaneous evaluation of material parameters using analytical transient eddy current models</i>	Proc. of 19th Intl. Workshop on ENDE	Submitted 24 Aug 2014

The relevance of this work, as it pertains to the Dodd and Deeds formalism [1], is discussed in Chapter 5. Finally, a summary of results is presented in Chapter 6, and an overview of future work is listed in Chapter 7.

"It is hoped that the ability to calculate these eddy-current phenomena accurately will lead to eddy-current instruments which can make direct measurements of the physical properties of a specimen without calibration standards."

- Dodd and Deeds 1969

## CHAPTER 2 – THEORY

This chapter, beginning with Maxwell's equations, presents a summary of electromagnetic field theory in the context of the Transient Eddy Current (TEC) technique, and reviews the mathematics necessary to formulate analytical solutions to boundary value problems.

### 2.1. Electrodynamics

Maxwell's field equations in matter [37], cast in vectorial form in SI units (International System of Units), are written as

$$\nabla \cdot \mathbf{E} = \frac{\rho}{\varepsilon}, \quad (1)$$

$$\nabla \cdot \mathbf{B} = 0, \quad (2)$$

$$\nabla \times \mathbf{E} = -\frac{d\mathbf{B}}{dt}, \quad (3)$$

$$\nabla \times \mathbf{B} = \mu \mathbf{j} + \mu \varepsilon \frac{d\mathbf{E}}{dt}, \quad (4)$$

where current density  $\mathbf{j}$  and charge density  $\rho$  are considered as the sources that establish the electromagnetic fields  $\mathbf{B}$  (magnetic flux density) and  $\mathbf{E}$  (electric field), respectively. Material parameters  $\mu$  and  $\varepsilon$  correspond to the medium's magnetic permeability and the electrical permittivity. Ohm's law, which relates the current density to the electric field – or alternatively, to the magnetic vector potential,  $\mathbf{A}$  – is given as [37]

$$\mathbf{j} = \sigma \mathbf{E}, \quad (5)$$

where  $\sigma$  is the medium's electrical conductivity. The magnetic flux density  $\mathbf{B}$  may be expressed as the curl of the magnetic vector potential such that

$$\mathbf{B} = \nabla \times \mathbf{A}. \quad (6)$$

Equation (6) is substituted into (3), such that

$$\nabla \times \mathbf{E} = -\frac{d\nabla \times \mathbf{A}}{dt} = -\nabla \times \frac{d\mathbf{A}}{dt}, \quad (7)$$

and therefore

$$\mathbf{E} = -\frac{d\mathbf{A}}{dt}. \quad (8)$$

From equation (8), Ohm's law may be expressed in terms of the magnetic vector potential as

$$\mathbf{j} = -\sigma \frac{d\mathbf{A}}{dt}. \quad (9)$$

Using the Coulomb gauge definition, i.e.  $\nabla \cdot \mathbf{A} = 0$ , equations (9), (8) and (6) are substituted into (4) to obtain the full wave equation

$$\nabla^2 \mathbf{A} = \mu\sigma \frac{d\mathbf{A}}{dt} + \mu\epsilon \frac{d^2 \mathbf{A}}{dt^2}. \quad (10)$$

In the magnetoquasistatic (MQS) approximation [37], the second derivative on the right-hand-side (RHS) of equation (10), which arises as a consequence of displacement currents, may be neglected. This approximation is valid at relatively long timescales, or alternatively at low frequencies (<50MHz), implied by eddy current diffusion in conducting metallic materials (typical eddy current instruments operate below 12MHz). The approximation can be understood through the idea that the

currents change sufficiently slowly that the system can be taken to be in equilibrium at all times. Thus, under MQS, the dominant electromagnetic phenomena are described by the diffusion equation:

$$\nabla^2 \mathbf{A} = \mu\sigma \frac{d\mathbf{A}}{dt}. \quad (11)$$

The vector Laplacian,  $\nabla^2$ , assumes a different form for different coordinate systems. In cylindrical coordinates, it is given as [39]

$$\nabla^2 \mathbf{A} = \begin{bmatrix} \frac{\partial^2 A_r}{\partial z^2} + \frac{\partial^2 A_r}{\partial r^2} + \frac{1}{r} \frac{\partial A_r}{\partial r} - \frac{A_r}{r^2} + \frac{1}{r^2} \frac{\partial^2 A_r}{\partial \phi^2} - \frac{2}{r^2} \frac{\partial A_\phi}{\partial \phi} \\ \frac{\partial^2 A_\phi}{\partial z^2} + \frac{\partial^2 A_\phi}{\partial r^2} + \frac{1}{r} \frac{\partial A_\phi}{\partial r} - \frac{A_\phi}{r^2} + \frac{1}{r^2} \frac{\partial^2 A_\phi}{\partial \phi^2} + \frac{2}{r^2} \frac{\partial A_r}{\partial \phi} \\ \frac{\partial^2 A_z}{\partial z^2} + \frac{\partial^2 A_z}{\partial r^2} + \frac{1}{r} \frac{\partial A_z}{\partial r} + \frac{1}{r^2} \frac{\partial^2 A_z}{\partial \phi^2} \end{bmatrix} \begin{matrix} \hat{\mathbf{r}} \\ \hat{\boldsymbol{\phi}} \\ \hat{\mathbf{z}} \end{matrix}, \quad (12)$$

and may be simplified when symmetries exist. For instance, consider Poisson's equation that describes the vector potential created by a current density:

$$\nabla^2 \mathbf{A} = -\mu \mathbf{j}. \quad (13)$$

If the current density is axially symmetric and circulating only in the  $\hat{\boldsymbol{\phi}}$  direction, such as in the case of a circularly symmetric coil, then  $A_{r,z} = 0$  and  $\frac{\partial A_\phi}{\partial \phi} = 0$ , and the vector Laplacian reduces to

$$\nabla^2 \mathbf{A} = \left[ \frac{\partial^2 A_\phi}{\partial z^2} + \frac{\partial^2 A_\phi}{\partial r^2} + \frac{1}{r} \frac{\partial A_\phi}{\partial r} - \frac{A_\phi}{r^2} \right] \hat{\boldsymbol{\phi}}. \quad (14)$$

The diffusion equation in (11), together with an additional set of constraints called boundary conditions, form the basis of an eddy current boundary value problem.

## 1.6. Magnetic Permeability

An external magnetic field  $\mathbf{H}$  will cause the atomic dipoles of a ferromagnet to align with the applied field [38]. The molecular field, arising from alignment due to quantum mechanical effects, yields a large internal and external magnetization field  $\mathbf{M}$  [40]. The total magnetic flux density,  $\mathbf{B}$ , is proportional to the sum of the applied field with the magnetization field such that

$$\mathbf{B} = \mu_0(\mathbf{H} + \mathbf{M}), \quad (15)$$

where  $\mu_0$  is the magnetic permeability of free space. For linear magnetic materials, the expression above can be re-expressed as

$$\mathbf{B} = \mu_0 \left(1 + \frac{M}{H}\right) \mathbf{H} = \mu \mathbf{H}, \quad (16)$$

where  $\mu$  is the magnetic permeability of the material. Generally, the relationship between applied field strength  $\mathbf{H}$  and magnetic flux density  $\mathbf{B}$  is not linear in ferromagnetic materials. The non-linear variation of  $\mu = B/H$  for a ferromagnetic material, such as commercial iron, is shown in Figure 2.

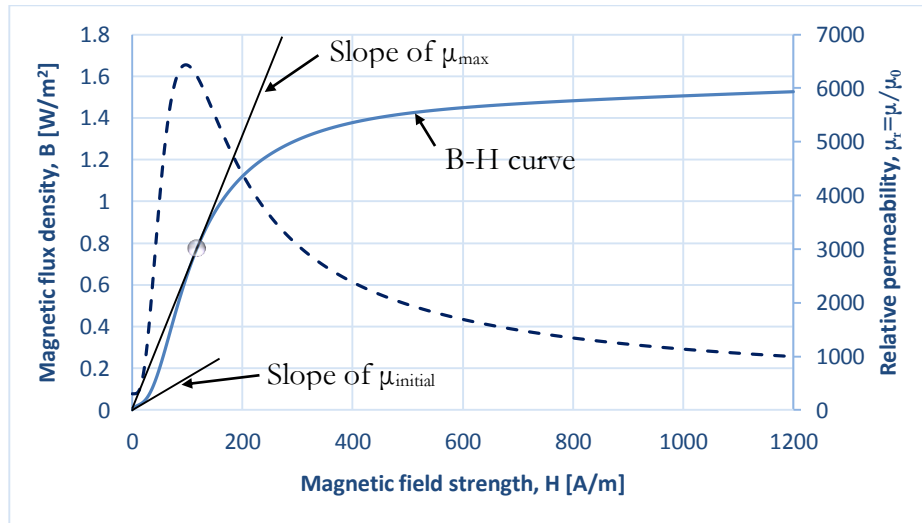


Figure 2: Magnetization curve of commercial iron. Permeability is given by the ratio  $B/H$ . (Redrawn from [41])

The permeability at low flux densities, called the initial permeability, is much less than the permeability at higher flux densities [40]. At low fields, the behavior of ferromagnetic materials is described by the Rayleigh law [40]. When a small external field  $\mathbf{H}$  is applied, domain wall motion is reversible. The initial permeability, the limit approached by the ratio of  $\mathbf{B}$  and  $\mathbf{H}$  for small applied fields, is, therefore, reversible and approximately linear. The permeability curves of various materials are shown to be linear when the applied field is sufficiently small (0 – 0.5 mT) [41]. This fact is of particular importance in eddy current testing, where the current flowing in the exciting coil is typically weak. The condition of weak fields and therefore, linear permeability greatly reduces the complexity of mathematical models.

The initial relative magnetic permeability of pure iron ranges between 200 and 250 [41][42], and is depressed considerably by the addition of carbon. Data of Gumlich [43] and Yensen [44] show that, in the high carbon range, the initial permeability lies between 100 and 150 for annealed alloys. Ferromagnetic carbon steel tubes of a similar composition are investigated in eddy current experiments in Chapter 4.

## 2.2. Material interface

In the magnetoquasistationary approximation for normally conducting media where surface currents vanish, and in axially symmetric problems where only the azimuthal, or  $\hat{\phi}$ , component of the magnetic vector potential exists, the boundary conditions at a radial interface, expressed in circular cylindrical coordinates, are derived in ANNEX B and given as [15]

$$\frac{A_1 + r \frac{\partial A_1}{\partial r}}{\mu_1} = \frac{A_2 + r \frac{\partial A_2}{\partial r}}{\mu_2}, \quad (17)$$

$$A_1 = A_2 . \tag{18}$$

these boundary conditions apply, for example, to the inner and outer walls of tubular structures such as a rod – shown in Figure 3 –, tube and borehole.

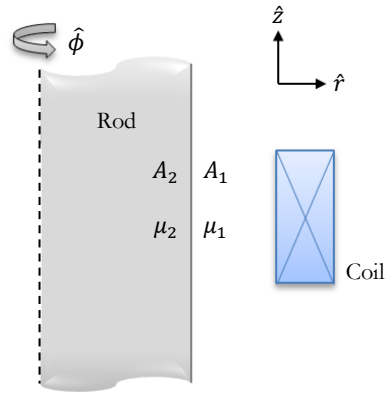


Figure 3: Cross-sectional view of a coil encircling a rod depicting a vertical boundary.

For the case of axially symmetric planar structures, such as a half-space – shown in Figure 4 –, plate and multilayer plate, the boundary conditions enforced at the planar interfaces are also derived in ANNEX B and are written as [15]

$$\frac{1}{\mu_1} \frac{\partial A_1}{\partial z} = \frac{1}{\mu_2} \frac{\partial A_2}{\partial z} , \tag{19}$$

$$A_1 = A_2 . \tag{20}$$

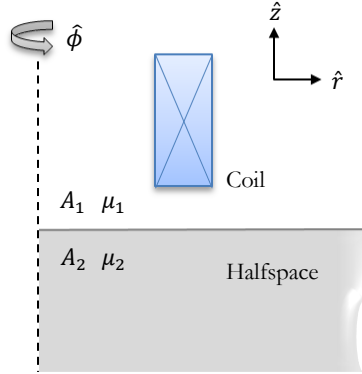


Figure 4: Cross-sectional view of a coil above a plate depicting a horizontal boundary.

### 2.3. Integral transforms

Integral transforms are the most convenient way of solving partial differential equations, such as the diffusion equation, for problems involving planar and tubular structures, which contain infinite domains with parallel interfaces. Three will be discussed here; the Fourier, the Cosine, and the Hankel transforms.

The non-unitary, angular frequency, Fourier transform [45] is defined as

$$F(\omega) = \int_{-\infty}^{\infty} e^{-j\omega t} f(t) dt, \quad (21)$$

where the frequency domain function  $F(\omega)$  is said to be the Fourier transform of the time domain function  $f(t)$ . The inverse Fourier transform is defined as

$$f(t) = \frac{1}{2\pi} \int_{-\infty}^{\infty} e^{j\omega t} F(\omega) d\omega. \quad (22)$$

A list of useful functions and their Fourier transforms are presented in Table 1.

Table 1: Useful Fourier transform rules.

Function	Fourier transform non-unitary, angular frequency	Remarks
$\frac{d^n f(t)}{dt^n}$	$(j\omega)^n F(\omega)$	Transform of a derivative.
$(f * i)(t)$	$F(\omega)I(\omega)$	Transform of a convolution.
$u(t)$	$\pi \left( \frac{1}{j\pi\omega} + \delta(\omega) \right)$	The function $u(t)$ is the Heaviside unit step function.
$\delta(t)$	1	The distribution $\delta(t)$ denotes the Dirac delta function, or unit impulse.
1	$2\pi\delta(\omega)$	Transform of a constant.
$\sin(\varpi t)$	$-j\pi(\delta(\omega - \varpi) - \delta(\omega + \varpi))$	Transform of a sine function.
$\cos(\varpi t)$	$\pi(\delta(\omega - \varpi) + \delta(\omega + \varpi))$	Transform of a cosine function.

When a solution is anticipated to be symmetric about the origin, the Fourier cosine transform [46], defined as

$$F(\lambda) = \int_0^{\infty} \cos(\lambda z) f(z) dz, \quad (23)$$

where the spatial frequency function  $F(\lambda)$  is said to be the transform of the spatial function  $f(z)$ , may be applied. Its inverse is given as

$$f(z) = \frac{1}{\pi} \int_0^{\infty} \cos(\lambda z) F(\lambda) d\lambda. \quad (24)$$

Functional Cosine transforms that will be useful in this work are listed in Table 2.

Table 2: Useful Fourier cosine transform rules.

Function	Fourier cosine transform non-unitary, angular frequency
$\frac{d^2 f(z)}{dz^2}$	$-\lambda^2 F(\lambda)$
$\delta(z)$	1
$\delta(z - h)$	$\cos(\lambda h)$

Finally, the first-order Hankel transform [47] may be used when the solution is anticipated to be axially symmetric. The forward transform is defined as

$$F(\gamma) = \int_0^\infty r J_1(\gamma r) f(r) dr, \quad (25)$$

where  $J_1(r)$  denotes a first-order Bessel function of the first kind [48], and where  $F(\gamma)$  is said to be the first-order Hankel transform of  $f(r)$ . The inverse transform is given as

$$f(r) = \int_0^\infty \gamma J_1(\gamma r) F(\gamma) d\gamma. \quad (26)$$

Useful first-order Hankel transforms used throughout this work are listed in Table 3.

Table 3: Useful first-order Hankel transform rules.

Function	First order Hankel transform
$\frac{d^2 f(r)}{dr^2} + \frac{1}{r} \frac{df(r)}{dr} - \frac{f(r)}{r^2}$	$-\gamma^2 F(\gamma)$
$\delta(r - a)$	$J_1(\gamma a)$

The integral transforms introduced above are well-suited for the solution of eddy current boundary value problems involving infinite domains with parallel interfaces. Such problems include rods, boreholes, tubes, plates, half-spaces and multi-layered structures. Problems involving corners and edges require more exquisite mathematics, such as truncated eigenfunction expansions and mode matching [28]. Such problems will not be addressed in this thesis, but will be addressed in future work.

## 2.4. Fourier series

A Fourier series [49] is an expansion of a periodic function in terms of an infinite sum of trigonometric functions. Fourier series make use of the orthogonality relationships of the sine and cosine functions. The computation and study of Fourier series is known as harmonic analysis. The Fourier series of a periodic function with period  $2P$  ( $P$  is the length of the pulse), periodic over the interval  $[0,2P]$ , is expressed as

$$f(t) = \frac{a_0}{2} + \sum_{n=1}^{\infty} a_n \cos\left(\frac{\pi n t}{P}\right) + b_n \sin\left(\frac{\pi n t}{P}\right), \quad (27)$$

where

$$a_0 = \frac{1}{P} \int_0^{2P} f(t) dt, \quad (28)$$

$$a_n = \frac{1}{P} \int_0^{2P} f(t) \cos\left(\frac{\pi n t}{P}\right) dt, \quad (29)$$

$$b_n = \frac{1}{P} \int_0^{2P} f(t) \sin\left(\frac{\pi n t}{P}\right) dt, \quad (30)$$

For example, the Fourier series representation of a 50% duty cycle square wave of amplitude  $v_0$  and of pulse length  $P$  is written as

$$v(t) = \frac{v_0}{2} + \frac{2v_0}{P} \sum_{n=1}^{\infty} \frac{\sin(\omega_n t)}{\omega_n}, \quad \omega_n \equiv \frac{(2n-1)\pi}{P}. \quad (31)$$

Equation (31) is plotted, in Figure 5, using 1, 3 and 10 terms (in addition to the constant term) in a truncated summation, alongside the square-waveform to which the series converges with an infinite number of terms.

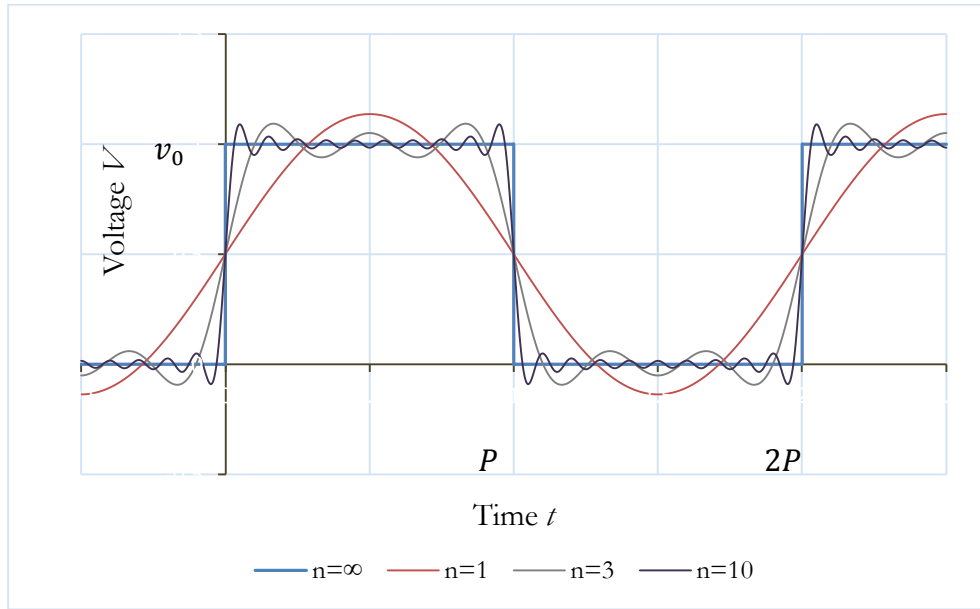


Figure 5: Fourier representation of a square wave with amplitude  $v_0$  pulse length  $P$ .

The Fourier transform of equation (31), which follows from transforms listed in Table 1, is written as

$$\pi v_0 \delta(\omega) - j \frac{2\pi v_0}{P} \sum_{n=1}^{\infty} \frac{\delta(\omega - \omega_n) - \delta(\omega + \omega_n)}{\omega_n}, \quad \omega_n \equiv \frac{(2n-1)\pi}{P}, \quad (32)$$

and will be useful throughout this work.

## 2.5. Convolution

Convolution theory [50] is central to the development of solutions to transient eddy current problems in this thesis. When used in conjunction with Kirchhoff's voltage law, feedback effects, arising between conducting, and even ferromagnetic, test pieces and the driving and sensing coils, can be properly addressed.

The impulse response of a system, defined as  $\hat{A}(t)$ , is the system's response when an impulse is applied at time  $t = 0$ . In causal systems, the response cannot occur before the onset of the input, such that  $\hat{A}(t) = 0$  when  $t < 0$ . Below, a delayed response  $\hat{A}(t - \tau)$  arises from an impulse applied at  $t = \tau$ .

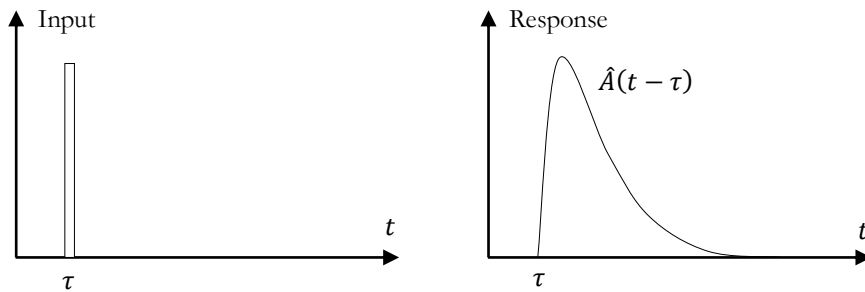


Figure 6: Input arising at time  $\tau$  and its response  $\hat{A}(t - \tau)$ .

Consider an arbitrary, yet continuous, input divided into rectangular pulses of length  $d\tau$ . Each pulse may be regarded as a Dirac impulse. If the input is  $i(t)$ , then the magnitude of a particular pulse centered around  $t = \tau$  is  $i(\tau)d\tau$ . The response is  $i(\tau)d\tau \hat{A}(t - \tau)$  as depicted in Figure 7.

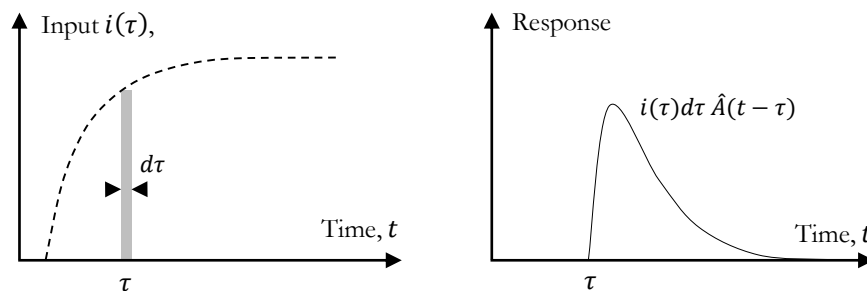


Figure 7: Response of a Dirac impulse from an arbitrary input.

Therefore, the total response to the complete input corresponds to the sum of the component responses such that  $A(t) = \sum i(\tau) d\tau \hat{A}(t - \tau)$ , as illustrated in Figure 8.

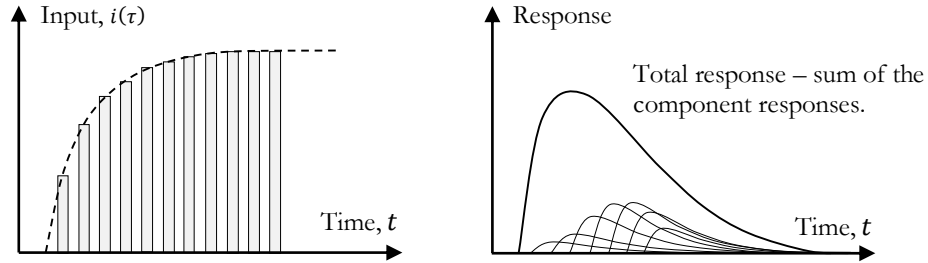


Figure 8: Total response to an arbitrary input is the sum of the component responses.

In the limit, as the pulses are made thinner and more numerous, the sum becomes an integral such that

$$A(t) = \int_{-\infty}^{\infty} i(\tau) \hat{A}(t - \tau) d\tau . \quad (33)$$

The integral is generally taken from  $-\infty$  to  $\infty$  as shown in equation (33). However, for causal input signals starting at  $t = 0$  such as driving signals in transient eddy current testing, the integral is from 0 to  $t$ , since  $\hat{A}(t - \tau) = 0$  when  $\tau < t$ , such that

$$A(t) = \int_0^t i(\tau) \hat{A}(t - \tau) d\tau . \quad (34)$$

The integral expression in (34) is called a convolution of  $\hat{A}(t)$  and  $i(t)$ . It is often written as

$$A(t) = i(t) * \hat{A}(t) = \hat{A}(t) * i(t) . \quad (35)$$

Convolution is useful for finding the response of a system to an arbitrary input in terms of the response to a standard function, which is usually the impulse. Arbitrary responses can also be

formulated in terms of the step response, as is done in Duhamel's theorem. [38] An important property of convolution is that in evaluating the integral, it does not matter which function is taken as a function of  $(\tau)$  as long the other is a function of  $(t - \tau)$ .

Another important property of convolution is that its Fourier transform is equivalent to the product of the component transforms, as shown in Table 1, such that

$$\int_{-\infty}^{\infty} (i(t) * \hat{A}(t)) e^{-j\omega t} dt = \hat{A}(\omega) I(\omega), \quad (36)$$

where  $\hat{A}(\omega)$  and  $I(\omega)$  are the Fourier transforms of the impulse response solution  $\hat{A}(t)$  and the input function  $i(t)$ , respectively.

## 2.6. Kirchhoff's voltage law

Differential equations, which describe the currents flowing in electrical circuits, are written using Kirchhoff's voltage law [51]. It will be shown in the manuscripts how feedback terms, which arise from conducting and magnetic test pieces, can be included in these differential equations using convolution theory.

The principle of conservation of energy implies that the directed sum of the electrical potential differences (voltage) around any closed network is zero [51]. The law can be stated as

$$\sum_{k=1}^N V_k = 0, \quad (37)$$

where there are  $N$  voltage sources in the circuit. Consider a series resistor, inductor and capacitor (RLC) circuit as shown in Figure 9.

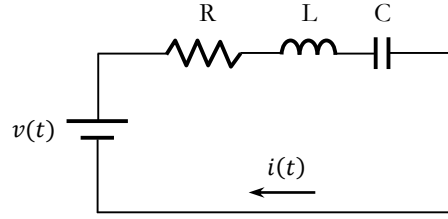


Figure 9: RLC series circuit.

Using Kirchhoff's voltage rule, we may write

$$v(t) = v_R(t) + v_L(t) + v_C(t), \quad (38)$$

where  $v(t)$ , the voltage supplied by the driving source, is equal to the sum of the voltages across the circuit components (resistor, inductor and capacitor). The constitutive relations are [51]

$$v_R(t) = R i(t), \quad (39)$$

$$v_L(t) = L \frac{d}{dt} i(t), \quad (40)$$

$$v_C(t) = \frac{1}{C} \int_{-\infty}^t i(\tau) d\tau. \quad (41)$$

Thus, the integro-differential equation, governing the time dependent current flowing in the circuit, is written as

$$v(t) = R i(t) + L \frac{d}{dt} i(t) + \frac{1}{C} \int_{-\infty}^t i(\tau) d\tau. \quad (42)$$

This equation is easily solved for the time-dependant current  $i(t)$  flowing in the circuit due to an applied voltage  $v(t)$ . In the case of a step excitation  $v(t) = v_0 u(t)$ , where  $u(t)$  is the Heaviside function defined in Table 1, equation (42) is differentiated with respect to time such that

$$v_0 \delta(t) = R \frac{di(t)}{dt} + L \frac{d^2 i(t)}{dt^2} + \frac{i(t)}{C}. \quad (43)$$

The Fourier transform of equation (43), using Table 1, is written as

$$v_0 = j\omega R I(\omega) - \omega^2 L I(\omega) + \frac{I(\omega)}{C}, \quad (44)$$

and solved for  $I(\omega)$  such that

$$I(\omega) = \frac{v_0}{\frac{1}{C} - \omega^2 L + j\omega R}. \quad (45)$$

The inverse Fourier transform of equation (45) yields three solutions, which depend on the relative magnitudes of the resistance  $R$ , inductance  $L$  and capacitance  $C$ . The damping factor  $\zeta$ , defined as the ratio of the damping frequency,  $\frac{R}{2L}$ , and the resonant frequency,  $\frac{1}{\sqrt{LC}}$ , is written [51]

$$\zeta \equiv \frac{R}{2} \sqrt{\frac{C}{L}}. \quad (46)$$

The underdamped response ( $\zeta < 1$ ) is

$$i(t) = \frac{v_0 \sin\left(\sqrt{\frac{1}{CL} - \frac{R^2}{4L^2}} t\right) e^{-\frac{R}{2L} t}}{4L \sqrt{\frac{1}{CL} - \frac{R^2}{4L^2}}}, \quad (47)$$

the critically damped response ( $\zeta = 1$ ) is

$$i(t) = v_0 \frac{t e^{-\frac{R}{2L} t}}{L}, \quad (48)$$

and finally, the overdamped response ( $\zeta > 1$ ) is written as

$$i(t) = v_0 \frac{\left( e^{\sqrt{\frac{1}{CL} - \frac{R^2}{4L^2}} t} - e^{-\sqrt{\frac{1}{CL} - \frac{R^2}{4L^2}} t} \right) e^{-\frac{R}{2L} t}}{2L \sqrt{\frac{1}{CL} - \frac{R^2}{4L^2}}}. \quad (49)$$

An alternate method of solving equation (42) is to substitute the Fourier representation of a square waveform instead of a Heaviside step function. Then, using equation (31), the differential equation, to which a solution is sought, becomes

$$\frac{v_0}{2} + \frac{2v_0}{P} \sum_{n=1}^{\infty} \frac{\sin(\varpi_n t)}{\varpi_n} = Ri(t) + L \frac{d}{dt} i(t) + \frac{1}{C} \int_{-\infty}^t i(\tau) d\tau. \quad (50)$$

Proceeding as before, equation (50) is differentiated with respect to time, yielding

$$\frac{2v_0}{P} \sum_{n=1}^{\infty} \cos(\varpi_n t) = R \frac{di(t)}{dt} + L \frac{d^2 i(t)}{dt^2} + \frac{i(t)}{C}, \quad (51)$$

and Fourier transformed so that

$$\frac{2v_0}{P} \sum_{n=1}^{\infty} \pi (\delta(\omega - \varpi_n) + \delta(\omega + \varpi_n)) = j\omega R I(\omega) - \omega^2 L I(\omega) + \frac{I(\omega)}{C}. \quad (52)$$

The transformed current function  $I(\omega)$  is isolated as

$$I(\omega) = \frac{2\pi v_0}{P} \sum_{n=1}^{\infty} \frac{\delta(\omega - \varpi_n) + \delta(\omega + \varpi_n)}{j\omega R - \omega^2 L + \frac{1}{C}}, \quad (53)$$

and the inverse Fourier transform is applied giving

$$i(t) = \frac{1}{2\pi} \int_{-\infty}^{\infty} \frac{2\pi v_0}{P} \sum_{n=1}^{\infty} \frac{\delta(\omega - \varpi_n) + \delta(\omega + \varpi_n)}{j\omega R - \omega^2 L + \frac{1}{C}} e^{j\omega t} d\omega. \quad (54)$$

The integral can be separated into two components:

$$i(t) = \frac{v_0}{P} \int_{-\infty}^{\infty} \sum_{n=1}^{\infty} \frac{\delta(\omega - \omega_n)}{j\omega R - \omega^2 L + \frac{1}{C}} e^{j\omega t} d\omega + \frac{v_0}{P} \int_{-\infty}^{\infty} \sum_{n=1}^{\infty} \frac{\delta(\omega + \omega_n)}{j\omega R - \omega^2 L + \frac{1}{C}} e^{j\omega t} d\omega. \quad (55)$$

In accordance with the sampling property [50], the Dirac delta functions destroy the integrals in which they lie, returning the kernels evaluated at  $\omega_n$  and  $-\omega_n$ , respectively, so that

$$i(t) = \frac{v_0}{P} \sum_{n=1}^{\infty} \frac{e^{j\omega_n t}}{j\omega_n R - \omega_n^2 L + \frac{1}{C}} + \frac{v_0}{P} \sum_{n=1}^{\infty} \frac{e^{-j\omega_n t}}{-j\omega_n R - \omega_n^2 L + \frac{1}{C}}. \quad (56)$$

Noting that the second term on the RHS of equation (56) is just the complex conjugate of the first. Since the sum of a complex function and its conjugate is equivalent to twice the real component<sup>1</sup>, equation (56) becomes

$$i(t) = \frac{2v_0}{P} \sum_{n=1}^{\infty} \Re \left( \frac{e^{j\omega_n t}}{j\omega_n R - \omega_n^2 L + \frac{1}{C}} \right). \quad (57)$$

Equation (57) may be re-written in trigonometric form as

$$i(t) = \frac{2v_0}{P} \sum_{n=1}^{\infty} \frac{1}{\omega_n} \frac{\left( \frac{1}{\omega_n C} - \omega_n L \right) \cos(\omega_n t) + R \sin(\omega_n t)}{\left( \frac{1}{\omega_n C} - \omega_n L \right)^2 + R^2}, \quad (58)$$

or, equivalently, as a superposition of phase shifted sine waves such that

$$i(t) = \frac{2v_0}{P} \sum_{n=1}^{\infty} \frac{\sin \left( \omega_n t - \arctan \left( \frac{\omega_n L}{R} - \frac{1}{\omega_n C R} \right) \right)}{\omega_n \sqrt{\left( \frac{1}{\omega_n C} - \omega_n L \right)^2 + R^2}}. \quad (59)$$

---

<sup>1</sup> Sum of a complex number with its conjugate:  $(x + jy) + (x - jy) = 2x$

Equation (59) is equivalent to all three solutions presented in (47), (48) and (49). Specifically, the series formulation is convergent for all  $\zeta$ , a notable advantage. As a demonstration, solution (59) is plotted, in Figure 10, alongside plots of solutions (47) and (49) for overdamped ( $\zeta = 1.05$ ) and underdamped ( $\zeta = 0.24$ ) systems, respectively.

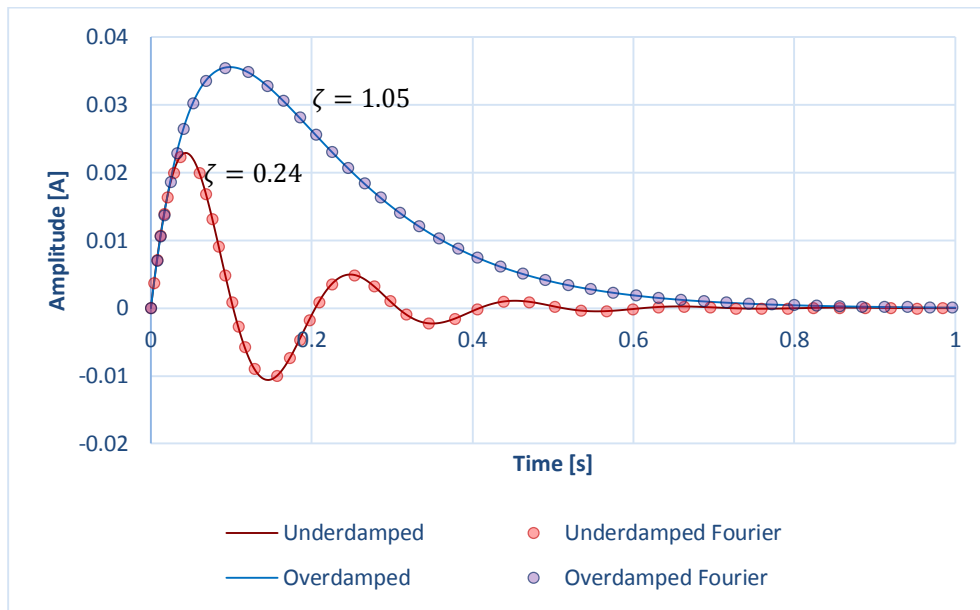


Figure 10: Plots of exact solutions (47) and (49), describing overdamped and underdamped systems, respectively, compared to an equivalent Fourier series representation (59).

Fourier superposition is, therefore, a powerful tool for the solution to differential equations. Exact analytical expressions for the RLC circuit's transient response are shown to be equivalent to the Fourier series solution, provided that the waveform's period is made long enough to encompass all of the transient effects. This method suffers, however, from the relatively high number of terms that must be included in the summation in order to ensure good convergence, which incurs a high computational cost. Despite this, Fourier superposition will be employed in the derivations of solutions in Chapter 4.

## 2.7. Computation of results

All computations are performed in Maplesoft's Maple 18 computational software [52]. Numerical integration is used to calculate the frequency-dependent complex inductance functions  $\mathcal{L}_1$ ,  $\mathcal{L}_2$  and  $\mathcal{M}$  (described in Chapter 4), and employs the NAG method d01akc, which uses adaptive Gauss 30-point and Kronrod 61-point rules [53]. Fourier series summations, performed to calculate probe response, include 250 terms in the computation in order to assure excellent convergence. For each term in the series, functions  $\mathcal{L}_1$ ,  $\mathcal{L}_2$  and  $\mathcal{M}$  must be computed. On average, 22 minutes are required, using an Intel® Core™ i7-4820K CPU at 3.70 GHz, to compute both the driver and the pickup response. An example worksheet containing the Maple code used to compute the transient driver and pickup responses of a coaxial probe encircling a ferromagnetic conducting rod is provided in Annex A.

Methods of reducing the incurred computation time are numerous. For example, the truncated region eigenfunction expansion (TREE) method [28] would be an excellent way to convert the integrals into summations, which has the potential to drastically reduce computation time. This approach is not taken here, however, this could be developed in the future in order to improve computational efficiency.

At this point, all aspects of the theory and computation of analytical results have been introduced. The following chapter will describe the details of the experiments performed to validate the theoretical models.

## CHAPTER 3 – EXPERIMENT

The experimental apparatus and method are described in this chapter. Transient eddy current measurements were performed on rod and tube geometries with ferromagnetic and non-ferromagnetic conductors in order to validate the analytical models using two different pulsing systems. An itemized list of the equipment necessary to acquire the experimental data and to characterize the test pieces is provided.

### 3.1. Pulser systems

This section describes the electronic pulse generating and measurement equipment that was used for signal generation and acquisition. Two different pulsing systems - one powered by battery and the other by a conventional power supply - were employed for the collection of experimental results presented in the manuscripts. Both in-house built systems were capable of transmit (driver-only) and transmit-receive (driver-pickup) functionality.

#### *- Battery Pulser*

The battery-powered pulser system, used to investigate tubular structures in manuscripts IV and V, are comprised of the following components:

- 12-Volt battery,
- National Instruments USB-6211 DAQ Board,
- Instrumentation Amplifier Chip (approximate signal gain of 150),
- Coaxial cables,
- Electromagnetic coils.

The National Instruments USB-6211 DAQ board has a maximum sampling rate of 250 kHz on a single channel. Consequently, transient voltages are sampled at 4  $\mu$ s increments. The relaxation time, defined as  $\tau \equiv \frac{L}{R}$ , associated with the probe used in conjunction with this system (L and R are later given in Table 5) is 198  $\mu$ s. Four relaxation times describe 98% of the transient signal, and correspond to 199 sampled points, which is a sufficient number of samples for a representative signal display and interpretation. However, it should be noted that coils with shorter relaxation times would require an acquisition board with a higher sampling rate in order to ensure good data density. The power supply is a battery, which provides a stable voltage source, yielding a superior signal-to-noise ratio in comparison to a conventional power supply. Driver voltage signals are measured across 2  $\Omega$  and 26.7  $\Omega$  resistors arranged in parallel, whereas pickup signals are measured across two 26.7  $\Omega$  resistors in series, as depicted by the circuit diagrams shown in Figure 11. In addition, an operational amplifier provides a signal gain of approximately 150. The coaxial cables are assumed to have negligible losses.

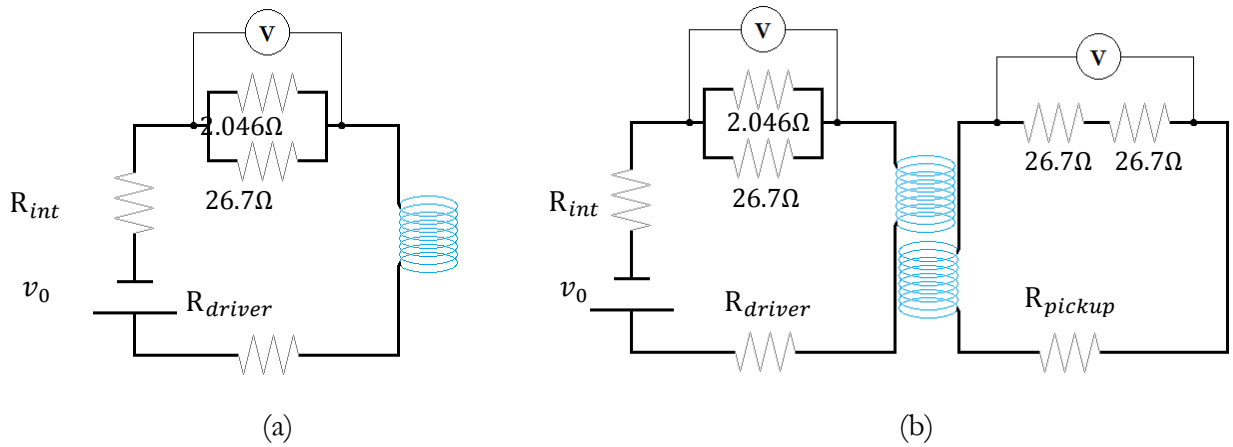


Figure 11: Driver (a) and driver-pickup (b) circuit diagrams for the battery pulser.

In order to accurately determine the value of the internal resistance and gain of the system, a set of calibration measurements were performed. A variable resistor was connected in lieu of the

driver coil shown in Figure 11 (a) above, and the transient voltage was recorded across the  $2 \Omega$  and  $26.7 \Omega$  parallel resistors. The equation for the steady-state current,  $i$ , flowing in the circuit, is written using Kirchhoff's voltage law, introduced in Section 2.6, as

$$v_0 = R_{int} i + R_{var} i + (2^{-1} + 26.7^{-1})^{-1} i, \quad (60)$$

and the voltage,  $\varepsilon$ , measured across the parallel resistors is written as

$$\varepsilon = G(2^{-1} + 26.7^{-1})^{-1} i, \quad (61)$$

where  $G$  is the signal gain from the operational amplifier. Equations (60) and (61) are solved and the resulting expression is recast into a linear form such that

$$\varepsilon^{-1} = \frac{(2^{-1} + 26.7^{-1})}{Gv_0} R_{var} + \frac{R_{int}(2^{-1} + 26.7^{-1}) + 1}{Gv_0}, \quad (62)$$

where  $\varepsilon^{-1}$  is the inverse of the measured steady state voltage,  $R_{var}$  is the resistance of the variable resistor,  $v_0$  is the amplitude of the applied voltage and  $R_{int}$  is the internal resistance of the pulser circuit. From equation (62), the expressions for the slope  $m$  and y-axis intercept  $b$ , respectively, are

$$m = \frac{(2^{-1} + 26.7^{-1})}{Gv_0}, \quad (63)$$

$$b = \frac{R_{int}(2^{-1} + 26.7^{-1}) + 1}{Gv_0}. \quad (64)$$

The inverse of the measured voltage,  $\varepsilon^{-1}$ , is plotted, in Figure 12, as a function of the variable resistance  $R_{var}$  for two different applied voltages, yielding linear relationships as prescribed by equation (62).

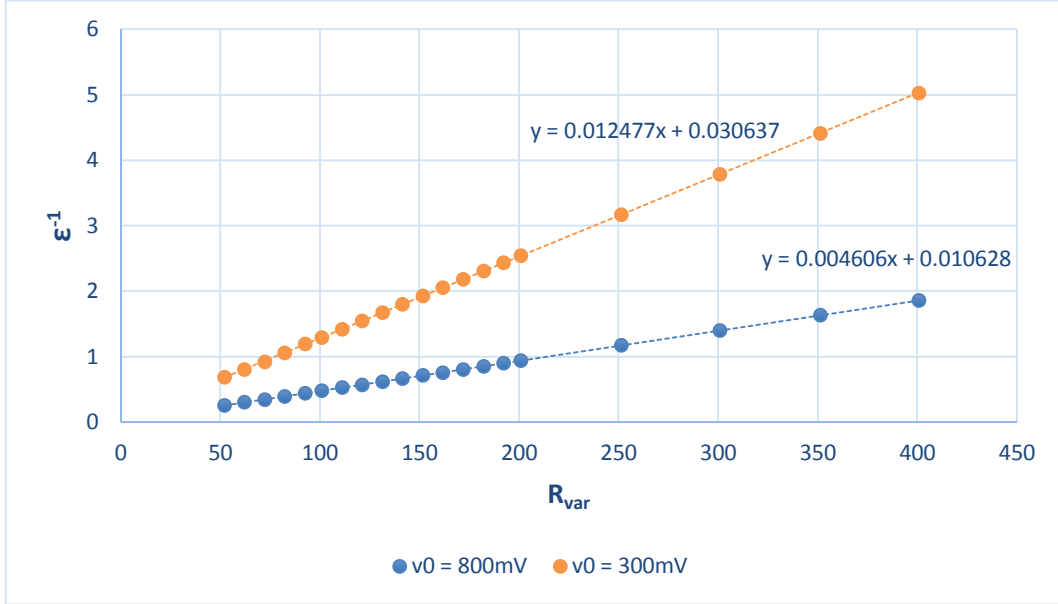


Figure 12: Battery pulser calibration plots.

The values  $R_{int}$  and  $G$  are calculated from the experimentally measured slopes  $m$  and y-axis intercepts  $b$ , using equations (63) and (64), and are listed in Table 4.

Table 4: Gain  $G$  and internal resistance  $R_{int}$  of the battery pulser calculated from linearized data sets.

$v_0$	800 mV	300 mV	
Slope $m$	0.00461	0.0125	
Intercept $b$	0.0106	0.0306	<i>Average</i>
$G$	146	144	<b>145</b>
$R_{int}$	0.448 $\Omega$	0.597 $\Omega$	<b>0.522 <math>\Omega</math></b>

In order to assess the quality of the driving signal, a 90  $\Omega$  resistor was connected, in place of a driver coil, to the pulse output terminal of the battery pulser. The normalized leading edge of the raw digitized square pulse excitation is shown in Figure 13.

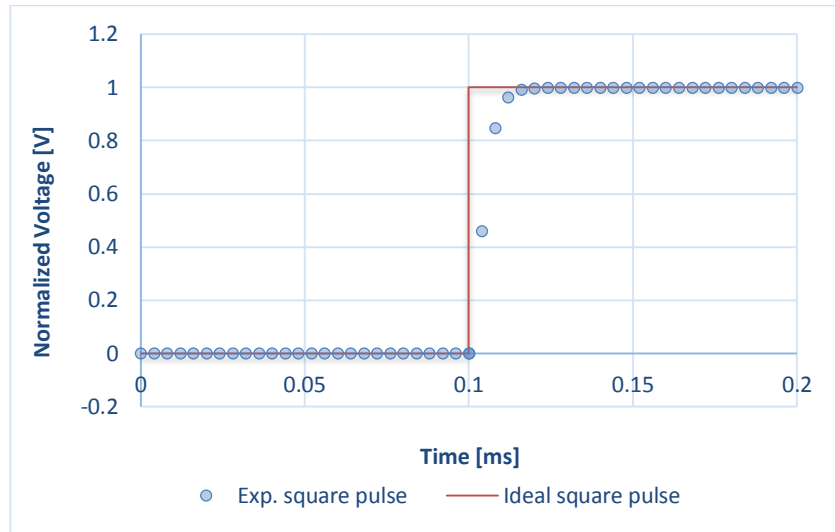


Figure 13: Leading edge of the square pulse generated by the battery pulser.

The driving signal (blue circle symbols) is not ideal (red line), as it requires approximately 16  $\mu\text{s}$  (four sampling increments) to switch states due to parasitic inductance and capacitance. Since the analytical models assume ideal square pulse excitations, distortions in the output signal will adversely affect agreement between the experimental and analytical results, particularly at early times. For coils with relatively long relaxation times, such as the ones used in this thesis, disagreement between experiment and theory becomes negligible.

*- Conventional power supply pulser*

The second pulser system, used to collect the experimental data for the rod experiments, comprises of the following components:

- Conventional 12-volt power supply,
- National Instruments USB-6343 DAQ board,
- Stanford Research Systems model SR560 Low noise pre-amplifier,
- 2.0  $\Omega$  and 50.0  $\Omega$  precision resistors,

- Coaxial cables,
- Electromagnetic coils.

Circuit diagrams representing the driver and driver-pickup circuitry are presented in Figure 14 (a) and (b), respectively.

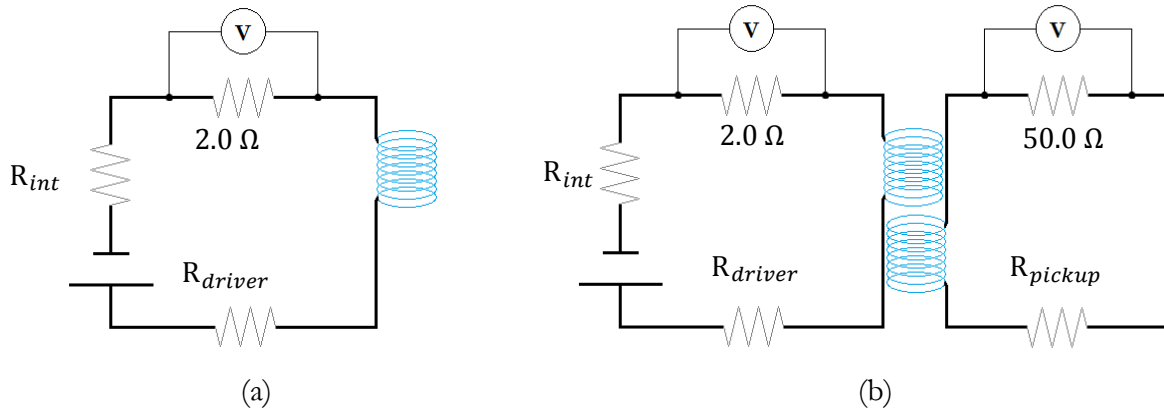


Figure 14: Driver (a) and driver-pickup (b) circuit diagrams for the conventional power supply pulser.

The National Instruments USB-6343 DAQ board has a maximum sampling rate of 500 kHz for a single channel, which corresponds to a voltage measurement every  $2 \mu\text{s}$ . The relaxation time associated with the experimental coils used in conjunction with this system is  $98.8 \mu\text{s}$  based on the coil properties listed in Table 6, which correspond to 197 sample points. Therefore, the 500 kHz sample rate is sufficient for recording a representative signal.

The leading edge of the normalized square waveform, or step, generated by the pulser and measured across a  $90 \Omega$  resistor is shown in Figure 15.

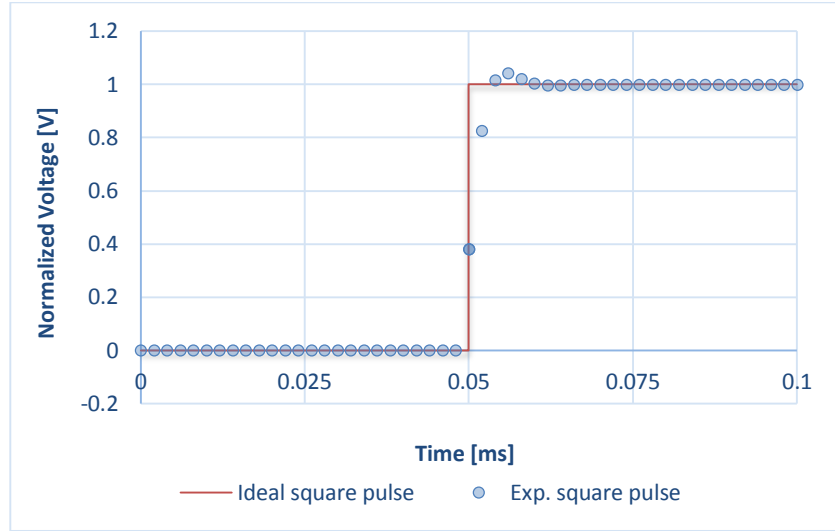


Figure 15: Leading edge of the square pulse generated by the conventional power supply pulser.

The step reaches its steady state within approximately  $10 \mu\text{s}$ , which is a short time relative to the relaxation times of the coils used in this work. The applied waveform, which differs from an ideal step function, resembles an underdamped transient; this is attributed to resistances, inductances and capacitances internal to the system. As mentioned previously, some experimental disagreement with analytical models, which describe responses to ideal square waveforms, will exist at early times. The discrepancy, however, is negligible at the timescales associated with the long-relaxation time coils ( $\tau = L/R \approx 150 \mu\text{s}$ ) used in this thesis. The effect, however, would become more apparent if coils with relatively short relaxation times were used. One way to compensate for this discrepancy would be to calculate the response to the experimental pulse rather than to an ideal square pulse. This strategy would also reduce ringing, which arises due to a step discontinuity (Heaviside function), and would, therefore, increase convergence rate and reduce computation time.

The value of the pulser’s internal resistance, obtained by performing the same calibration procedure performed with the battery pulser, was found to be  $2.76 \Omega$ . The low noise signal amplifier produces a known user-selected gain, which can be factored out of the experimental results. Having

determined all resistance values in the system, the circuit equations may now be solved with inductors, and even capacitors, as demonstrated in section 2.6. Such solutions are pertinent to eddy current non-destructive testing and will be developed in the manuscripts presented in Chapter 4.

### 3.2. Electromagnetic coils

A critical factor for achieving good agreement between theory and experiment is the manufacturing quality of the driving and sensing coils. Two coaxial driver-pickup probes were wound; one in tandem configuration (designed for the investigation of tubes) and the other in an encircling configuration (designed for rods). Both probes are shown in Figure 16.



Figure 16: Tandem driver-pickup tube probe (left) and encircling driver-pickup rod probe (right).

The coils were carefully wound with known number of turns, uniform turn density, rectangular cross-section and windings precisely perpendicular to coil axes. Additionally, each winding was laid precisely adjacent to the previous one in order to obtain a tight packing and, thus, a maximum fill-factor. Precisely manufactured coils are critical for experimental validation, since the analytical models assume ideal coil characteristics. Though it may be possible to model non-uniform turn density and non-perpendicular windings analytically, the position of the wire would have to be recorded while winding the coils; resulting in unnecessarily complex mathematics.

The physical dimensions of each coil were measured using a micrometer, and the number of turns was recorded during the winding process. The coils' resistance values were measured using a Keithley 2182 nanovoltmeter and a Keithley 6221 DC and AC current source. Finally, the self- and mutual inductance coefficients were extracted by performing a least-squares fit between driver-only experimental data and theory. The details of this procedure are explained in “*Concerning the Derivation of Exact Solutions to Inductive Circuit Problems for Eddy Current Testing*” in Chapter 4. The physical dimensions and electrical properties of the tandem probe (shown on the left in Figure 16) are listed in Table 5.

Table 5: Tandem probe characteristics.

<b>Coil:</b>	<b>Driver</b>	<b>Receiver</b>
Number of turns :	838	887
Wire gage :	36 AWG	36 AWG
Length :	9.01 mm	11.09 mm
Inner radius :	10.73 mm	10.71 mm
Outer radius :	12.54 mm	12.26 mm
Resistance :	87.6 $\Omega$	92.4 $\Omega$
Self-Inductance :	17.4 mH	17.6 mH
Inner-edge gap :	3.83 mm	
Mutual Inductance :	3.73 mH	

The encircling probe's characteristics are listed in Table 6.

Table 6: Encircling probe characteristics.

<b>Coil:</b>	<b>Driver</b>	<b>Pickup</b>
--------------	---------------	---------------

Number of turns :	991	787
Wire gage :	36 AWG	36 AWG
Length :	14.97 mm	14.98 mm
Inner radius :	8.21 mm	5.93 mm
Outer radius :	9.47 mm	7.03 mm
Resistance :	80.80 $\Omega$	47.55 $\Omega$
Self-Inductance :	12.26 mH	4.70 mH
Center offset :	0.025 mm	
Mutual Inductance :	5.28 mH	

Diagrams showing the relative dimensions and construction of the coils are provided in each of the manuscripts presented in Chapter 4.

### 3.3. Rods and Tubes

The following section provides a description of the conducting and ferromagnetic rods and tubes that were investigated in experiments. Physical dimensions, such as rod radius and tube wall thickness, were measured with a micrometer. Conductivity values are measured by the four-point method, which uses separate pairs of current-carrying and voltage-sensing electrodes [54]. Relative magnetic permeability values were calculated from the area under transient pickup signals using a novel inverse algorithm developed in the manuscript entitled “*Simultaneous evaluation of material parameters using analytical transient eddy current models*”.



Figure 17: Assorted aluminum, stainless steel, brass and carbon steel tubes with  $\frac{3}{4}$ " outer diameter.

Manuscripts II and III develop and validate solutions for the transient response of a driver coil and of a driver-pickup probe to a conducting and ferromagnetic rod. The electrical conductivities, relative magnetic permeabilities and radii of the test rods are listed in Table 7 below:

Table 7: Rod characteristics.

<b>Rod :</b>	<b>Copper</b>	<b>Brass</b>	<b>Steel</b>
Radius :	3.17 mm	3.19 mm	3.01 mm
Conductivity :	58.14 MS·m <sup>-1</sup>	12.44 MS·m <sup>-1</sup>	4.30 MS·m <sup>-1</sup>
Relative permeability :	1	1	107

The geometrical and electrical characteristics of the tube specimens, used to perform validation experiments in manuscripts IV and V, are listed in Table 8 on the following page:

Table 8: Tube specifications.

<b>Tube :</b>	<b>Brass</b>	<b>Steel</b>
---------------	--------------	--------------

Wall thickness :	1.65 mm (.065 in)	1.24 mm (.049 in)
Outer diameter :	19.05 mm (¾ in)	19.05 mm (¾ in)
Conductivity :	15.74 MS·m <sup>-1</sup>	7.022 MS·m <sup>-1</sup>
Relative permeability :	1.013	119.8

The magnetic permeabilities of the carbon steel rod and tube presented above are assumed constant in the analytical models developed in Chapter 4. The assumption of linear permeability, which has been introduced in Chapter 2, is justified in the next section.

### 3.4. Linear permeability

In what follows, two simple experiments confirm that the magnetization fields, generated during transient eddy current data collection, are well within the Rayleigh regime, where  $\mathbf{B}$  depends linearly upon  $\mathbf{H}$ .

The magnetic vector potential generated by a circular coil with length  $l$ , inner radius  $a$ , outer radius  $b$ , number of turns  $N$ , resistance  $R$  and carrying voltage  $v_0$  is written as

$$\boldsymbol{\psi}(r, z) = \frac{v_0}{R} \frac{2\mu_0 N}{\pi l(b-a)} \int_0^\infty \frac{\cos(\lambda z) \sin\left(\frac{\lambda l}{2}\right)}{\lambda} I_1(\lambda r) \int_a^b r K_1(\lambda r) dr d\lambda \hat{\boldsymbol{\phi}}. \quad (65)$$

The magnetic field strength  $\mathbf{H}$  is given by the curl of vector potential  $\boldsymbol{\psi}$ . In cylindrical coordinates, the axial component of the applied field is given by

$$H_z(r, z) = (\nabla \times \boldsymbol{\psi}(r, z)) \cdot \hat{\mathbf{z}} = \frac{1}{r} \frac{d}{dr} (r\psi(r, z)) \quad (66)$$

$$= \frac{v_0}{R} \frac{2\mu_0 N}{\pi l(b-a)} \int_0^\infty \cos(\lambda z) \sin\left(\frac{\lambda l}{2}\right) I_0(\lambda r) \int_a^b r K_1(\lambda r) dr d\lambda. \quad (67)$$

The largest value of  $H_z$  will occur at the center of the coil, and therefore, is given as

$$H_z(0,0) = \frac{v_0}{R} \frac{2\mu_0 n}{\pi} \int_0^\infty \sin\left(\frac{\lambda l}{2}\right) \int_a^b r K_1(\lambda r) dr d\lambda. \quad (68)$$

For the tandem probe (Table 5), the maximum field strength is calculated to be

$$H_z(0,0) \cong 2.82 \cdot 10^{-4} \text{ A} \cdot \text{m}^{-1}, \quad (69)$$

and, for the encircling probe (Table 6), is

$$H_z(0,0) \cong 2.86 \cdot 10^{-3} \text{ A} \cdot \text{m}^{-1}. \quad (70)$$

These values are well within the Rayleigh regime described by Bozorth.

In what follows, an experiment is performed to confirm the validity of the linear permeability assumption. Mathematical expressions, developed in Chapter 4, describe the functional dependence between the area under a transient pickup signal and the magnetic permeability of the specimen. Thus, the magnitude of difference between the area under the leading edge signal and the area under the trailing edge signal will be indicative of the amount of hysteresis. Infusion and effusion eddy current signals, generated by the leading and trailing edges of a square wave excitation, are obtained for the case of ferromagnetic tubes and plotted in Figure 18 on the next page.

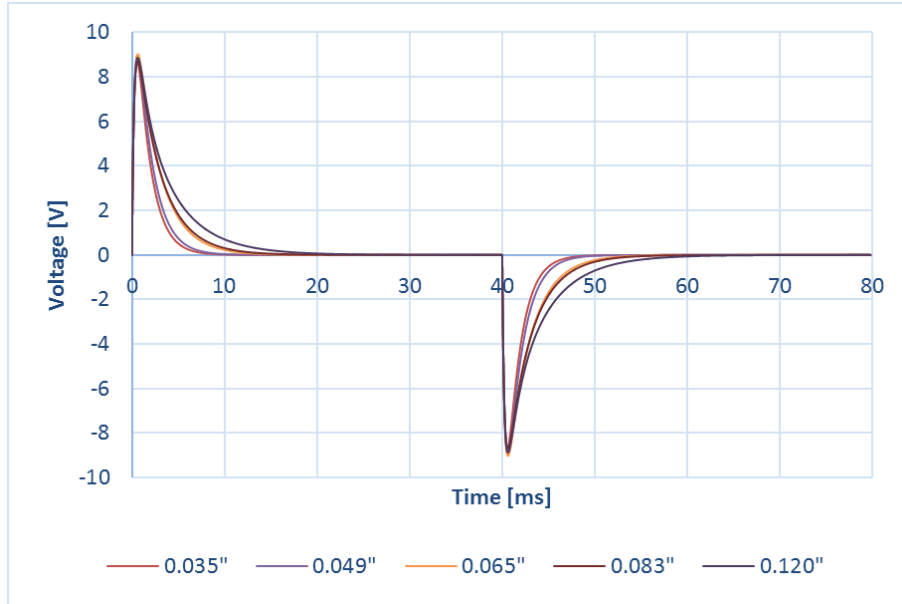


Figure 18: Transient responses to the leading and trailing edges of a square wave excitation.

The areas under the pickup signals shown in Figure 18 are listed in Table 9.

Table 9: Areas under the transient leading and trailing edge signals shown in Figure 18.

Steel tube thickness:	0.89 mm (0.035 in)	1.24 mm (0.049 in)	1.65 mm (0.065 in)	2.11 mm (0.083 in)	3.05 mm (0.120 in)
Area under leading edge:	18.94	21.41	28.72	29.18	36.08
Area under trailing edge:	-18.90	-21.37	-28.66	-29.13	-36.01
% difference:	0.20%	0.17%	0.19%	0.20%	0.18%

The signal areas, between the leading and trailing edge regimes, all differ by approximately 0.2%. Thus, the effects of hysteresis are negligible and, therefore, the specimen's permeability can be assumed to be constant.

In a second experiment, the areas under transient pickup signals are measured for different applied voltages. Mathematical expressions, developed in Chapter 4, suggest that transient signals are proportional to the amplitude of the applied voltage step,  $v_0$ . The expressions are only valid,

however, if the relationship between  $\mathbf{B}$  and  $\mathbf{H}$  is linear. A plot of transient signal areas as a function of applied voltage is shown in Figure 19.

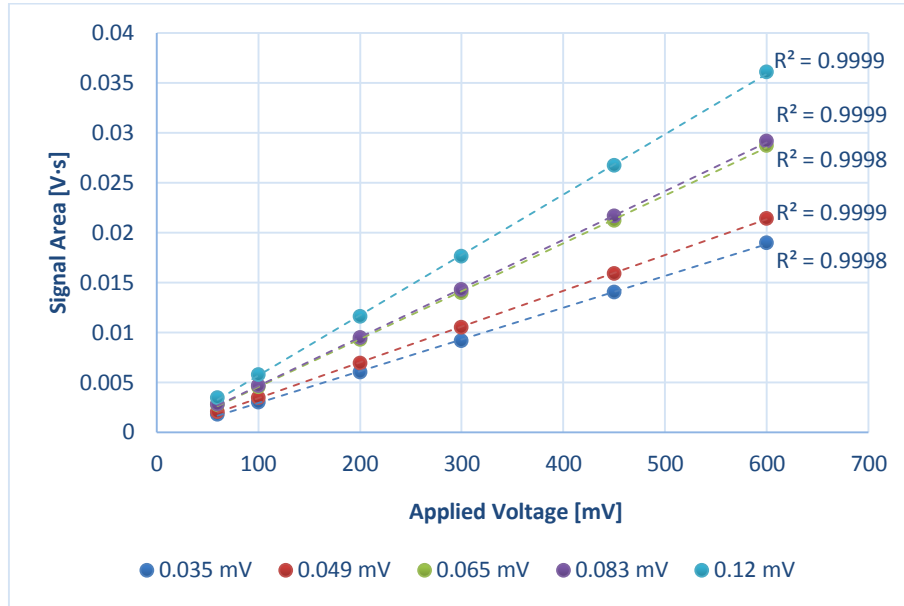


Figure 19: Areas under transient response signals for various tubes at various input voltages.

The areas under the ferromagnetic tube signals are observed to scale linearly with the applied voltage,  $v_0$ , in support of the linear permeability assumption. It is clear that the materials considered in this thesis are operating in the linear permeability regime.

### 3.5. Experimental results

This section discusses the post-processing and formatting of experimental results. Good pulsing system design and probe quality contribute to the data's excellent signal-to-noise ratio. Additionally, twenty signal waveforms are recorded and averaged for each experiment. Noise levels are significantly low - 0.4 mV approx. in a typical pickup signal with a peak value of 3 V as shown in Figure 20 - negating the requirement for any additional filtering or averaging. Two examples of

measured transient pickup signals, acquired in air and in the presence of a brass tube, are plotted in Figure 20.

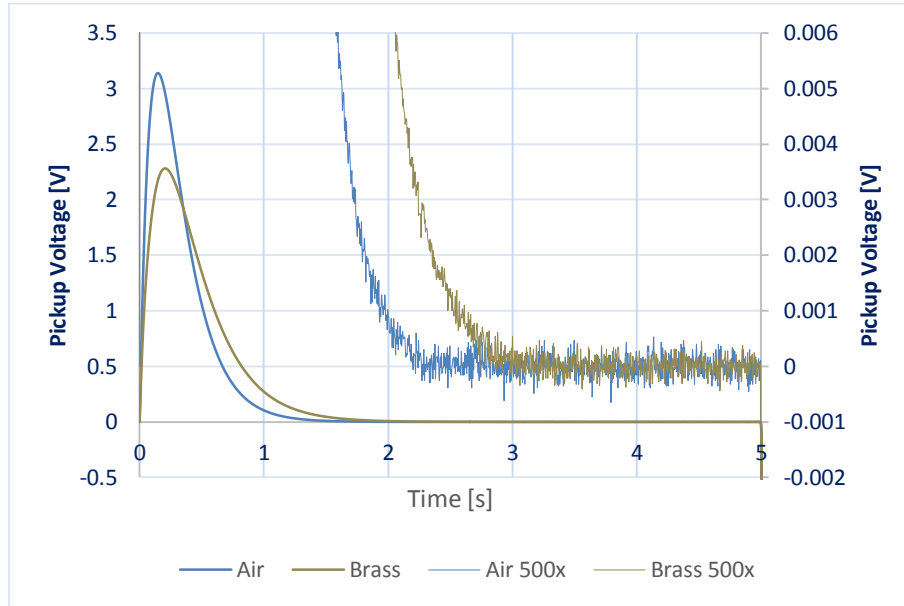


Figure 20: Air (blue) and brass tube (orange) pickup signals; 1x (left axis) and 500x (right axis) zoom.

Signals are observed to be sampled at sufficiently small time intervals, so as to produce an accurate signal representation, and to contain very little electronic noise ( $\approx 0.5$  mV as seen in Figure 20). Measurement error bars are too small to depict.

In order to validate the analytical circuit models, voltage signals are converted, in accordance with Ohm's Law  $V = IR$ , to yield the transient currents flowing in the driver and pickup circuits. For example, a voltage signal, sensed by the pickup coil in the circuit described in Figure 11 (b), would be divided by  $53.4 \Omega$  (two  $26.7 \Omega$  resistors in series). Additionally, the signal must also be divided by the system gain (145 as listed in Table 4). The transient current is plotted as a solid line, with vertical and horizontal axes displaying units of milliamps and milliseconds, respectively, as shown in Figure 21.

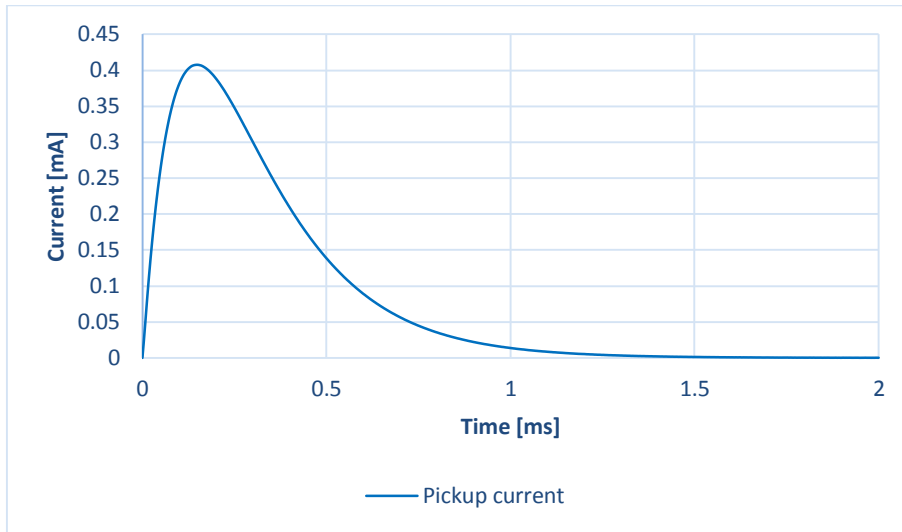


Figure 21: Formatted experimental data.

Later, in Chapter 4, theoretical predictions will be plotted, using circle symbols, alongside the experimental data in order to validate the analytical models, an example of which is shown in Figure 22.

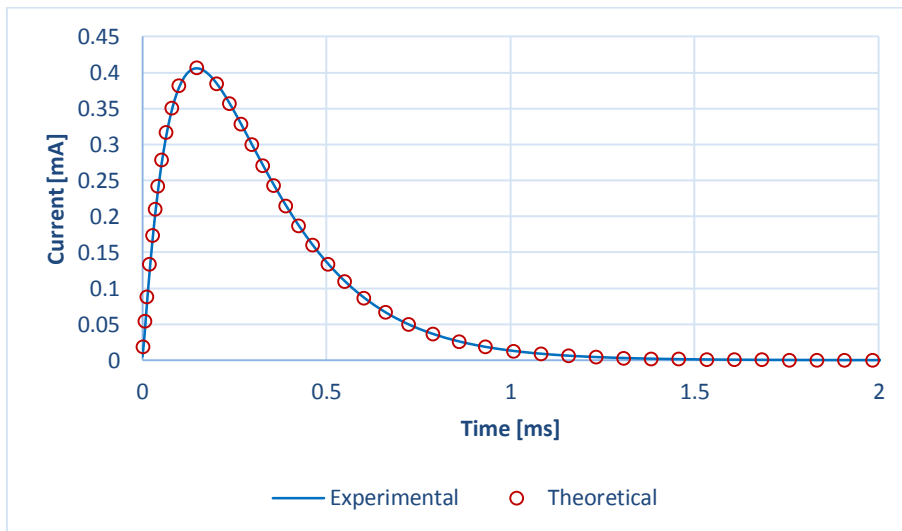


Figure 22: Experimental and theoretical results; graphical overlay format.

The following chapters contain the manuscripts, upon which these basic considerations have been built.

## CHAPTER 4 – MANUSCRIPTS

**Manuscript 1:** “Concerning the derivation of exact solutions to inductive circuit problems for eddy current testing”. NDT&E Intl. Accepted 30 Jul 2014.

NB: As noted by Dr. Theodoulidis, the double integral expression for the self-inductance of a coil in air given in equation (28) can be simplified using the following integral identity:

$$\int_0^{\infty} \frac{\sin^2(ax) dx}{x^2(b^2 + x^2)} = \frac{\pi}{4b^2} \left[ 2a - \frac{1}{b} (1 - e^{-2ab}) \right] \quad [a > 0, b > 0] \quad (71)$$

NB: As noted by Dr. Morelli, the magnetic vector potential in an axisymmetric system (a circular coaxial coil encircling a rod for example) has only one vector component (the  $\hat{\phi}$  component) and the field can, thus, be considered as scalar in nature. This is true for all axisymmetric systems.

# Concerning the derivation of exact solutions to inductive circuit problems for eddy current testing

D.R. Desjardins<sup>1</sup>, T.W. Krause<sup>2</sup>, A.Tetervak and L. Clapham<sup>1</sup>

*1. Department of Physics, Queen's University, Kingston, ON, Canada, K7L 3N6*

*2. Department of Physics, Royal Military College of Canada, Kingston, ON, Canada, K7K 7B4*

**Abstract** – A novel strategy, which enables the derivation of exact solutions describing all electromagnetic interactions arising in inductively coupled circuits, is developed. Differential circuit equations are formulated in terms of the magnetic fields arising in inductive systems, using Faraday's law and convolution, and solved using the Fourier transform. The approach is valid for systems containing any number of driving and receiving coils, and may be extended to include nearby conducting and ferromagnetic structures. Furthermore, arbitrary excitation waveforms, such as a sinusoid or a square wave for applications in conventional and transient eddy current, respectively, may be considered. In this first work, the general theory is presented and subsequently applied to the simple case of a coaxial driver and receiver coil configuration. Theoretical expressions for the self- and mutual inductance coefficients are shown to fall out of the theory naturally. Experimental results, obtained for a square wave function excitation, are found to be in excellent agreement with the analytical predictions.

**Key Words**– Transient Eddy Current, Inductive Coils, Mutual Inductance

## I. Introduction

Eddy current non-destructive testing (NDT) is one of several technologies making use of the precise generation and measurement of magnetic fields. Mathematical models describing the transient electromagnetic interactions, which arise between field generating and sensing coils in close proximity to conducting structures, enable the determination of these structures' geometrical and material characteristics. This capability is critically important to the aeronautical, nuclear and petrochemical industries for example [1], which monitor the structural health of their physical assets for economic and safety reasons. Research in eddy current theory had already begun by 1921 when Wwedensky [2] calculated the diffusion of magnetic fields impressed upon rigid conducting cylinders. Later, the pioneering work of Dodd and Deeds [3] in the late 1960's had led to the formulation of solutions to harmonic induction problems using a magnetic vector potential formalism. More recently, theoretical work has been performed by Morozova [4], Fan [5], Bowler [6]-[8], Theodoulidis [9][10] and many others [11]-[10] with the aim of modeling induced voltages or coil impedance changes for applications in NDT. A persistent challenge to the development of driver-pickup models, however, has been a lack of agreement with experimental results in cases where magnetic structures, which exhibit strong feedback effects, are considered. This is quite inopportune since steel, and many other materials commonly encountered in industry, are ferromagnetic. Furthermore, the additional magnetic flux, generated by the magnetization of such structures, enhances the induced eddy current densities [11]. These incentives provide the motivation for the development of exact mathematical models, which would facilitate the quantitative analysis and interpretation of experimental signals.

This work is the first to incorporate electromagnetic field solutions directly into Kirchoff's circuit equations. The strategy yields exact expressions that describe all the electromagnetic

interactions arising in inductively coupled systems. Thus, feedback effects, which have historically posed a challenge to the development of transient eddy current models, are completely addressed. In this work, the methodology for solutions to general eddy current problems is developed in full, but only applied to the simpler case of a coaxial driver and pickup coil configuration. Initial validation of the theory in this simple case demonstrates the effectiveness of the methodology. In subsequent works, the theory will be applied to inductive circuit problems containing ferromagnetic conducting structures, such as half-spaces, plates, rods and tubes. Thus, in a series of works that will follow, the complexity and number of variables considered will be iteratively increased along with more general validation of the theory and exploration of its potential applications.

In the simpler case, where no conducting structure is present, electromagnetic interactions arise solely from the inductive coupling of the coils. To this end, solutions to two-coil inductive circuit problems have already been obtained [16] in the traditional manner; differential circuit equations are formulated in terms of constant coefficients  $L$  and  $M$ , the self- and mutual inductance coefficients, respectively. However, the manner in which  $L$  and  $M$  come to appear in these equations, although understood, is not explicitly shown. In what follows, the circuit equations are formulated from first principles using Faraday's law and convolution theory [50]. In doing so, the correct solutions, which describe the transient currents flowing in the coupled driver and pickup circuits, are achieved and validated experimentally. More importantly, expressions for  $L$  and  $M$  are shown to fall out of the theory naturally. This work is in preparation for subsequent addition of other inductive elements. In particular, it will be shown in future work that additional inductance effects, associated with the presence of ferromagnetic conducting structures, emerge from the theory.

## II. Theoretical Development

In consideration of what follows, a circular pickup coil is centered about the axis of a larger encircling driver coil. In accordance with Maxwell's equations, a time-varying current flowing in the driver coil will induce a current in the pickup. The current induced in the pickup gives rise to a transient magnetic field, which, in turn, generates an opposing current within the driver coil. The circuit equations describing the resultant time-dependent currents  $i_1$  and  $i_2$  flowing in the driver and pickup coils, respectively, are written using Kirchhoff's laws in the following general form

$$R_1 i_1(t) = v(t) + \varepsilon_1(t) \quad (1)$$

$$R_2 i_2(t) = \varepsilon_2(t), \quad (2)$$

where  $v$  is any time-dependent excitation voltage - step, harmonic, multi-frequency, ramp, saw-tooth, etc. -  $R_1$  and  $R_2$  are the total circuit resistances, and  $\varepsilon_1$  and  $\varepsilon_2$  are the total time-dependent voltages induced in the driver and pickup coils, respectively. Both  $\varepsilon_1$  and  $\varepsilon_2$  have three components; one arising from the field generated by the driver coil, another from the field generated by the receiver coil and the third from transient eddy current fields emanating from a conducting sample when present. A challenge in the development of analytical transient eddy current models has been the inability to formulate expressions for these feedback terms.

In what follows, induced voltages  $\varepsilon_1$  and  $\varepsilon_2$  are expressed in terms of the unknown current functions  $i_1$  and  $i_2$  using convolution integrals, and substituted back into the circuit equations. Beginning with Faraday's law, a voltage  $\varepsilon$  is induced within a current loop,  $C$ , and is proportional to the time-derivative of the magnetic flux normal to the area,  $S$ , enclosed by that loop such that [18]

$$\varepsilon(t) = -\frac{d}{dt} \oiint_S \mathbf{B}(r, z, t) \cdot d\mathbf{S}, \quad (3)$$

where  $d\mathbf{S}$  is the differential surface element. A magnetic vector potential formalism is adopted in order to take advantage of the circular (azimuthal) symmetry of the problem. The magnetic flux density  $\mathbf{B}$  is written as the curl of  $\mathbf{A}$ , and in accordance with Stokes' Theorem, the surface integral is recast into a contour integral. Finally,  $\mathbf{A}$  contains only an azimuthal vector component and is symmetric about the axis. Thus, the voltage induced within a current loop due to a time-varying vector potential is expressed as

$$\varepsilon(t) = -\frac{d}{dt} \oint_S (\nabla \times \mathbf{A}(r, z, t)) \cdot d\mathbf{S} = -\frac{d}{dt} \oint_C \mathbf{A}(r, z, t) \cdot d\mathbf{l} = -2\pi r \frac{d}{dt} A(r, z, t). \quad (4)$$

For a circular multi-turn coil with a rectangular cross-section, the current loop expression in (4) is integrated over the cross-sectional area of the coil,  $\Sigma$ , and multiplied by a turn density so that

$$\varepsilon(t) = -\frac{2\pi N}{l(b-a)} \frac{d}{dt} \iint_{\Sigma} r A(r, z, t) dr dz, \quad (5)$$

where  $N$  is the number of turns,  $l$  is the coil length,  $a$  and  $b$  are the inner and outer coil radii, respectively. The time-dependence of the magnetic vector potential  $A$  is not explicitly known. It can, however, be expressed as the convolution of the system's unit impulse response [50] with a yet unknown time-dependent current function such that

$$A(r, z, t) = \hat{A}(r, z, t) * i(t) \equiv \int_0^t \hat{A}(r, z, t - \tau) i(\tau) d\tau, \quad (6)$$

where  $\hat{A}$  is the system's unit impulse response and  $A$  is the actual system response resulting from the onset of the time-dependent current  $i$ . Thus,  $A$  inherits the time-dependence and relative magnitude of  $i$ , as expected. In an inductive system composed of  $m$  coils, there are  $m$  unit impulse response solutions, associated with their respective current functions, existing in superposition. The straightforward generalization of (6), which describes the total magnetic vector potential  $A$  in a multi-coil system, is

$$A(r, z, t) = \hat{A}_{\langle 1 \rangle}(r, z, t) * i_1(t) + \hat{A}_{\langle 2 \rangle}(r, z, t) * i_2(t) + \dots + \hat{A}_{\langle m \rangle}(r, z, t) * i_m(t), \quad (7)$$

where the number in the subscript angle-brackets  $\langle \ \rangle$  specifies the coil from which the potential arises. Equation (7) is substituted into (5) and the total time-dependent voltage induced in the  $k^{\text{th}}$  coil of a system of  $m$  coils, now expressed in terms of the unknown current functions, may be written as

$$\varepsilon_k(t) = -\frac{2\pi N_k}{l_k(b_k - a_k)} \frac{d}{dt} \oint\!\!\!\oint^{[k]} r(\hat{A}_{\langle 1 \rangle} * i_1 + \hat{A}_{\langle 2 \rangle} * i_2 + \dots + \hat{A}_{\langle m \rangle} * i_m) dr dz, \quad (8)$$

where the number in the superscript square-brackets  $[ \ ]$  specifies the coil over which the cross-sectional surface integral is performed. Additionally, these unit impulse responses can be decomposed into component contributions; contributions from the field generated solely by the coils, denoted  $\hat{\psi}$ , and contributions from eddy current fields (in anticipation of the development of general solutions), denoted  $\hat{\Xi}$ , arising from the presence of a conducting sample such that

$$\hat{A}_{\langle k \rangle}(r, z, t) = \hat{\psi}_{\langle k \rangle}(r, z, t) + \hat{\Xi}_{\langle k \rangle}(r, z, t). \quad (9)$$

Equation (8) is the generalized mathematical formulation of the voltages induced in a multi-coil system, which may also include conducting samples. Unable to calculate the driver signal directly, previous authors have resorted to convoluting the impulse response with an experimentally measured driver signal, in order to calculate a pickup coil's response [10][11]. This semi-analytical approach fails to consider the interaction between the pickup coil and the sample, which hinders agreement with experimental results, particularly at early times. The strategy employed in this work, however, is to substitute equation (8) back into the circuit equations, which are then solved for unknown current functions  $i_1$  and  $i_2$ . This simple manipulation enables the formulation of complete solutions for the transient responses of driver and pickup coils, negating the requirement of experimental input. In this work, solutions arising from the application of this strategy are validated

for a simple driver-pickup system in air. Future works will consider increasingly complex systems, including nearby conductors and different coil configurations.

In a two-coil inductive system, in the absence of a conducting structure,  $\hat{\mathbf{E}}_{(k)} = \mathbf{0}$  and so the impulse response,  $\hat{A}_{(k)}$ , due to the  $k^{\text{th}}$  coil is simply the unit impulse coil field,  $\hat{\psi}_{(k)}$ . Therefore, induced voltages  $\varepsilon_1$  and  $\varepsilon_2$  in circuit equations (1) and (2) may be expressed as

$$\varepsilon_1(t) = -\frac{2\pi N_1}{l_1(b_1 - a_1)} \frac{d}{dt} \iint^{[1]} r \left( \hat{\psi}_{(1)}(r, z, t) * i_1(t) + \hat{\psi}_{(2)}(r, z, t) * i_2(t) \right) dr dz, \quad (10)$$

$$\varepsilon_2(t) = -\frac{2\pi N_2}{l_2(b_2 - a_2)} \frac{d}{dt} \iint^{[2]} r \left( \hat{\psi}_{(1)}(r, z, t) * i_1(t) + \hat{\psi}_{(2)}(r, z, t) * i_2(t) \right) dr dz. \quad (11)$$

The magnetic vector potential generated by a coil following a unit impulse excitation is developed in what follows. Poisson's equation [18] for an infinitesimal current loop of radius  $r$  located on the plane  $z = \mathfrak{z}$  carrying a unit impulse current  $i = \delta(t)$  is expressed as

$$\nabla^2 \hat{\psi}(r, z, t) = -\mu_0 \delta(r - r) \delta(z - \mathfrak{z}) \delta(t), \quad (12)$$

where  $\delta(t)$  is a Dirac delta function [50]. The vector Laplacian is recast into its differential operator form for the appropriate cylindrical geometry where

$$\left( \frac{\partial^2}{\partial r^2} + \frac{1}{r} \frac{\partial}{\partial r} - \frac{1}{r^2} + \frac{\partial^2}{\partial z^2} \right) \hat{\psi}(r, z, t) = -\mu_0 \delta(r - r) \delta(z - \mathfrak{z}) \delta(t). \quad (13)$$

Since the field is symmetric in  $\phi$  and about the plane  $z = \mathfrak{z}$ , a first-order Hankel transform [19] with parameter  $\gamma$  separates the radial coordinate  $r$  and a Fourier cosine integral transform [19] with parameter  $\lambda$  separates the axial coordinate  $z$  such that equation (13) becomes

$$(-\gamma^2 - \lambda^2) \hat{\psi}(\gamma, \lambda, t) = -\mu_0 r J_1(\gamma r) \cos(\lambda \mathfrak{z}) \delta(t). \quad (14)$$

The transformed solution is isolated as

$$\hat{\psi}(\gamma, \lambda, t) = \mu_0 \frac{r J_1(\gamma r) \cos(\lambda z)}{\gamma^2 + \lambda^2} \delta(t). \quad (15)$$

The inverse Hankel and cosine integral transforms of (15) are taken, and the resulting expression describes the magnetic vector potential generated by a single circular loop carrying a unitary current impulse such that

$$\hat{\psi}(r, z, t) = \frac{\mu_0}{\pi} \int_0^\infty \int_0^\infty \gamma J_1(\gamma r) \cos(\lambda z) \frac{r J_1(\gamma r) \cos(\lambda z)}{\gamma^2 + \lambda^2} d\gamma d\lambda \delta(t). \quad (16)$$

The single loop solution is integrated over the physical dimensions of an arbitrarily-sized coil and multiplied by a cross-sectional coil-turn density. The height  $z$  of the plane containing the loop must be integrated about the origin in order to preserve the problem's symmetry, thereby retaining the validity of the Fourier cosine transform. Thus, (16) is integrated from  $z = -\frac{l}{2}$  to  $\frac{l}{2}$  and from  $r = a$  to  $r = b$  giving

$$\hat{\psi}(r, z, t) = \frac{2\mu_0 n}{\pi} \int_0^\infty \int_0^\infty \gamma J_1(\gamma r) \cos(\lambda z) \frac{\int_a^b r J_1(\gamma r) dr \sin\left(\frac{\lambda l}{2}\right)}{\lambda(\gamma^2 + \lambda^2)} d\gamma d\lambda \delta(t), \quad (17)$$

where  $l$  is the coil length,  $a$  and  $b$  are the inner and outer radii,  $n \equiv \frac{N}{l(b-a)}$  is the turn density and  $\delta(t)$  is the current impulse [50]. This double integral solution is convergent for all  $r$  and  $z$ , even within the boundaries of the coil itself. However, one of the inverse transforms can be carried out in order to simplify the solution. This simplification leads to restrictions on the resulting solutions' regions of convergence, however.

In order to solve a boundary value problem, equation (17) would be matched at a material interface. The inverse Hankel transform of (17) could be carried out to yield

$$\hat{\psi}(r, z, t) = \frac{2\mu_0 n}{\pi} \int_0^\infty \frac{\cos(\lambda z) \sin\left(\frac{\lambda l}{2}\right)}{\lambda} \left\{ \begin{array}{l} I_1(\lambda r) \int_a^b r K_1(\lambda r) dr \quad r \leq a \\ K_1(\lambda r) \int_a^b r I_1(\lambda r) dr \quad r \geq b \end{array} \right\} d\lambda \delta(t). \quad (18)$$

Equation (18) is valid in the region  $z = ]-\infty, \infty[$  and  $r = [0, a] \cup [b, \infty[$  and is, therefore, suitable for solving boundary value problems with vertical interfaces, as in the case of a rod or a tube extending in  $z$  for instance.

If, however, the boundary value problem of interest has a horizontal boundary - a horizontal plate, which extends in  $r$  for instance - the inverse Fourier cosine transform in (17) would be carried out to yield

$$\hat{\psi}(r, z, t) = \frac{\mu_0 n}{2} \int_0^\infty I_1(\gamma r) \frac{\int_a^b r J_1(\gamma r) dr}{\gamma} \left( e^{\frac{\gamma l}{2}} - e^{-\frac{\gamma l}{2}} \right) \left\{ \begin{array}{l} e^{-\gamma z} \quad z \geq l/2 \\ e^{\gamma z} \quad z \leq -l/2 \end{array} \right\} d\gamma \delta(t), \quad (19)$$

which is valid for the region  $r = ]-\infty, \infty[$  and  $z = ]-\infty, -\frac{l}{2}] \cup [\frac{l}{2}, \infty[$ .

The expressions in (10) and (11) for the induced voltages are substituted into circuit equations (1) and (2). A non-unitary Fourier transform, defined as  $\mathcal{F}\{f(t)\} \equiv \int_{-\infty}^\infty f(t) e^{-j\omega t} dt$  with angular frequency  $\omega$ , is applied in order to separate the  $t$  coordinate and the circuit equations become

$$R_1 I_1(\omega) = V(\omega) - j\omega 2\pi n_1 \iint^{[1]} r \left( \hat{\psi}_{(1)}(r, z) I_1(\omega) + \hat{\psi}_{(2)}(r, z) I_2(\omega) \right) dr dz, \quad (20)$$

$$R_2 I_2(\omega) = -j\omega 2\pi n_2 \iint^{[2]} r \left( \hat{\psi}_{(1)}(r, z) I_1(\omega) + \hat{\psi}_{(2)}(r, z) I_2(\omega) \right) dr dz, \quad (21)$$

where  $I(\omega)$  and  $V(\omega)$  are the Fourier transforms of the current function  $i(t)$ . Since the Fourier transform of a convolution is simply the product of the transforms [19],  $I_1$  and  $I_2$  can now be removed from the cross-sectional integrals so that

$$R_1 I_1(\omega) = V(\omega) - j\omega 2\pi n_1 \left( \oint\!\!\!\oint^{[1]} r \hat{\psi}_{(1)}(r, z) dr dz \cdot I_1(\omega) + \oint\!\!\!\oint^{[1]} r \hat{\psi}_{(2)}(r, z) dr dz \cdot I_2(\omega) \right), \quad (22)$$

$$R_2 I_2(\omega) = -j\omega 2\pi n_2 \left( \oint\!\!\!\oint^{[2]} r \hat{\psi}_{(1)}(r, z) dr dz \cdot I_1(\omega) + \oint\!\!\!\oint^{[2]} r \hat{\psi}_{(2)}(r, z) dr dz \cdot I_2(\omega) \right). \quad (23)$$

In anticipation of the final result, the following coefficients are defined:

$$L_1 \equiv 2\pi n_1 \oint\!\!\!\oint^{[1]} r \hat{\psi}_{(1)}(r, z) dr dz, \quad (24)$$

$$M_{12} \equiv 2\pi n_1 \oint\!\!\!\oint^{[1]} r \hat{\psi}_{(2)}(r, z) dr dz, \quad (25)$$

$$L_2 \equiv 2\pi n_2 \oint\!\!\!\oint^{[2]} r \hat{\psi}_{(2)}(r, z) dr dz, \quad (26)$$

$$M_{21} \equiv 2\pi n_2 \oint\!\!\!\oint^{[2]} r \hat{\psi}_{(1)}(r, z) dr dz. \quad (27)$$

The time dependence of  $\hat{\psi}_{(1)}$  and  $\hat{\psi}_{(2)}$  is a Dirac impulse whose Fourier transform is  $\mathcal{F}\{\delta(t)\} = 1$ , thus, the cross-sectional integrals yield constant coefficients. It will be shown that these constants correspond to the self- and mutual inductance coefficients.

Equation (24) requires that the static vector potential  $\psi_{(1)}$ , which arises from the driver coil, be integrated over the cross-section of the driver coil itself. Solution (17) applies, since it converges within the coil's own domain. Substitution of (17) into (24) and (26) yields

$$L_1 = 8\mu_0 n_1^2 \int_0^\infty \int_0^\infty \frac{\left( \int_{a_1}^{b_1} r I_1(\gamma r) dr \right)^2 \sin^2\left(\frac{\lambda l_1}{2}\right)}{\lambda^2(\gamma^2 + \lambda^2)} d\gamma d\lambda, \quad (28)$$

and

$$L_2 = 8\mu_0 n_2^2 \int_0^\infty \int_0^\infty \frac{\left( \int_{a_2}^{b_2} r I_1(\lambda r) dr \right)^2 \sin^2\left(\frac{\lambda l_2}{2}\right)}{\lambda^2(\gamma^2 + \lambda^2)} d\gamma d\lambda. \quad (29)$$

One of the simplified solutions, (18) or (19), may be substituted into equations (25) and (27) depending on the relative geometry, or overlap, of the coils. In the problem at hand, the coils are located about the same axis and their centers are separated by a distance  $d$  along that axis as shown in Figure 23 below.

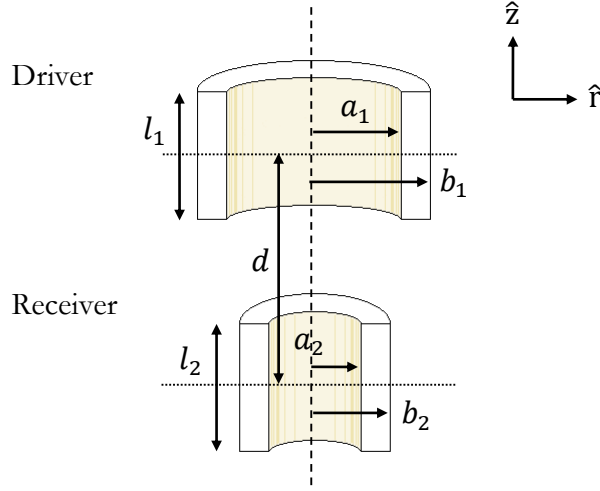


Figure 23: Coaxial coil configuration with coil dimensions.

There is no radial overlap since the inner radius of the driver lies beyond the outer radius of the pickup. Therefore, solution (18) for  $r \geq b$  is substituted into the equation for  $M_{12}$  so that

$$M_{12} = 2\pi n_1 \oint \int^{[1]} r \left( \frac{2\mu_0 n_2}{\pi} \int_0^\infty \frac{\cos(\lambda z) \sin\left(\frac{\lambda l_2}{2}\right)}{\lambda} K_1(\lambda r) \int_{a_2}^{b_2} r I_1(\lambda r) dr d\lambda \right) dr dz. \quad (30)$$

The cross-section integral in (30) is performed for  $z = d - \frac{l_1}{2}$  to  $z = d + \frac{l_1}{2}$  and for  $r = a_1$  to  $r = b_2$  and the resulting expression is

$$M_{12} = 8\mu_0 n_1 n_2 \int_0^\infty \cos(\lambda d) \frac{\sin\left(\frac{\lambda l_1}{2}\right) \sin\left(\frac{\lambda l_2}{2}\right)}{\lambda^2} \int_{a_1}^{b_1} r K_1(\lambda r) dr \int_{a_2}^{b_2} r I_1(\lambda r) dr d\lambda. \quad (31)$$

Proceeding in the same manner, the expression for  $M_{21}$ , fourth equation in (24), is evaluated as

$$M_{21} = 8\mu_0 n_1 n_2 \int_0^\infty \cos(\lambda d) \frac{\sin\left(\frac{\lambda l_2}{2}\right) \sin\left(\frac{\lambda l_1}{2}\right)}{\lambda^2} \int_{a_2}^{b_2} r I_1(\lambda r) dr \int_{a_1}^{b_1} r K_1(\lambda r) dr d\lambda. \quad (32)$$

Expressions (31) and (32) are exactly equivalent, as expected since the mutual inductance coefficient  $M$  is defined as

$$M \equiv M_{21} = M_{12}. \quad (33)$$

This integral expression for the mutual induction coefficient, of course, has been known for a long time [20].

Using the definitions in equations (24)-(27), which have arisen naturally from the theory, the Fourier transformed circuit equations in (22) and (23) are written as

$$R_1 I_1(\omega) = V(\omega) - j\omega L_1 I_1(\omega) - j\omega M I_2(\omega), \quad (34)$$

$$R_2 I_2(\omega) = -j\omega M I_1(\omega) - j\omega L_2 I_2(\omega), \quad (35)$$

with solutions

$$I_1(\omega) = \frac{(R_2 + j\omega L_2)V(\omega)}{(R_1 + j\omega L_1)(R_2 + j\omega L_2) + \omega^2 M^2}, \quad (36)$$

$$I_2(\omega) = -\frac{j\omega M V(\omega)}{(R_1 + j\omega L_1)(R_2 + j\omega L_2) + \omega^2 M^2}. \quad (37)$$

The time-domain solutions are obtained by applying the appropriate inverse Fourier transform, defined as  $\mathcal{F}^{-1}\{F(\omega)\} \equiv \frac{1}{2\pi} \int_{-\infty}^{\infty} F(\omega) e^{j\omega t} d\omega$ , to equations (36) and (37) such that

$$i_1(t) = \frac{1}{2\pi} \int_{-\infty}^{\infty} \frac{(R_2 + j\omega L_2)V(\omega)}{(R_1 + j\omega L_1)(R_2 + j\omega L_2) + \omega^2 M^2} e^{j\omega t} d\omega, \quad (38)$$

$$i_2(t) = -\frac{1}{2\pi} \int_{-\infty}^{\infty} \frac{j\omega M_{21} V(\omega)}{(R_1 + j\omega L_1)(R_2 + j\omega L_2) + \omega^2 M^2} e^{j\omega t} d\omega, \quad (39)$$

where  $V(\omega)$  is the Fourier transform of the arbitrary time-dependent excitation function  $v(t)$ . Suppose a step function is chosen for pulsed eddy current applications. Then  $v(t) = v_0 u(t)$ , where  $u(t)$  is a Heaviside function and  $v_0$  is the amplitude of the voltage step. Its Fourier transform is [21]

$$V(\omega) = v_0 \left( \pi \delta(\omega) + \frac{1}{j\omega} \right). \quad (40)$$

Equation (40) is substituted into (38) and (39) and the inverse transforms are evaluated analytically in closed form as

$$i_1(t) = \frac{v_0}{R_1} \left( 1 - \frac{(e^{-\alpha t} + e^{-\beta t})}{2} + \frac{(L_1 R_2 - L_2 R_1)(e^{-\alpha t} - e^{-\beta t})}{2(\alpha - \beta)(L_1 L_2 - M^2)} \right), \quad (41)$$

$$i_2(t) = \frac{v_0 M (e^{-\alpha t} - e^{-\beta t})}{(\alpha - \beta)(L_1 L_2 - M^2)}, \quad (42)$$

where

$$\alpha \equiv \frac{(L_1 R_2 + L_2 R_1) + \sqrt{(L_1 R_2 + L_2 R_1)^2 - 4R_1 R_2 (L_1 L_2 - M^2)}}{2(L_1 L_2 - M^2)}, \quad (43)$$

$$\beta \equiv \frac{(L_1 R_2 + L_2 R_1) - \sqrt{(L_1 R_2 + L_2 R_1)^2 - 4R_1 R_2 (L_1 L_2 - M^2)}}{2(L_1 L_2 - M^2)}, \quad (44)$$

consistent with solutions reported in the literature [16].

Alternatively, if a sinusoidal function is assumed as in the case of applications in conventional eddy current, then  $v(t) = v_0 \sin(\omega t)$ , where  $v_0$  is the amplitude of a sinusoid with angular frequency  $\omega$ . Its Fourier transform is [21]

$$V(\omega) = -j\pi v_0 (\delta(\omega - \omega) - \delta(\omega + \omega)). \quad (45)$$

Equation (45) is substituted into (38) and (39) and the inverse transforms are evaluated in closed form as

$$i_1(t) = v_0 \sqrt{\omega^2 L_2^2 + R_2^2} \frac{\sin\left(\omega t - \arctan\left(\omega \frac{L_1 R_2^2 + \omega^2 L_2 (L_1 L_2 - M^2)}{R_1 R_2^2 + \omega^2 (R_1 L_2^2 + M^2 R_2)}\right)\right)}{\sqrt{(R_1 R_2 - \omega^2 (L_1 L_2 - M^2))^2 + \omega^2 (L_1 R_2 + L_2 R_1)^2}}, \quad (46)$$

$$i_2(t) = -v_0 \omega M \frac{\sin\left(\omega t - \arctan\left(\frac{\omega^2 (L_1 L_2 - M^2) - R_1 R_2}{\omega (L_1 R_2 + L_2 R_1)}\right)\right)}{\sqrt{(R_1 R_2 - \omega^2 (L_1 L_2 - M^2))^2 + \omega^2 (L_1 R_2 + L_2 R_1)^2}}. \quad (47)$$

Furthermore, any Fourier series representation of a time-dependent excitation waveform  $v(t)$  may be selected and substituted into solutions (38) and (39). The Fourier transform of a Fourier series produces a weighted sum of Dirac delta functions, which replaces the integral with a readily computable summation via the sampling theorem [50]. Therefore, the pickup response to an arbitrary waveform excitation may be constructed as a superposition of the solution in (47).

In what follows, solutions (41) and (42), which describe the transient currents flowing through the driver and pickup circuits, respectively, are validated by experiment.

### III. Experimental Results

A power supply with an internal resistance of 2.46  $\Omega$  generates a 4.53 V square pulse excitation. Coaxial cables with negligible losses rout the pulse through a 2.00  $\Omega$  resistor to a 80.8  $\Omega$  driving coil. A 47.6  $\Omega$  pickup coil is connected in series with a 50.0  $\Omega$  termination resistor and to a National Instruments signal acquisition card (NI6211 USB DAQ board). Transient voltages are measured and recorded across the 2.00  $\Omega$  and 50.0  $\Omega$  resistors in the driver and receiver circuits, respectively. The transient currents flowing through the circuits are related to the experimentally measured voltages in accordance with Ohm's Law (i.e.  $i_{1,\text{exp}} = v_{1,\text{exp}}/2.00\Omega$  and  $i_{2,\text{exp}} = v_{2,\text{exp}}/50.0\Omega$ ). The inductively coupled circuit is depicted in Figure 24,

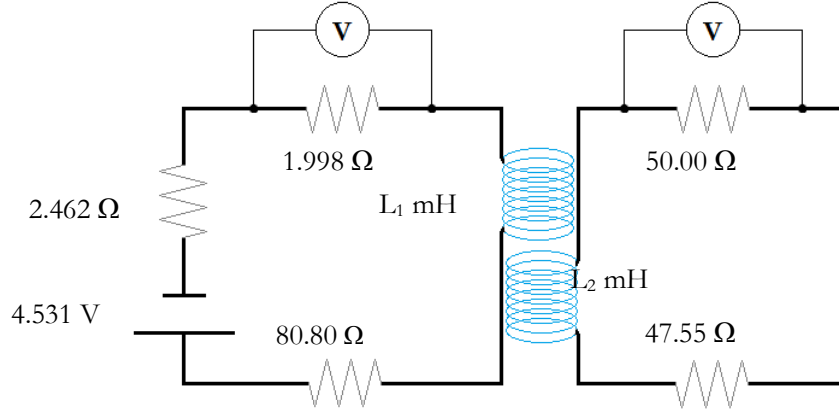


Figure 24: Diagram representing the experimental driver and pickup circuit.

and the driver and pickup coil characteristics are listed in Table X below.

Table X: Coil characteristics.

Coil:	Driver	Pickup
Number of turns :	991	787
Wire gage [AWG] :	36	36
Length [mm] :	14.97	14.98
Inner radius [mm] :	8.21	5.93
Outer radius [mm] :	9.47	7.03
Resistance [ $\Omega$ ] :	80.80	47.55

The coils were carefully wound with known number of turns, uniform turns density and windings exactly perpendicular to coil axes. The centers of the coaxial coils forming the probe were separated by a distance  $d$  of 0.025 mm along the axis. Expressions (28), (29) and (31), the self- and mutual inductance coefficients, were calculated using Maple's numerical integration package.

The experimental self-inductance values were obtained using Maple's Fit command [22]. The model function in (48) was fit to the driver-only experimental signal, for each coil, such that the resulting self-inductance value  $L$  minimized the least-squares error.

$$i(t) = \frac{v_0}{R} \left( 1 - e^{-\frac{R}{L}t} \right). \quad (48)$$

Similarly, the experimental value for the mutual inductance coefficient  $M$  was obtained by fitting equation (42) to the measured pickup signal, using the experimental self-inductance values and measured resistance values. The calculated values are presented alongside the experimental values in Table XI below.

Table XI: Comparison of the calculated and measured self- and mutual inductance coefficients.

	<b>Calculated</b>	<b>Experiment</b>
Driver self-inductance ( $L_1$ )	12.264 mH	12.249 mH
Pickup self-inductance ( $L_2$ )	4.7043 mH	4.7067 mH
Mutual inductance ( $M$ )	5.2766 mH	5.2791 mH

The total circuit resistances (the sums of the resistance values for their respective circuits shown in Figure 24) are  $R_1 = 85.26 \Omega$ , and  $R_2 = 97.55 \Omega$ . These values are substituted into solutions (41) and (42) and the resulting expressions are plotted alongside the experimental results shown in Figure 25.

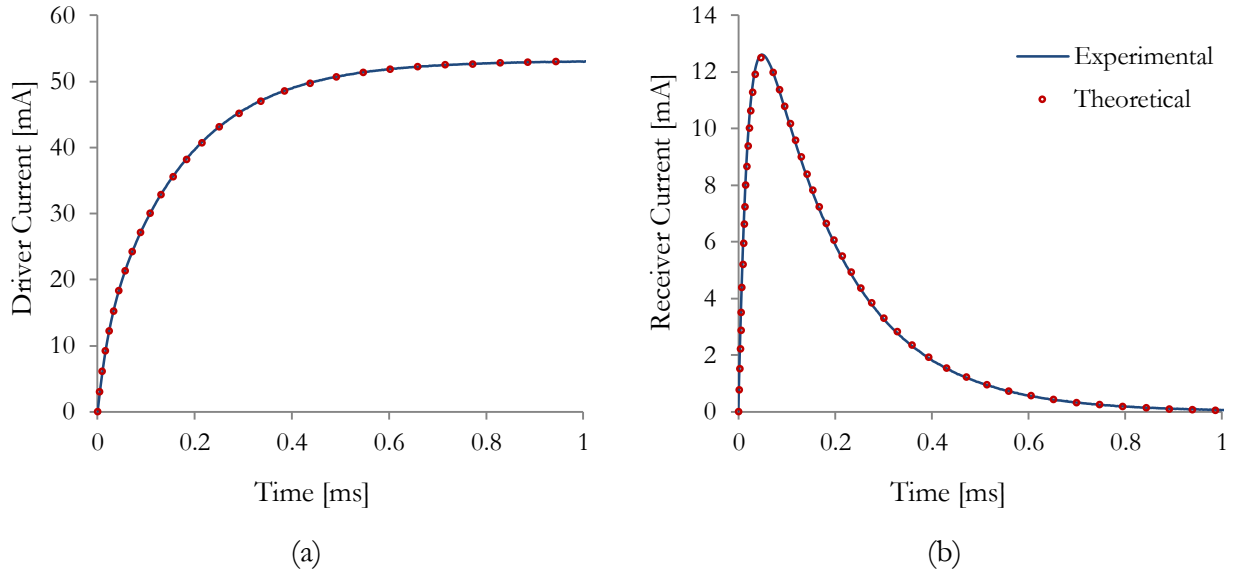


Figure 25: Experimental and theoretical results for the transient currents flowing through the coaxial driver (a) and pickup (b) coils. The outer coil is the driver and the inner coil is the receiver.

An additional verification of the theory is conducted by interchanging the coils in the system. In this second experiment, the inner coil is the driver and the outer coil is the receiver. The results are presented in Figure 26 below.

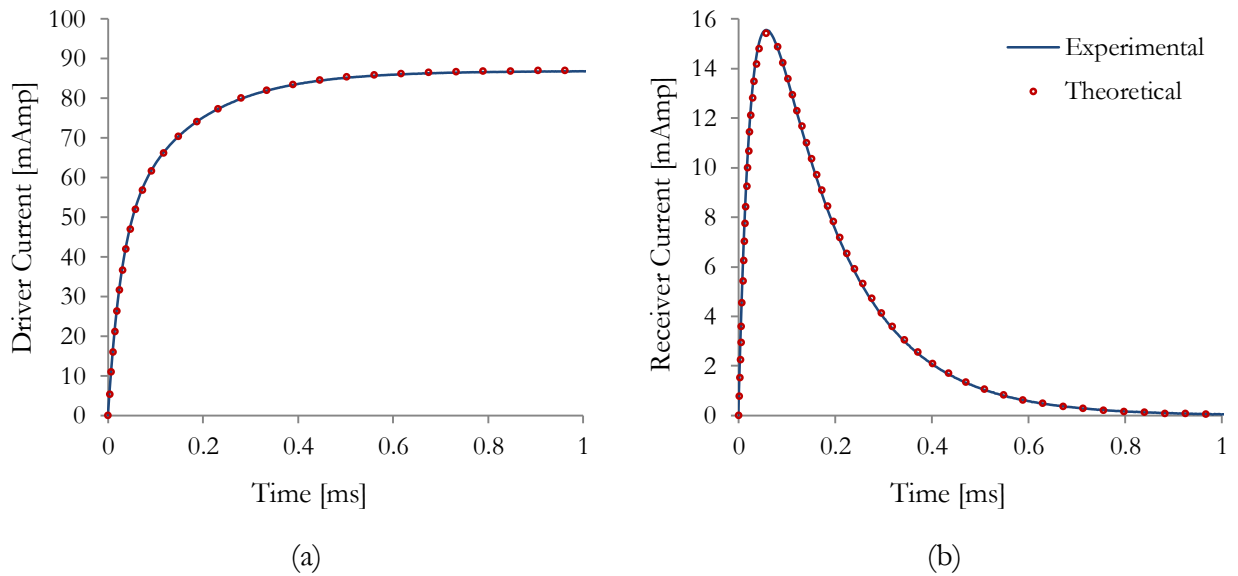


Figure 26: Experimental and theoretical results for the transient currents flowing through the coaxial driver (a) and pickup (b) coils. The outer coil is the receiver and the inner coil is the driver.

The experimental and theoretical results are in excellent agreement. This confirms the solutions for the self- and mutual inductance coefficients,  $L$  and  $M$ , respectively. The theory, from which these experimentally validated solutions have emerged, sets the stage for the consideration of more complicated effects arising from nearby conducting and ferromagnetic structures.

#### **IV. Conclusion**

A novel approach for the derivation of exact solutions to inductively coupled circuit problems has been developed. Induced voltages were written as convolutions of unit impulse response solutions together with their corresponding time-dependent current functions, and substituted into the corresponding differential circuit equations. In this first work, the circuit equations were solved for the simple case of a coaxial driver and pickup probe configuration. Time-independent expressions, which ultimately corresponded to the self- and mutual inductance coefficients, naturally arise as a consequence of the theory. The generality of the approach allows for consideration of any number of driver and pickup coils in inductive circuit problems. Furthermore, solutions can be obtained for coupled circuits in which driver coils are excited by arbitrary waveforms. Finally, this novel approach may be used to correctly address the inductive coupling effects that arise in the presence of ferromagnetic and/or conducting structures. This will be the focus of subsequent works.

#### **V. References**

- [1] Burke SK, Ibrahim ME. Mutual impedance of air-cored coils above a conductive plate. *J Phys D: Appl Phys* 2004;37:1857-1868.
- [2] Von Wwedensky B. Concerning the eddy currents generated by a spontaneous change of magnetization. *Annalen der Physik* 1921;64:609-620.

- [3] Dodd CV, Deeds WE. Analytical solutions to eddy-current probe-coil problems. *J Appl Phys* 1968;39:2829-2838.
- [4] Morozova GM, Polygalov VF, Epov MI, Mogilatov VS. Transient electromagnetic field of a current loop centered on the axis of a hollow magnetic cylinder. *Russian Geo and Geophys* 2000;41:1435-1444.
- [5] Fan M, Huang P, Ye B, Hou D, Zhang G, Zhou Z. Analytical modeling for transient probe response in pulsed eddy current testing. *NDT & E Int* 2009;42:376-383.
- [6] Bowler JR, Theodoulidis TP. Coil impedance variation due to induced current at the edge of a conductive plate. *J Phys D: Appl Phys* 2006;39:2862-2868.
- [7] Bowler JR, Theodoulidis T. Eddy currents induced in a conducting rod of finite length by a coaxial encircling coil. *J Phys D: Appl Phys* 2005;38:2861–2868.
- [8] Bowler JR, Theodoulidis T, Xie H, Ji Y. Evaluation of eddy-current probe signals due to cracks in fastener holes. *IEEE Trans on Magn* 2012;48:1159-1170.
- [9] Theodoulidis T, Bowler JR. Eddy current coil interaction with a right-angled conductive wedge. *Proc R Soc A* 2005;461:3123-3139. doi: 10.1098/rspa.2005.1509.
- [10] Theodoulidis T. Developments in calculating the transient eddy-current response from a conductive plate. *IEEE Trans on Magn* 2008;44:1894-1896.
- [11] Simm A, Theodoulidis T, Poulakis N, Tian GY. Investigation of the magnetic field response from eddy current inspection of defects. *Int J Adv Manuf Technol* 2011;54:223-230.
- [12] Sun H, Bowler JR, Theodoulidis T. Eddy Currents induced in a finite length layered rod by a coaxial coil. *IEEE Trans on Magn* 2005;41:2455-2461.
- [13] Harfield N, Bowler JR. Solution of the two-dimensional problem of a crack in a uniform field in eddy-current non-destructive evaluation. *J Phys D: Appl Phys* 1995;28:2197-2205.

- [14] Yoshida Y, Bowler JR. Vector potential integral formulation for eddy-current probe response to cracks. *IEEE Trans on Magn* 2000;36:461-469.
- [15] Desjardins D, Krause TW, Gauthier N. Analytical modeling of the transient response of a coil encircling a ferromagnetic conducting rod in pulsed eddy current testing. *NDT&E Int* 2013;60:127-131.
- [16] Goldman S. *Transformation Calculus and Electrical Transients*. New York: Prentice Hall; 1949.
- [17] Liboff RL. *Introductory quantum mechanics*. 2<sup>nd</sup> ed. Reading; Addison-Wesley; 1992.
- [18] Griffiths DJ. *Introduction to Electrodynamics*. 3rd ed. Upper Saddle River: Prentice-Hall; 1999.
- [19] Gaskill JD. *Linear Systems, Fourier Transforms, and Optics*. New York: John Wiley & Sons; 1978.
- [20] Havelock, T. H., "On certain Bessel integrals and the coefficients of mutual induction of coaxial coils," *Phil. Mag.*, Vol. 15, 332-345, 1908.
- [21] Kammler D. *A First Course in Fourier Analysis*. New York: University Press; 2000.
- [22] Statistics[Fit] – Fit a model function to data. (2014). Retrieved January 07, 2014, from <http://www.maplesoft.com/support/help/Maple/view.aspx?path=Statistics%2FFit>

**Manuscript 2:** “*Transient response of a driver coil in transient eddy current testing*”. NDT&E Intl. Accepted  
01 Apr 2015.

Author contributions: D.R Desjardins (theory, experiment, primary writer), T.W. Krause (editor, literature survey suggestions), and L. Clapham.

# Transient response of a driver coil in transient eddy current testing

D.R. Desjardins<sup>1\*</sup>, T.W. Krause<sup>2</sup> and L. Clapham<sup>1</sup>

1. Department of Physics, Queen's University, Kingston, ON, Canada, K7L 3N6

2. Department of Physics, Royal Military College of Canada, Kingston, ON, Canada, K7K 7B4

**Abstract** – A solution is presented for the case of a driver coil encircling a ferromagnetic conducting rod. The differential circuit equation is formulated in terms of the rod's impulse response using convolution theory, and solved by Fourier transform. The final solution accounts for feedback between the ferromagnetic rod and the driver coil, providing correct voltage response of the coil. Also arising from the solution is an analytical expression for the complex inductance in the circuit, which accounts for real (inductive) and imaginary (loss) elements associated with the rod. Experimental results, obtained for the case of square wave excitation, show excellent agreement.

**Key Words**– Transient Eddy Current, Ferromagnetic, Rod, Analytical Modeling, Complex Inductance

## I. Introduction

Research in eddy current theory has grown considerably in recent years due to increasing demands for magnetically sensitive non-destructive testing capabilities. Aging nuclear and petrochemical facilities, as well as aircraft and naval fleets, which need to be monitored and maintained, are examples of the benefactors of such technologies. Much work [3]-[10] has been devoted to the development of theoretical models, which aim to predict induced voltages or impedance changes in interrogating coils for applications in eddy current testing. To date, analytical models that predict coil impedance change as a function of an applied sinusoidal current frequency

---

\* Corresponding author: dandesja@gmail.com

have been very successful. By contrast, transient eddy current models have been developed on the assumption of an invariant current excitation, as was done in [14][13][26] for example, which is problematic, since changing inspection conditions and variations in material characteristics modify the applied current signal via magnetic coupling effects. A limited number solutions predicting voltage transients have been developed, and achieving agreement between theory and experiment remains a challenge, particularly at early times and when considering ferromagnetic materials [11]. Ferromagnetic conductors, such as steel, exhibit stronger and thereby more complicated feedback effects between driver and sample circuit elements. Since steel is a commonly encountered construction material, complete models, which correctly account for these complex electromagnetic interactions, are of significant interest. This work considers a coil's voltage response to an abruptly applied voltage step, instead of a current step. Unlike current, a prescribed excitation voltage will remain invariant under changing inspection conditions. Ultimately, model-assisted analyses of experimental data may provide a direct method for the extraction of values such as liftoff, wall thickness, conductivity, permeability and other material and geometrical characteristics of interest.

Previously [17], an approach, in which differential circuit equations were formulated in terms of the magnetic fields arising in an inductive system, was developed and applied for the simple case of a pair of coaxial coils. Expressions, which corresponded to the self- and mutual inductance coefficients, arose naturally from the theory. In this work, the theory is extended to consider the inductive effects of ferromagnetic and conducting structures on a driver coil. In particular, it will be shown that an additional inductance coefficient, which describes the inductive coupling of the coil with a structure, emerges from the theory. Experimental results validate the theory. The resulting analytical model provides a complete understanding of the way in which geometrical and material parameters affect measured coil responses. Furthermore, the theory may be extended to systems

containing multiple sensing coils. This will be the focus of subsequent works prepared by the authors.

In following with the theory developed in [17], the impulse response of a long ferromagnetic conducting rod will be directly incorporated into the differential circuit equation via a convolution integral [18], and the resulting equation will be solved by Fourier transform.

## II. Theory

A circular driver coil is centered about the axis of a long, ferromagnetic and conducting rod with magnetic permeability  $\mu$  and conductivity  $\sigma$  as depicted in Figure 27. In accordance with Maxwell's equations, a time-varying current flowing in the driver coil will induce eddy currents within the volume of the rod. These eddy currents give rise to a transient magnetic field which, in turn, generates an opposing current within the driver coil. The magnetic vector potential, arising from the magnetization and induction of eddy currents within a rod following an impulse excitation, is developed first.

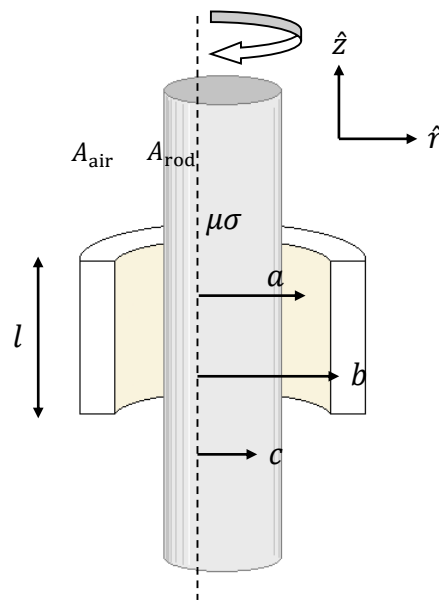


Figure 27: Diagram of a coil encircling a long rod.

The solution for the air region surrounding the rod is the superposition of magnetization and eddy current fields together with the time-dependent excitation field generated by the coil. Consider the case in which the coil carries a current impulse,  $i(t) = \delta(t)$ , where  $\delta(t)$  is a Dirac delta function [18]. Then, the system impulse response outside of the rod, defined as  $\hat{A}_{\text{air}}(r, z, t)$ , is the superposition of an impulse excitation, denoted  $\hat{\psi}(r, z, t)$ , together with the impulse response of the rod, defined as  $\hat{\Xi}(r, z, t)$ , according to

$$\hat{A}_{\text{air}}(r, \lambda, t) = \hat{\psi}(r, \lambda, t) + \hat{\Xi}(r, \lambda, t). \quad (1)$$

The impulse excitation field has been developed in [1] and is given here as

$$\hat{\psi}(r, \lambda, t) = \psi(r, \lambda)\delta(t) = 2\mu_0 n \frac{\sin\left(\frac{\lambda l}{2}\right)}{\lambda} \left\{ \begin{array}{l} I_1(\lambda r) \int_a^b r K_1(\lambda r) dr \quad r \leq a \\ K_1(\lambda r) \int_a^b r I_1(\lambda r) dr \quad r \geq b \end{array} \right\} \delta(t), \quad (2)$$

where  $l$  is the coil's length,  $a$  and  $b$  are its inner and outer radii, as shown in Figure 27,  $n \equiv \frac{N}{l(b-a)}$  is the coil's turn density, and  $\delta(t)$  is the current unit impulse.

The rod's impulse response for the air region,  $\hat{\Xi}(r, z, t)$ , which describes the magnetic vector potential associated solely with magnetization and eddy current effects, obeys Laplace's equation [18]. The vector Laplacian is recast into its differential operator form for the appropriate cylindrical geometry, and the resulting expression's axial coordinate,  $z$ , is separated by means of a Fourier cosine transform [19] with parameter  $\lambda$  such that

$$\left( \frac{\partial^2}{\partial r^2} + \frac{1}{r} \frac{\partial}{\partial r} - \frac{1}{r^2} - \lambda^2 \right) \hat{\Xi}(r, \lambda, t) = 0. \quad (3)$$

Equation (3) is Bessel's modified differential equation. The allowable solution is the first-order modified Bessel function of the second kind written as

$$\hat{\Xi}(r, \lambda, t) = \mathcal{A}(\lambda, t)K_1(\lambda r), \quad (4)$$

where  $\mathcal{A}(\lambda, t)$  is an unknown coefficient. Equations (4) and (2) are substituted into (1), and a Fourier transform, defined as  $\mathcal{F}\{f(t)\} \equiv \int_{-\infty}^{\infty} f(t)e^{-j\omega t} dt$  with angular frequency  $\omega$ , is applied to the resulting expression giving

$$\hat{A}_{\text{air}}(r, \lambda, \omega) = \psi(r, \lambda) + \mathcal{A}(\lambda, \omega)K_1(\lambda r), \quad (5)$$

where  $\hat{A}_{\text{air}}(r, \lambda, \omega) = \mathcal{F}\{\hat{A}_{\text{air}}(r, \lambda, t)\}$ . It is noted that the Fourier transform of  $\hat{\psi}(r, \lambda, t)$  is frequency-independent since  $\int_{-\infty}^{\infty} \delta(t)e^{-j\omega t} dt = 1$ .

The diffusion equation [18], which governs the time-dependent evolution of the magnetic vector potential inside the rod, is written as

$$\nabla^2 \hat{A}_{\text{rod}}(r, z, t) = \mu_r \mu_0 \sigma \frac{\partial}{\partial t} \hat{A}_{\text{rod}}(r, z, t), \quad (6)$$

The  $z$  coordinate is separated by means of a Fourier cosine transform and the  $t$  coordinate separated by a Fourier transform, such that

$$\left( \frac{\partial^2}{\partial r^2} + \frac{1}{r} \frac{\partial}{\partial r} - \frac{1}{r^2} - \lambda^2 \right) \hat{A}_{\text{rod}}(r, \lambda, \omega) = j\omega \mu_r \mu_0 \sigma \hat{A}_{\text{rod}}(r, \lambda, \omega). \quad (7)$$

The allowable solution to the differential equation in (7) is the first-order modified Bessel function of the first kind written as

$$\hat{A}_{\text{rod}}(r, \lambda, \omega) = \mathcal{B}(\lambda, \omega)I_1(\Lambda r), \quad (8)$$

where  $\mathcal{B}(\lambda, \omega)$  is an unknown coefficient and  $\Lambda$  is defined as

$$\Lambda \equiv \sqrt{\lambda^2 + j\omega \mu_r \mu_0 \sigma}. \quad (9)$$

Exterior and interior solutions (5) and (8), respectively, are matched at the rod's boundary, at which  $r = c$  as shown in Figure 27, using the appropriate boundary conditions [21]

$$\hat{A}_{\text{air}}(c, \lambda, \omega) = \hat{A}_{\text{rod}}(c, \lambda, \omega), \quad (10)$$

$$\mu_r \left( \hat{A}_{\text{air}}(c, \lambda, \omega) + c \hat{A}'_{\text{air}}(c, \lambda, \omega) \right) = \hat{A}_{\text{rod}}(c, \lambda, \omega) + c \hat{A}'_{\text{rod}}(c, \lambda, \omega), \quad (11)$$

where the primes denote differentiation with respect to  $r$ . Boundary equations (10) and (11) are solved for unknown Bessel coefficients  $\mathcal{A}(\lambda, \omega)$  and  $\mathcal{B}(\lambda, \omega)$  :

$$\mathcal{A}(\lambda, \omega) = 2\mu_0 n \int_a^b r K_1(\lambda r) dr \frac{\sin\left(\frac{\lambda l}{2}\right) \mu_r \lambda I_0(\lambda c) I_1(\Lambda c) - \Lambda I_1(\lambda c) I_0(\Lambda c)}{\lambda \mu_r \lambda K_0(\lambda c) I_1(\Lambda c) + \Lambda K_1(\lambda c) I_0(\Lambda c)}, \quad (12)$$

$$\mathcal{B}(\lambda, \omega) = 2\mu_r \mu_0 n \int_a^b r K_1(\lambda r) dr \frac{\sin\left(\frac{\lambda l}{2}\right) (K_0(\lambda c) I_1(\lambda c) + I_0(\lambda c) K_1(\lambda c))}{\mu_r \lambda K_0(\lambda c) I_1(\Lambda c) + \Lambda K_1(\lambda c) I_0(\Lambda c)}. \quad (13)$$

Finally, the frequency-domain impulse responses are written as

$$\hat{\mathcal{E}}(r, z, \omega) = \frac{1}{\pi} \int_0^\infty \mathcal{A}(\lambda, \omega) K_1(\lambda r) \cos(\lambda z) d\lambda, \quad (14)$$

$$\hat{A}_{\text{rod}}(r, z, \omega) = \frac{1}{\pi} \int_0^\infty \mathcal{B}(\lambda, \omega) I_1(\Lambda r) \cos(\lambda z) d\lambda, \quad (15)$$

where  $\mathcal{A}(\lambda, \omega)$  and  $\mathcal{B}(\lambda, \omega)$  are given in (12) and (13), respectively, and  $\Lambda$  is defined in (9).

In what follows, the rod's impulse response in the region containing the driver coil, equation (14), is substituted into the differential circuit equation, as performed previously [17]. The circuit equation, which describes the resultant time-dependent current  $i$  flowing in the driver coil, is written using Kirchhoff's laws in the following general form

$$Ri(t) = v(t) + \varepsilon(t), \quad (16)$$

where  $v(t)$  is any time-dependent excitation voltage - step, harmonic, multi-frequency, ramp, saw-tooth, etc. -  $R$  is the total driver circuit resistance, and  $\varepsilon(t)$  is the total time-dependent back-emf induced in the driver coil. The function  $\varepsilon$  is expected to have two components; one arising from the field generated by the driver coil itself and another from transient eddy current fields emanating from the ferromagnetic conducting structure. Induced voltage  $\varepsilon(t)$  can be expressed as the convolution of the system's impulse response with the yet unknown time-dependent current function [1] such that

$$\varepsilon(t) = -2\pi n \frac{d}{dt} \int_{-\frac{l}{2}}^{\frac{l}{2}} \int_a^b r \hat{A}_{\text{air}}(r, z, t) * i(t) \, dr dz, \quad (17)$$

where  $\hat{A}_{\text{air}}(r, z, t)$  is the system's impulse response in the region containing the coil, and where the surface integral is performed over the cross-section of that coil. Equation (1) is substituted into (17) then into (16) to obtain

$$Ri(t) = v(t) - 2\pi n \frac{d}{dt} \int_{-\frac{l}{2}}^{\frac{l}{2}} \int_a^b r \left( \hat{\psi}(r, z, t) + \hat{\Xi}(r, z, t) \right) * i(t) \, dr dz. \quad (18)$$

It has been shown previously [17] that

$$2\pi n \frac{d}{dt} \int_{-\frac{l}{2}}^{\frac{l}{2}} \int_a^b r \hat{\psi}(r, z, t) * i(t) \, dr dz = L \frac{d}{dt} i(t), \quad (19)$$

where the self-inductance coefficient,  $L$ , was expressed as

$$L \equiv 8\mu_0 n \int_0^\infty \int_0^\infty \gamma \frac{\left( \int_a^b r J_1(\gamma r) \, dr \right)^2 \sin^2\left(\frac{\lambda l}{2}\right)}{\lambda^2(\gamma^2 + \lambda^2)} \, d\gamma \, d\lambda, \quad (20)$$

with number of turns  $N$ , length  $l$ , inner radius  $a$  and outer radius  $b$ . As explained in [17], the double integral expression for the magnetic vector potential generated by a circular coil,  $\hat{\psi}(r, z, t)$ , converges for all  $r$  and  $z$ , including the region within the coil itself. Integration of this expression over the coil's own cross-section yields its self-inductance. This double integral expression can be expressed in terms of generalized hypergeometric functions as was done by Conway [22]. Equation (20) is an idealized approximation, however. It is well-known that the self-inductance of a coil is frequency-dependent [23]. Particularly at higher frequencies, skin effects, capacitive coupling between the windings and electrical resonance effects introduce deviations from the ideal case. However, these effects are negligible at the low frequencies implied by transient eddy current, and are not treated in this theory.

Using (19), the circuit equation is rewritten as

$$v(t) = Ri(t) + L \frac{d}{dt} i(t) + 2\pi n \frac{d}{dt} \int_{-\frac{l}{2}}^{\frac{l}{2}} \int_a^b r \hat{\Xi}(r, z, t) * i(t) dr dz. \quad (21)$$

The solution for time-dependent current  $i(t)$  in equation (21) is sought. The convolution integral prohibits  $i(t)$  from being separated from  $\hat{\Xi}(r, z, t)$ . However, the Fourier transform of a convolution is simply the product of the transforms [18]. Thus, by Fourier transforming (21) such that

$$V(\omega) = RI(\omega) + j\omega LI(\omega) + j\omega 2\pi n \int_{-\frac{l}{2}}^{\frac{l}{2}} \int_a^b r \hat{\Xi}(r, z, \omega) I(\omega) dr dz, \quad (22)$$

the Fourier transformed current function,  $I(\omega)$ , can be removed from the integral. The solution to equation (22) is evaluated as

$$I(\omega) = \frac{V(\omega)}{R + j\omega(L + \mathcal{L})}, \quad (23)$$

where we have defined

$$\mathcal{L} \equiv 2\pi n \int_{-\frac{l}{2}}^{\frac{l}{2}} \int_a^b r \hat{\mathbf{E}}(r, z, \omega) \, dr dz. \quad (24)$$

Equation (14) is substituted into (24), and the cross-section integral is performed for  $z$  from  $-l/2$  to  $l/2$  and for  $r$  from  $a$  to  $b$ , yielding

$$\mathcal{L} \equiv 8\mu_0 n^2 \int_0^\infty \frac{\sin^2\left(\frac{\lambda l}{2}\right)}{\lambda^2} \left( \int_a^b r K_1(\lambda r) \, dr \right)^2 \frac{\mu_r \lambda I_0(\lambda c) I_1(\lambda c) - \Lambda I_1(\lambda c) I_0(\lambda c)}{\mu_r \lambda K_0(\lambda c) I_1(\lambda c) + \Lambda K_1(\lambda c) I_0(\lambda c)} \, d\lambda. \quad (25)$$

The frequency-dependent function  $\mathcal{L}$  can be described as a complex-valued inductance arising from the electromagnetic coupling of the coil with the rod. In order to understand its physical significance, consider the following.  $\mathcal{L}$  can be decomposed as  $\mathcal{L} = \Re(\mathcal{L}) + j \Im(\mathcal{L})$  where  $\Re(\mathcal{L})$  and  $\Im(\mathcal{L})$  are the real and imaginary components of  $\mathcal{L}$ , respectively. Now, consider the impedance that is implied:  $Z = j\omega\mathcal{L}$ , [18] where  $\omega$  represents the angular frequency. It is expanded as

$$Z = j\omega \Re(\mathcal{L}) - \omega \Im(\mathcal{L}). \quad (26)$$

The imaginary part of the inductance contributes a real part to the impedance, associated with losses [18]. The  $\omega \Im(\mathcal{L})$  term can be interpreted as the frequency-dependent part of the circuit's resistance. The real part of the inductance forms the imaginary part of the impedance, associated with inductive energy storage.

The general solution, expressed in the time domain, is obtained by applying an inverse Fourier transform to (23) such that

$$i(t) = \frac{1}{2\pi} \int_{-\infty}^{\infty} \frac{V(\omega)}{R + j\omega(L + \mathcal{L})} e^{j\omega t} d\omega. \quad (27)$$

where  $V(\omega)$  is the Fourier transform of the excitation function,  $v(t)$ , applied to the driver coil. Suppose a sinusoidal function is chosen for applications in conventional eddy current. Then  $v(t) = v_0 \sin(\omega t)$  where  $v_0$  is the amplitude of a sinusoid with angular frequency  $\omega$ . Its Fourier transform [24] is

$$V(\omega) = -j\pi v_0 (\delta(\omega - \omega) - \delta(\omega + \omega)). \quad (28)$$

Equation (28) is substituted into (27) and the inverse transform is evaluated as

$$i(t) = -\frac{jv_0}{2} \left( \frac{e^{j\omega t}}{R + j\omega(L + \mathcal{L}(\omega))} - \frac{e^{-j\omega t}}{R - j\omega(L + \mathcal{L}(-\omega))} \right). \quad (29)$$

Note that the second term in the parentheses is simply the complex conjugate of the first. The difference between a function and its complex conjugate is twice the imaginary component of the function [24]; thus, equation (29) is re-written in terms of trigonometric functions as

$$i(t) = v_0 \frac{(R - \omega \Im(\mathcal{L})) \sin(\omega t) - \cos(\omega t) \omega (L + \Re(\mathcal{L}))}{(R - \omega \Im(\mathcal{L}))^2 + \omega^2 (L + \Re(\mathcal{L}))^2}, \quad (30)$$

where  $\mathcal{L}$  is a complex-valued inductance evaluated at  $\omega = \omega$  using equation (25). Equation (30) may be alternatively expressed as a sine wave with a phase shift as:

$$i(t) = v_0 \frac{\sin\left(\omega t - \arctan\left(\frac{\omega(L + \Re(\mathcal{L}))}{R - \omega \Im(\mathcal{L})}\right)\right)}{\sqrt{(R - \omega \Im(\mathcal{L}))^2 + \omega^2 (L + \Re(\mathcal{L}))^2}}, \quad (31)$$

Equation (31) is the final closed-form solution describing the current flowing through a driver coil coupled to a ferromagnetic conducting structure and driven by a sinusoidal voltage  $v(t) = v_0 \sin(\omega t)$ .

Furthermore, the formulation of (31) enables a direct treatment of the phase and amplitude arising from inductive coupling effects.

In general, *any* time-dependent excitation waveform (periodic function)  $v(t)$  may be expressed as a Fourier series. The Fourier transform of a superposition of cosine and sine waves (i.e. Fourier series) will consist of a summation of weighted Dirac functions, whose effect under the integral in (27) is to select out a set of particular frequencies in accordance with the sampling theorem [18]. Thus, the Fourier series corresponding to a periodic square wave with a 50% duty cycle and having amplitude  $v_0$  and pulse duration  $P$  (i.e. period  $2P$ ) may be expressed as

$$v(t) = \frac{v_0}{2} + \frac{2v_0}{P} \sum_{n=1}^{\infty} \frac{\sin(\omega_n t)}{\omega_n}, \quad (32)$$

where we have defined

$$\omega_n \equiv \frac{(2n-1)\pi}{P}. \quad (33)$$

It is important to note that the amplitudes of the frequencies, that form the square wave excitation, vary as  $\omega_n^{-1}$ ; transient eddy current is dominated by lower frequency effects. A Fourier transform is applied to equation (32) such that

$$V(\omega) = \pi v_0 \delta(\omega) + \frac{2\pi v_0}{P} \sum_{n=1}^{\infty} \frac{\delta(\omega - \omega_n) - \delta(\omega + \omega_n)}{j\omega_n}, \quad (34)$$

Equation (34) is substituted into (27) yielding

$$i(t) = \frac{v_0}{2R} + \frac{v_0}{P} \sum_{n=1}^{\infty} \frac{e^{j\omega_n t}}{j\omega_n (R + j\omega_n (L + \mathcal{L}(\omega_n)))} + \frac{v_0}{P} \sum_{n=1}^{\infty} \frac{e^{-j\omega_n t}}{-j\omega_n (R - j\omega_n (L + \mathcal{L}(-\omega_n)))}. \quad (35)$$

As before, the second summation term in equation (35) is the complex conjugate of the first. The sum, however, of a function with its complex conjugate is equivalent to twice the real component of the function. [24] Finally, equation (35) is re-written in terms of trigonometric functions as

$$i(t) = \frac{v_0}{2R} + \frac{2v_0}{P} \sum_{n=1}^{\infty} \frac{(R - \varpi_n \Im(\mathcal{L})) \sin(\varpi_n t) - \cos(\varpi_n t) \varpi_n (L + \Re(\mathcal{L}))}{\varpi_n \left( (R - \varpi_n \Im(\mathcal{L}))^2 + \varpi_n^2 (L + \Re(\mathcal{L}))^2 \right)}, \quad (36)$$

where  $\varpi_n$  is defined in equation (33) and  $\mathcal{L}$  is evaluated at  $\omega = \varpi_n$  for each  $n$ . Equation (36) may also be recast into a series of phase-shifted sine waves such that

$$i(t) = \frac{v_0}{2R} + \frac{2v_0}{P} \sum_{n=1}^{\infty} \frac{\sin\left(\varpi_n t - \arctan\left(\frac{\varpi_n (L + \Re(\mathcal{L}))}{R - \varpi_n \Im(\mathcal{L})}\right)\right)}{\varpi_n \sqrt{(R - \varpi_n \Im(\mathcal{L}))^2 + \varpi_n^2 (L + \Re(\mathcal{L}))^2}}, \quad (37)$$

where the real and imaginary parts of the complex function  $\mathcal{L}$  need only be evaluated at discrete frequencies  $\varpi_n$ . Equation (37) is the final solution describing the resultant current flowing through a driver coil coupled to a ferromagnetic conducting structure and driven by a square waveform voltage with amplitude  $v_0$  and period  $P$ .

### III. Experimental Results

A power supply with an internal resistance of 2.46  $\Omega$  was used to generate a 4.53 V square pulse excitation. Coaxial cables with negligible losses route the pulse through a 2.00  $\Omega$  resistor to a 47.6  $\Omega$  driving coil. A National Instruments signal acquisition card (NI6211 USB DAQ board) measures and records the transient potential difference across the 2.00  $\Omega$  resistor at 2  $\mu$ s intervals. The transient current flowing through the circuit is related to the experimentally measured voltage in accordance with Ohm's Law (i.e.  $i_{\text{exp}} = v_{\text{exp}}/2.00\Omega$ ). The driver circuit is depicted in Figure 24,

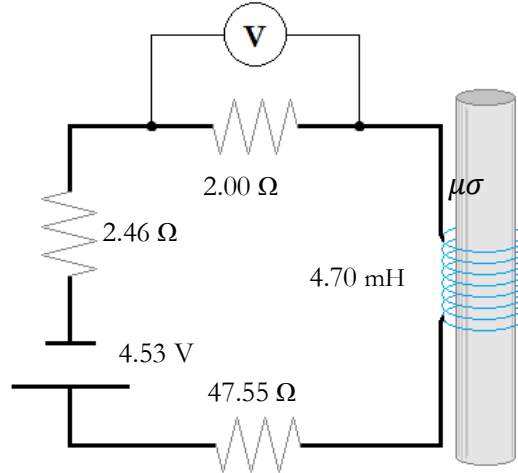


Figure 28: Circuit diagram depicting the driver circuit with the long ferromagnetic conducting rod.

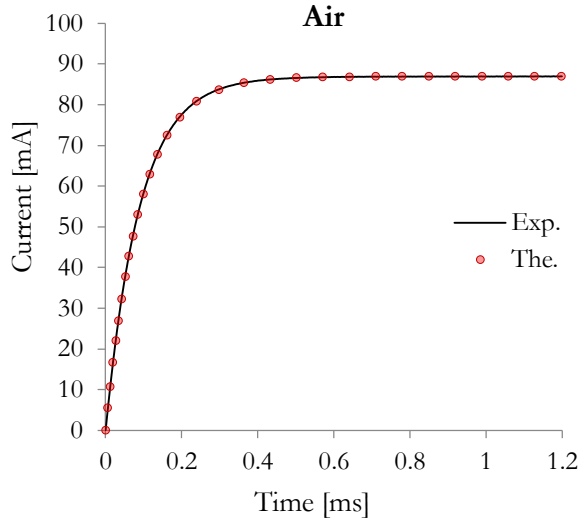
and the coil and rod characteristics are listed in table 1 below.

Coil: Driver		Rod : Copper Brass Steel			
Number of turns :	787	Radius [mm] :	3.172	3.191	3.005
Wire gage [AWG] :	36	Conductivity [ $\text{MS}\cdot\text{m}^{-1}$ ] :	58.14	12.44	4.30
Length [mm] :	14.98	Relative Permeability :	1	1	107
Inner radius [mm] :	5.93				
Outer radius [mm] :	7.03				
Resistance [ $\Omega$ ] :	47.55				
Inductance [mH] :	4.704				

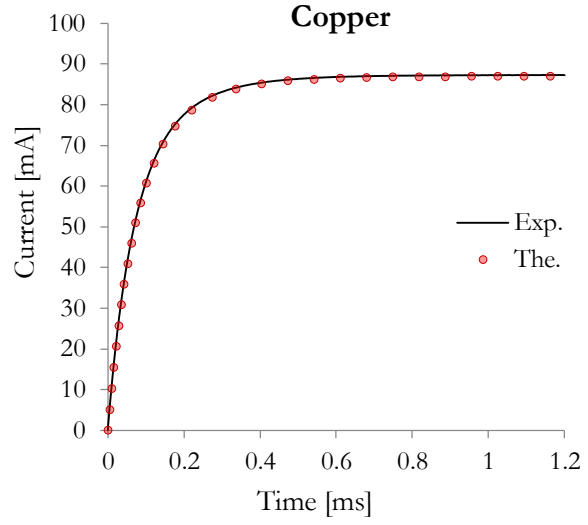
Table 12: Coil and rod geometrical, electrical and material characteristics.

The coil was carefully wound with known number of turns, uniform turns density and windings exactly perpendicular to coil axis. The value of the rod's relative magnetic permeability, calculated using an extension of the theory presented here, is typical of steels [26].

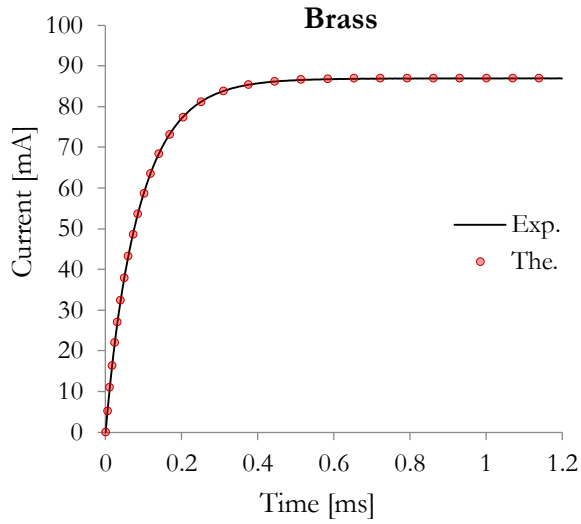
Solution (36) is plotted in Figure 29, using the values listed in Table 12, and compared with experimental results for rods, which are non-conducting non-magnetic (air), conducting non-magnetic (copper and brass) and conducting magnetic (steel). All computations are performed in Maplesoft's Maple 18 computational software [27]. Numerical integration is used to calculate the frequency-dependent complex inductance functions  $\mathcal{L}_1$ ,  $\mathcal{L}_2$  and  $\mathcal{M}$ , and employs the NAG method d01akc, which uses adaptive Gauss 30-point and Kronrod 61-point rules [28]. Fourier series summations, performed to calculate probe response, include 300 terms in the computation in order to assure excellent convergence. For a square wave with a 3 ms period, this corresponds to summing the effects of frequencies up to approximately 100kHz. For each term in the series, functions  $\mathcal{L}_1$ ,  $\mathcal{L}_2$  and  $\mathcal{M}$  must be computed. The experimental and theoretical results are in excellent agreement.



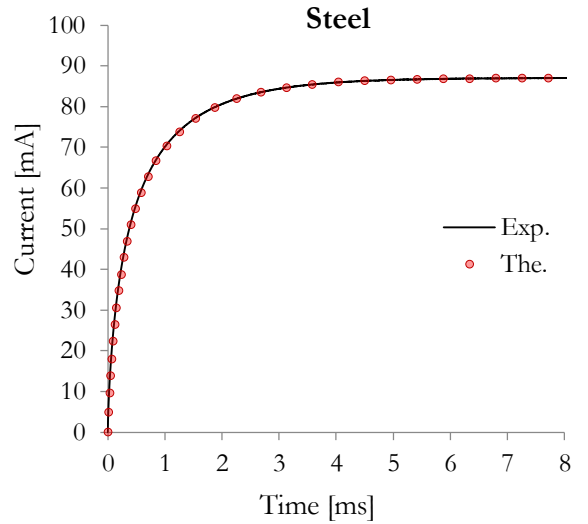
(a)



(b)



(c)



(d)

Figure 29: Experimental and theoretical results of the transient current in the driver circuit following the application of a square wave excitation to a coil in air (a) and encircling a copper rod (b), a brass rod (c) and a steel rod (d).

## IV. Discussion

The longer time-scale, associated with the steel rod results shown in Figure 3(d), follows from stronger electromagnetic interactions arising between the coil and the sample due to magnetization [21] effects. The theory, from which the experimentally validated solution has emerged, sets the stage

for the consideration of an inductive system, which contains a driver coil, a pickup coil and a ferromagnetic conducting structure.

A description of an additional inductance effect, associated with the presence of a ferromagnetic conducting structure, has emerged from the theory. This quantity, denoted  $\mathcal{L}$ , is a frequency-dependent complex-valued inductance, which depends on the geometry and material of the conducting structure, as expected. Whereas  $L$  represents the direct coupling of the coil with itself,  $\mathcal{L}$  can be interpreted as the indirect coupling of the coil with itself through the sample. These coupling effects are schematically represented in Figure 30 below.

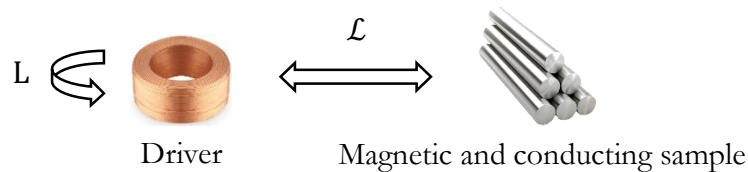


Figure 30: Schematic description of the coupling coefficients.

The imaginary part of the complex inductance is associated with losses, while the real part is associated with inductive energy storage. It may be more natural to consider the coupling effects of the material using  $\mathcal{L}$ , since it arises naturally from the theory, as opposed to  $Z$ , which is defined by convention as  $R + j\omega L$ .

The solution in equation (36) is valid for magnetic and conducting structures of various geometries provided that  $\mathcal{L}$  can be obtained by solving the appropriate boundary value problem. Thus, this theory can be straightforwardly extended to inductive circuit problems containing other ferromagnetic conducting structures, such as half-spaces, plates, rods, tubes, spheres and right-angled wedges [9] for instance. Mathematical models developed in this manner may be used to analyse experimental data and provide a direct method for the extraction of values such as liftoff,

wall thickness, conductivity, permeability and other material and geometrical characteristics of interest. Additionally, a comprehensive theoretical comparison of the eddy current densities induced within conducting structures, as arising from harmonic and square-wave transients, may now be conducted. Such a study would highlight the similarities and differences between transient and conventional eddy current testing for example, and corroborate other long-standing semi-empirical results such as the skin depth equation. In subsequent work, the theory will be extended to a case that includes both a driver and a pickup coil.

## V. Summary

A novel approach for the calculation of induced electrical transients for applications in non-destructive eddy current testing, developed in [17], was applied to the case of a driver coil encircling a long ferromagnetic conducting rod. The differential circuit equation was formulated in terms of the rod's impulse response using convolution theory. Solutions, for applications in both conventional and pulsed eddy current, were developed. The former is in closed-form and the latter in series-form. The final solutions account for each of the electromagnetic coupling effects arising in the system, and provide correct time-domain voltage responses of a coil under both harmonic and transient regimes. Additionally, an analytical expression for the complex inductance in the circuit, which accounts for real (inductive) and imaginary (loss) elements associated with the rod, has arisen from the theory. Experimental results, obtained for the case of square wave excitation, are in excellent agreement with the analytical equations.

## VI. References

- [1] Dodd CV, Deeds WE. Analytical solutions to eddy-current probe-coil problems. *J Appl Phys* 1968;39:2829-2838.

- [2] Bowler JR, Theodoulidis TP. Coil impedance variation due to induced current at the edge of a conductive plate. *J Phys D: Appl Phys* 2006;39:2862-2868.
- [3] Fan M, Huang P, Ye B, Hou D, Zhang G, Zhou Z. Analytical modeling for transient probe response in pulsed eddy current testing. *NDT & E Int* 2009;42:376-383.
- [4] Burke SK, Theodoulidis T. Impedance of a horizontal coil in a borehole: a model for eddy current borehole probes. *J Phys D: Appl Phys* 2004;37:485-494.
- [5] Bowler JR, Theodoulidis T. Eddy currents induced in a conducting rod of finite length by a coaxial encircling coil. *J Phys D: Appl Phys* 2005;38:2861-2868.
- [6] Bowler JR, Theodoulidis T, Xie H, Ji Y. Evaluation of eddy-current probe signals due to cracks in fastener holes. *IEEE Trans on Magn* 2012;48:1159-1170.
- [7] Theodoulidis T, Bowler JR. Eddy current coil interaction with a right-angled conductive wedge. *Proc R Soc A* 2005;461:3123-3139. doi: 10.1098/rspa.2005.1509.
- [8] Theodoulidis T. Developments in calculating the transient eddy-current response from a conductive plate. *IEEE Trans on Magn* 2008;44:1894-1896.
- [9] Simm A, Theodoulidis T, Poulakis N, Tian GY. Investigation of the magnetic field response from eddy current inspection of defects. *Int J Adv Manuf Technol* 2011;54:223-230.
- [10] Sun H, Bowler JR, Theodoulidis T. Eddy Currents induced in a finite length layered rod by a coaxial coil. *IEEE Trans on Magn* 2005;41:2455-2461.
- [11] Morozova GM, Polygalov VF, Epov MI, Mogilatov VS. Transient electromagnetic field of a current loop centered on the axis of a hollow magnetic cylinder. *Russian Geo and Geophys* 2000;41:1435-1444.
- [12] Xuan L, Zeng Z, Shanker B, Udpa L. Meshless method for numerical modeling of pulsed eddy currents. *IEEE Trans of Magn* 2004;40:3457-3461.

- [13] Yoshida Y, Bowler JR. Vector potential integral formulation for eddy-current probe response to cracks. *IEEE Trans on Magn* 2000;36:461-469.
- [14] Burke SK, Hugo GR. Transient eddy current NDE for hidden corrosion in multilayer structures. *Review of Progress in Quantitative Nondestructive Evaluation*, Vol 17, Plenum Press, New York, 1998.
- [15] T. Theodoulidis, Developments in calculating the transient eddy-current response from a conductive plate, *IEEE Trans. on Magn.* 44 (2008) 1894-1896.
- [16] J.R. Bowler, F. Fu, Transient eddy-current driver pickup probe response due to a conductive plate, *IEEE Trans. on Magn.* 42 (2006) 2029-2037.
- [17] Desjardins D, Krause TW, Tetervak A, Clapham L. Concerning the derivation of exact solutions to inductive circuit problems for eddy current testing. *NDT&E Int* 2014;68:128-135.
- [18] Liboff RL. *Introductory quantum mechanics*. 2<sup>nd</sup> ed. Reading; Addison-Wesley; 1992.
- [19] Griffiths DJ. *Introduction to Electrodynamics* 3rd Ed. Upper Saddle River: Prentice-Hall; 1999.
- [20] Gaskill JD. *Linear Systems, Fourier Transforms, and Optics*. New York: John Wiley & Sons; 1978.
- [21] Desjardins D, Krause TW, Gauthier N. Analytical modeling of the transient response of a coil encircling a ferromagnetic conducting rod in pulsed eddy current testing. *NDT&E Int* 2013;60:127-131.
- [22] J.T. Cowway. Analytical solutions for the self- and mutual inductance of concentric coplanar disk coils. *IEEE transactions on magnetics*, Vol. 49, No. 3, March 2013, pp 1135-1142.

- [23] D.J. Harrison, L.D. Jones, S.K. Burke, Posada, "Benchmark problems for defect size and shape determination in eddy-current non-destructive evaluation", Journal of Non-destructive Evaluation, Vol.15, No.1, pp.21-34, 1996.
- [24] Kammler D. A First Course in Fourier Analysis. New York: University Press; 2000.
- [25] Anton H. Elementary Linear Algebra. 8th ed. New York: Wiley; 2000.
- [26] Woolman J, Mottram RA. Mechanical and Physical Properties of the BS En Steels. Pergamon Press;1964.
- [27] Maple 18. (2014). Retrieved May 26, 2014, from <http://www.maplesoft.com/products/Maple/>
- [28] Maple online help: Numerical Integration. (2014). Retrieved June 26, 2014, from <http://www.maplesoft.com/support/help/Maple/view.aspx?path=evalf/Int&term=evalf/int>

**Manuscript 3:** “*Transient response of a driver-pickup probe in transient eddy current testing*”. NDT&E Intl.

Accepted 28 Apr 2015.

Author contributions: D.R Desjardins (theory, experiment, primary writer), T.W. Krause (editor, literature survey suggestions), and L. Clapham.

# Transient response of a driver-pickup coil probe in transient eddy current testing

D. Desjardins<sup>1,2</sup>, T.W. Krause<sup>2</sup> and L. Clapham<sup>1</sup>

1. Department of Physics, Queen's University, Kingston, ON, Canada, K7L 3N6

2. Department of Physics, Royal Military College of Canada, Kingston, ON, Canada, K7K 7B4

**Abstract** – Novel solutions that correctly incorporate all electromagnetic interactions arising in inductively coupled circuits are presented for the case of a coaxial driver and pickup coil probe encircling a long ferromagnetic conducting rod. The differential circuit equations are formulated in terms of the rod's impulse response using convolution theory, and solved by Fourier transform. The solutions presented here are the first to account for feedback between a ferromagnetic conductor and the driver and pickup coils, providing correct voltage response of the coils. Experimental results, obtained for the case of square wave excitation, are in excellent agreement with the analytical equations.

**Key Words** – Transient; Eddy Current; Analytical; Response

## I. Introduction

Driver-pickup eddy current non-destructive testing is a well-established method for the inspection of metallic objects [1]. It is relatively inexpensive, fast and reliable in comparison with other inspection technologies. These qualities make eddy current a desirable inspection method in industry [2][3], where it is employed to monitor the structural health of industrial assets. To this end, considerable efforts have been made to develop mathematical models that enable the interpretation of inspection data. The common approach is to formulate time-harmonic solutions, which describe the electromagnetic fields in a system, in order to calculate the change in a coil's impedance as it

---

<sup>2</sup> Corresponding author: dandesja@gmail.com

interacts with a conducting structure [4]-[8]. In a less developed approach, transient eddy current models consider the voltage induced in a pickup circuit [9]-[14] given a prescribed current that has been applied to a driver coil. Under voltage control, changing material characteristics and inspection geometries will distort the resultant current signal through feedback effects. In order to circumvent the feedback challenge, the common approach has been to employ current control systems. In such systems, however, the level of signal distortion from feedback effects is largely dependent on the quality of the current generator. Consequently, a persistent challenge for the development of transient driver-pickup models, particularly under voltage control, has been a lack of experimental agreement, particularly in cases where ferromagnetic materials, such as steel, exhibit stronger inductive coupling effects. In transient eddy current experiments, for instance, agreement with experimental data is limited to later times when feedback effects become less prominent [11]. In other cases, authors often assume non-magnetic samples for experimental validation [1]-[4], constrained sample geometries [4], and resort to fitted parameters [3] or convenient smoothing functions [9]. In some instances [9]-[13], analytical models have been presented with limited or no experimental support. In other cases, solutions are most frequently formulated for time-harmonic excitations for applications in conventional eddy current [15], and less often for general excitations, which include square waveforms for applications in pulsed eddy current.

Recently, a novel analytical approach, whereby electromagnetic field solutions are incorporated directly into Kirchhoff's circuit equations, and solved in terms of an applied voltage (instead of current), was developed [1]. This approach accounts for all electromagnetic interactions arising in inductively coupled systems and, thus, addresses the feedback problem. The theory was applied to the simple case of a driver coil encircling a ferromagnetic conducting rod [17]. The coil's calculated response to a step excitation was in excellent agreement with experimental results. In particular, it was shown that the interaction between the conductor and the driver coil could be

understood and represented as a complex frequency-dependent self-inductance coefficient. Previous works make mention of complex inductances [18], but this phenomenon was not clearly described in terms of electromagnetic processes. The analytical expression for this complex coefficient, which accounts for real (inductive) and imaginary (resistive) elements associated with the rod, fell out of the theory naturally. Thus, electromagnetic field theory and circuit theory have been intuitively combined to provide a complete model of eddy current induction phenomena.

In this work, the theory developed in [1] and [17] is extended to include a pickup coil. The coupled circuit equations, which describe the currents flowing in the driver and pickup, are formulated in terms of a conducting and ferromagnetic rod's impulse response using convolution theory, and solved by Fourier transform. The resulting solutions account for the self-coupling of the driver and pickup coils through the sample (complex self-inductance), and for the mutual coupling of the coils through the sample (complex mutual inductance). All electromagnetic coupling and feedback effects are, therefore, incorporated into the model. Experimental results, obtained for the case of square wave excitation, are in excellent agreement with the analytical equations. The exact time-harmonic solutions, for applications in conventional eddy current testing, are also given.

## II. Theory

A description of the model geometry is as follows. A pickup coil is centered about the axis of a larger encircling driver coil, as shown in Figure 31, where  $b_1 > a_1 > b_2 > a_2$ . These coaxial coils are centered about the axis of a long, ferromagnetic and conducting rod.

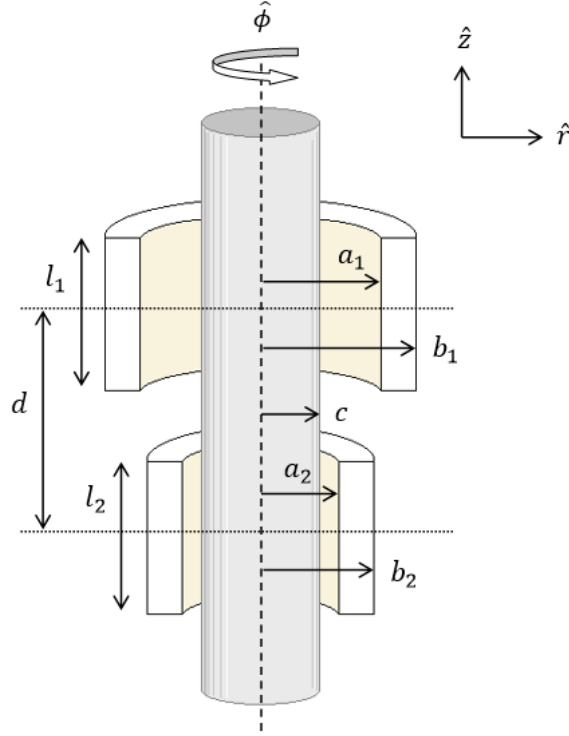


Figure 31: Coaxial driver coil, pickup coil and rod configuration.

In accordance with Maxwell's equations, time-varying currents flowing in the driver and pickup coils will induce eddy currents within the volume of the rod. These eddy currents give rise to transient magnetic fields which, in turn, induce currents within the coils. The circuit equations describing the resultant time-dependent currents  $i_1(t)$  and  $i_2(t)$  flowing in the driver and pickup, respectively, are written using Kirchhoff's laws in the following general form

$$R_1 i_1(t) = v(t) + \varepsilon_1(t), \quad (1)$$

$$R_2 i_2(t) = \varepsilon_2(t), \quad (2)$$

where  $v(t)$  is any time-dependent excitation voltage - step, harmonic, multi-frequency, ramp, sawtooth, etc. -  $R_1$  and  $R_2$  are the total circuit resistances, and  $\varepsilon_1(t)$  and  $\varepsilon_2(t)$  are the total time-dependent voltages induced in the driver and pickup coils, respectively. Both  $\varepsilon_1(t)$  and  $\varepsilon_2(t)$  have

three components; one arising from the field generated by the driver coil, another from the transient field generated by the receiver coil and the third from transient eddy current and magnetization fields emanating from a ferromagnetic conducting sample. Following the steps in [1][17], induced voltages  $\varepsilon_1(t)$  and  $\varepsilon_2(t)$  are expressed as the convolution of the system's impulse response with the as yet unknown time-dependent current functions  $i_1(t)$  and  $i_2(t)$  such that

$$\varepsilon_1(t) = -\frac{2\pi N_1}{l_1(b_1 - a_1)} \frac{d}{dt} \iint_{S_1} r \left( (\hat{\psi}_1(r, z, t) + \hat{\Xi}_1(r, z, t)) * i_1(t) \right. \\ \left. + (\hat{\psi}_2(r, z, t) + \hat{\Xi}_2(r, z, t)) * i_2(t) \right) dr dz, \quad (3)$$

$$\varepsilon_2(t) = -\frac{2\pi N_2}{l_2(b_2 - a_2)} \frac{d}{dt} \iint_{S_2} r \left( (\hat{\psi}_1(r, z, t) + \hat{\Xi}_1(r, z, t)) * i_1(t) \right. \\ \left. + (\hat{\psi}_2(r, z, t) + \hat{\Xi}_2(r, z, t)) * i_2(t) \right) dr dz. \quad (4)$$

where  $\hat{\psi}(r, z, t) = \hat{\psi}(r, z)\delta(t)$  corresponds to the magnetic vector potential generated by a coil carrying an impulse current, and  $\hat{\Xi}(r, z, t)$  is the impulse response of the conducting structure in the air region surrounding the rod. The number in the subscript of  $\hat{\psi}$  and  $\hat{\Xi}$  specifies the coil from which the potentials arise, whereas  $S_1$  and  $S_2$  specify the coil cross-section over which the potential is integrated. Equations (3) and (4) are substituted into the circuit equations in (1) and (2), to which a Fourier transform, defined as  $\mathcal{F}\{f(t)\} \equiv \int_{-\infty}^{\infty} f(t)e^{-j\omega t} dt$  where  $\omega$  is angular frequency, is applied giving

$$R_1 I_1(\omega) = V(\omega) - j\omega \frac{2\pi N_1}{l_1(b_1 - a_1)} \iint_{S_1} r \left( (\hat{\psi}_1(r, z) + \hat{\Xi}_1(r, z, \omega)) I_1(\omega) \right. \\ \left. + (\hat{\psi}_2(r, z) + \hat{\Xi}_2(r, z, \omega)) I_2(\omega) \right) dr dz, \quad (5)$$

$$\begin{aligned}
R_2 I_2(\omega) = -j\omega \frac{2\pi N_2}{l_2(b_2 - a_2)} \iint_{S_2} r \left( (\hat{\psi}_1(r, z) + \hat{\Xi}_1(r, z, \omega)) I_1(\omega) \right. \\
\left. + (\hat{\psi}_2(r, z) + \hat{\Xi}_2(r, z, \omega)) I_2(\omega) \right) dr dz, \tag{6}
\end{aligned}$$

where  $I(\omega) \equiv \mathcal{F}\{i(t)\}$ . Thus, transformed current functions  $I_1(\omega)$  and  $I_2(\omega)$  can be removed from the integrals and the coupled equations can be solved. For conciseness, and in anticipation of the final result, the following definitions are made

$$L_1 \equiv \frac{2\pi N_1}{l_1(b_1 - a_1)} \int_{-\frac{l_1}{2}}^{\frac{l_1}{2}} \int_{a_1}^{b_1} r \hat{\psi}_1(r, z) dr dz, \tag{7}$$

$$L_2 \equiv \frac{2\pi N_2}{l_2(b_2 - a_2)} \int_{-\frac{l_2}{2}}^{\frac{l_2}{2}} \int_{a_2}^{b_2} r \hat{\psi}_2(r, z) dr dz, \tag{8}$$

$$M \equiv \frac{2\pi N_1}{l_1(b_1 - a_1)} \int_{d-\frac{l_1}{2}}^{d+\frac{l_1}{2}} \int_{a_1}^{b_1} r \hat{\psi}_2(r, z) dr dz = \frac{2\pi N_2}{l_2(b_2 - a_2)} \int_{d-\frac{l_2}{2}}^{d+\frac{l_2}{2}} \int_{a_2}^{b_2} r \hat{\psi}_1(r, z) dr dz, \tag{9}$$

$$\mathcal{L}_1 \equiv \frac{2\pi N_1}{l_1(b_1 - a_1)} \int_{-\frac{l_1}{2}}^{\frac{l_1}{2}} \int_{a_1}^{b_1} r \hat{\Xi}_1(r, z, \omega) dr dz, \tag{10}$$

$$\mathcal{L}_2 \equiv \frac{2\pi N_2}{l_2(b_2 - a_2)} \int_{-\frac{l_2}{2}}^{\frac{l_2}{2}} \int_{a_2}^{b_2} r \hat{\Xi}_2(r, z, \omega) dr dz, \tag{11}$$

$$\mathcal{M} \equiv \frac{2\pi N_1}{l_1(b_1 - a_1)} \int_{d-\frac{l_1}{2}}^{d+\frac{l_1}{2}} \int_{a_1}^{b_1} r \hat{\Xi}_2(r, z, \omega) dr dz = \frac{2\pi N_2}{l_2(b_2 - a_2)} \int_{d-\frac{l_2}{2}}^{d+\frac{l_2}{2}} \int_{a_2}^{b_2} r \hat{\Xi}_1(r, z, \omega) dr dz, \tag{12}$$

where  $L_1$  and  $L_2$  are the self-inductance coefficients of the driver and pickup coils respectively and  $M$  is the mutual inductance coefficient. The limits of integration correspond to the dimensions and relative positions of the coils shown in Figure 31. Expressions for equations (7), (8) and (9) have been developed previously in [1] and are given here as

$$L_1 = \frac{8\mu_0 N_1^2}{l_1^2 (b_1 - a_1)^2} \int_0^\infty \int_0^\infty \frac{\gamma \left( \int_{a_1}^{b_1} r J_1(\gamma r) dr \right)^2 \sin^2 \left( \frac{\lambda l_1}{2} \right)}{\lambda^2 (\gamma^2 + \lambda^2)} d\gamma d\lambda, \quad (13)$$

$$L_2 = \frac{8\mu_0 N_2^2}{l_2^2 (b_2 - a_2)^2} \int_0^\infty \int_0^\infty \frac{\gamma \left( \int_{a_2}^{b_2} r J_1(\gamma r) dr \right)^2 \sin^2 \left( \frac{\lambda l_2}{2} \right)}{\lambda^2 (\gamma^2 + \lambda^2)} d\gamma d\lambda, \quad (14)$$

$$M = \frac{8\mu_0 N_1 N_2}{l_1 (b_1 - a_1) l_2 (b_2 - a_2)} \int_0^\infty \frac{\sin \left( \frac{\lambda l_1}{2} \right) \cos(\lambda d) \sin \left( \frac{\lambda l_2}{2} \right)}{\lambda^2} \int_{a_1}^{b_1} r K_1(\lambda r) dr \int_{a_2}^{b_2} r I_1(\lambda r) dr d\lambda, \quad (15)$$

where  $N_1$  and  $N_2$  are the coils' number of turns,  $l_1$  and  $l_2$  are their lengths,  $a_1$  and  $b_1$ , and  $a_2$  and  $b_2$ , are their inner and outer radii, respectively, and  $d$  is the axial distance between the midpoints of the driver and pickup coils as shown in Figure 31. As explained in [1], the double integral expression for the magnetic vector potential generated by a concentric coil,  $\hat{\psi}(r, z, t)$ , converges for all  $r$  and  $z$ , even within the region of the coil itself. The coil's self-inductance is obtained by integrating this expression over the cross-section of the coil. Note that this double integral expression can be compactly expressed in terms of generalized hypergeometric functions [22]. It should be noted that equations (15) is valid for  $a_1 > b_2$ , i.e. the pickup coil lies entirely within the region enclosed by a larger driver coil. Other driver-pickup coil configurations require the appropriate choice, based upon convergence region considerations, for the expression governing the magnetic vector potential (solutions (18) and (19) presented in [1]. Equations (13)-(15) are valid in the low-frequency regime. At higher frequencies, skin effects, parasitic capacitance and electrical resonance effects become apparent [23]. These effects are negligible at the low frequencies considered in this work. Expressions for equations (10), (11) and (12) are developed in what follows.

The magnetic vector potential impulse response, associated with magnetization effects and induced eddy current densities, for the air region surrounding a long ferromagnetic conducting rod has been developed previously in [17] and is given here as

$$\hat{\mathbb{E}}(\mathbf{r}, \mathbf{z}, \omega) = \frac{1}{\pi} \int_0^\infty \mathcal{A}(\lambda, \omega) K_1(\lambda r) \cos(\lambda z) d\lambda, \quad (16)$$

with

$$\mathcal{A}(\lambda, \omega) = \frac{2\mu_0 N}{l(b-a)} \int_a^b r K_1(\lambda r) dr \frac{\sin\left(\frac{\lambda l}{2}\right)}{\lambda} \frac{\mu_r \lambda I_0(\lambda c) I_1(\Lambda c) - \Lambda I_1(\lambda c) I_0(\Lambda c)}{\mu_r \lambda K_0(\lambda c) I_1(\Lambda c) + \Lambda K_1(\lambda c) I_0(\Lambda c)}, \quad (17)$$

$$\Lambda \equiv \sqrt{\lambda^2 + j\omega\mu_r\mu_0\sigma}, \quad (18)$$

where  $c$  is the rod radius,  $\sigma$  is its conductivity and  $\mu_r$  its relative magnetic permeability. Equation (14)

is substituted into equations (10), (11) and (12) giving

$$\mathcal{L}_1 = \frac{8\mu_0 N_1^2}{l_1^2 (b_1 - a_1)^2} \int_0^\infty \left( \int_{a_1}^{b_1} r K_1(\lambda r) dr \right)^2 \frac{\sin^2\left(\frac{\lambda l_1}{2}\right)}{\lambda^2} \frac{\mu_r \lambda I_0(\lambda c) I_1(\Lambda c) - \Lambda I_1(\lambda c) I_0(\Lambda c)}{\mu_r \lambda K_0(\lambda c) I_1(\Lambda c) + \Lambda K_1(\lambda c) I_0(\Lambda c)} d\lambda, \quad (19)$$

$$\mathcal{L}_2 = \frac{8\mu_0 N_2^2}{l_2^2 (b_2 - a_2)^2} \int_0^\infty \left( \int_{a_2}^{b_2} r K_1(\lambda r) dr \right)^2 \frac{\sin^2\left(\frac{\lambda l_2}{2}\right)}{\lambda^2} \frac{\mu_r \lambda I_0(\lambda c) I_1(\Lambda c) - \Lambda I_1(\lambda c) I_0(\Lambda c)}{\mu_r \lambda K_0(\lambda c) I_1(\Lambda c) + \Lambda K_1(\lambda c) I_0(\Lambda c)} d\lambda, \quad (20)$$

$$\begin{aligned} \mathcal{M} &= \frac{8\mu_0 N_1 N_2}{l_1 l_2 (b_1 - a_1)(b_2 - a_2)} \int_0^\infty \int_{a_1}^{b_1} r K_1(\lambda r) dr \int_{a_2}^{b_2} r K_1(\lambda r) dr \\ &\quad \times \frac{\sin\left(\frac{\lambda l_1}{2}\right) \cos(\lambda d) \sin\left(\frac{\lambda l_2}{2}\right)}{\lambda^2} \frac{\mu_r \lambda I_0(\lambda c) I_1(\Lambda c) - \Lambda I_1(\lambda c) I_0(\Lambda c)}{\mu_r \lambda K_0(\lambda c) I_1(\Lambda c) + \Lambda K_1(\lambda c) I_0(\Lambda c)} d\lambda. \end{aligned} \quad (21)$$

$\mathcal{L}_1$  and  $\mathcal{L}_2$  are frequency-dependent complex-valued inductances describing self-coupling of the driver and pickup coil, individually, through the conducting structure [17]. Similarly,  $\mathcal{M}$  describes the mutual coupling of the driver and pickup coils through the sample. Using the coefficients defined in (7)-(12), the Fourier transformed circuit equations in (5) and (6) are concisely re-written as

$$\mathbf{R}_1 \mathbf{I}_1(\omega) = V(\omega) - j\omega(\mathbf{L}_1 + \mathcal{L}_1) \mathbf{I}_1(\omega) - j\omega(\mathbf{M} + \mathcal{M}) \mathbf{I}_2(\omega), \quad (22)$$

$$R_2 I_2(\omega) = -j\omega(M + \mathcal{M})I_1(\omega) - j\omega(L_2 + \mathcal{L}_2)I_2(\omega). \quad (23)$$

Functions  $I_1(\omega)$  and  $I_2(\omega)$  are isolated as

$$I_1(\omega) = \frac{V(\omega)(R_2 + j\omega(L_2 + \mathcal{L}_2))}{(R_1 + j\omega(L_1 + \mathcal{L}_1))(R_2 + j\omega(L_2 + \mathcal{L}_2)) + \omega^2(M + \mathcal{M})^2}, \quad (24)$$

$$I_2(\omega) = \frac{-j\omega V(\omega)(M + \mathcal{M})}{(R_1 + j\omega(L_1 + \mathcal{L}_1))(R_2 + j\omega(L_2 + \mathcal{L}_2)) + \omega^2(M + \mathcal{M})^2}. \quad (25)$$

Finally, the complete time-domain solutions are obtained by applying inverse Fourier transforms to equations (24) and (25) such that

$$i_1(t) = \frac{1}{2\pi} \int_{-\infty}^{\infty} \frac{V(\omega)(R_2 + j\omega(L_2 + \mathcal{L}_2))e^{j\omega t}}{(R_1 + j\omega(L_1 + \mathcal{L}_1))(R_2 + j\omega(L_2 + \mathcal{L}_2)) + \omega^2(M + \mathcal{M})^2} d\omega, \quad (26)$$

$$i_2(t) = \frac{1}{2\pi} \int_{-\infty}^{\infty} \frac{-j\omega V(\omega)(M + \mathcal{M})e^{j\omega t}}{(R_1 + j\omega(L_1 + \mathcal{L}_1))(R_2 + j\omega(L_2 + \mathcal{L}_2)) + \omega^2(M + \mathcal{M})^2} d\omega, \quad (27)$$

where  $V(\omega)$  is the Fourier transform of an arbitrary time-dependent function. A sinusoidal function is appropriate for applications in conventional eddy current. Then  $v(t) = v_0 \sin(\omega t)$  where  $v_0$  is the amplitude of a sinusoid with angular frequency  $\omega$ . Its Fourier transform [21] is

$$V(\omega) = -j\pi v_0 (\delta(\omega - \omega) - \delta(\omega + \omega)). \quad (28)$$

Equation (28) is substituted into equations (26) and (27) to obtain

$$i_1(t) = -\frac{jv_0}{2} \left( \frac{(R_2 + j\omega(L_2 + \mathcal{L}_2))e^{j\omega t}}{(R_1 + j\omega(L_1 + \mathcal{L}_1))(R_2 + j\omega(L_2 + \mathcal{L}_2)) + \omega^2(M + \mathcal{M})^2} - \frac{(R_2 - j\omega(L_2 + \mathcal{L}_2))e^{-j\omega t}}{(R_1 - j\omega(L_1 + \mathcal{L}_1))(R_2 - j\omega(L_2 + \mathcal{L}_2)) + \omega^2(M + \mathcal{M})^2} \right), \quad (29)$$

$$i_2(t) = -\frac{jv_0}{2} \left( \frac{j\varpi(M + \mathcal{M})e^{j\varpi t}}{(\mathcal{R}_1 + j\varpi(L_1 + \mathcal{L}_1))(\mathcal{R}_2 + j\varpi(L_2 + \mathcal{L}_2)) + \varpi^2(M + \mathcal{M})^2} - \frac{-j\varpi(M + \mathcal{M})e^{-j\varpi t}}{(\mathcal{R}_1 - j\varpi(L_1 + \mathcal{L}_1))(\mathcal{R}_2 - j\varpi(L_2 + \mathcal{L}_2)) + \varpi^2(M + \mathcal{M})^2} \right). \quad (30)$$

The second term is the complex conjugate of the first in both equations (29) and (30). The difference of a function with its complex conjugate is equal to twice the imaginary part of that function, and so equations (29) and (30) are rewritten as

$$i_1(t) = v_0 \text{Im} \left( \frac{(\mathcal{R}_2 + j\varpi(L_2 + \mathcal{L}_2))e^{j\varpi t}}{(\mathcal{R}_1 + j\varpi(L_1 + \mathcal{L}_1))(\mathcal{R}_2 + j\varpi(L_2 + \mathcal{L}_2)) + \varpi^2(M + \mathcal{M})^2} \right), \quad (31)$$

$$i_2(t) = v_0 \text{Im} \left( \frac{j\varpi(M + \mathcal{M})e^{j\varpi t}}{(\mathcal{R}_1 + j\varpi(L_1 + \mathcal{L}_1))(\mathcal{R}_2 + j\varpi(L_2 + \mathcal{L}_2)) + \varpi^2(M + \mathcal{M})^2} \right). \quad (32)$$

Solutions (31) and (32) may be recast in terms of trigonometric functions such that

$$i_1(t) = v_0 \left( \frac{\alpha\varpi(L_2 + \Re(\mathcal{L}_2)) - \beta(\mathcal{R}_2 - \varpi\Im(\mathcal{L}_2))}{\alpha^2 + \beta^2} \cos(\varpi t) + \sin(\varpi t) \frac{\beta\varpi(L_2 + \Re(\mathcal{L}_2)) + \alpha(\mathcal{R}_2 - \varpi\Im(\mathcal{L}_2))}{\alpha^2 + \beta^2} \right), \quad (33)$$

$$i_2(t) = v_0\varpi \left( \frac{(\alpha(M + \Re(\mathcal{M})) + \beta\Im(\mathcal{M})) \cos(\varpi t) + \sin(\varpi t) (\beta(M + \Re(\mathcal{M})) - \alpha\Im(\mathcal{M}))}{\alpha^2 + \beta^2} \right), \quad (34)$$

where

$$\alpha \equiv (\mathcal{R}_1 - \varpi\Im(\mathcal{L}_1))(\mathcal{R}_2 - \varpi\Im(\mathcal{L}_2)) - \varpi^2(L_1 + \Re(\mathcal{L}_1))(L_2 + \Re(\mathcal{L}_2)) + \varpi^2(\Im(\mathcal{M})^2 - (M + \Re(\mathcal{M}))^2) \quad (35)$$

$$\beta \equiv \varpi(L_2 + \Re(\mathcal{L}_2))(\mathcal{R}_1 - \varpi\Im(\mathcal{L}_1)) + \varpi(L_1 + \Re(\mathcal{L}_1))(\mathcal{R}_2 - \varpi\Im(\mathcal{L}_2)) + 2\varpi^2\Im(\mathcal{M})(M + \Re(\mathcal{M})) \quad (36)$$

Equations (33) and (34) may, alternatively, be re-expressed as phase-shifted sine waves such that

$$i_1(t) = v_0 \sqrt{\frac{\varpi^2 (\mathcal{L}_2 + \Re(\mathcal{L}_2))^2 + (\mathcal{R}_2 - \varpi \Im(\mathcal{L}_2))^2}{\alpha^2 + \beta^2}} \sin(\varpi t - \arctan\left(\frac{(\mathcal{R}_2 - \varpi \Im(\mathcal{L}_2))\beta - \alpha\varpi(\mathcal{L}_2 + \Re(\mathcal{L}_2))}{(\mathcal{L}_2 + \Re(\mathcal{L}_2))\beta\varpi + \alpha(\mathcal{R}_2 - \varpi \Im(\mathcal{L}_2))}\right)), \quad (37)$$

$$i_2(t) = v_0 \varpi \sqrt{\frac{(\mathcal{M} + \Re(\mathcal{M}))^2 + \Im(\mathcal{M})^2}{\alpha^2 + \beta^2}} \sin\left(\varpi t - \arctan\left(\frac{\Im(\mathcal{M})\beta + \alpha(\mathcal{M} + \Re(\mathcal{M}))}{\Im(\mathcal{M})\alpha - \beta(\mathcal{M} + \Re(\mathcal{M}))}\right)\right), \quad (38)$$

Equations (37) and (38) are the exact closed-form solutions to circuit equations (1) and (2) given a harmonic excitation for applications in conventional eddy current testing.

Consider an arbitrary excitation waveform  $v(t)$  expressed as a Fourier series. Its Fourier transform,  $V(\omega)$ , will always consist of a weighted sum of Dirac delta functions whose effect, under the integrals in equations (26) and (27), is to select out a set of particular frequencies in accordance with the sampling theorem. Thus, frequency-dependent functions  $\mathcal{L}_1$ ,  $\mathcal{L}_2$  and  $\mathcal{M}$  need only be evaluated at specific frequencies, and the integral becomes a readily computable sum. Consider a square-wave excitation for applications in transient eddy current testing. The Fourier series representation of a square wave with pulse duration  $P$  (period  $2P$ ), amplitude  $v_0$  and a 50% duty cycle is given as

$$v(t) = \frac{v_0}{2} + \frac{2v_0}{\pi} \sum_{n=1}^{\infty} \frac{\sin\left(\frac{(2n-1)\pi}{P} t\right)}{2n-1}, \quad (39)$$

whose Fourier transform is

$$V(\omega) = \pi v_0 \delta(\omega) + \frac{2\pi v_0}{P} \sum_{n=1}^{\infty} \frac{\delta(\omega - \varpi_n)}{j\varpi_n} + \frac{2\pi v_0}{P} \sum_{n=1}^{\infty} \frac{\delta(\omega + \varpi_n)}{-j\varpi_n}, \quad (40)$$

where we have defined

$$\varpi_n \equiv \frac{(2n-1)\pi}{P}. \quad (41)$$

The pulse duration is made sufficiently long so that any eddy current signals decay to undetectable levels. The duty cycle is unimportant in this case, since only the leading edge of the waveform is considered. Equation (40) is substituted into solutions (26) and (27). As before, the second summation term is the complex conjugate of the first. The sum, however, of a function with its complex conjugate is equivalent to twice the real component of the function. Thus, the resulting solutions are written as

$$i_1(t) = \frac{v_0}{2R_1} + \frac{2v_0}{P} \sum_{n=1}^{\infty} \operatorname{Re} \left( \frac{e^{j\varpi_n t}}{j\varpi_n} \frac{R_2 + j\varpi_n(L_2 + \mathcal{L}_2)}{(R_1 + j\varpi_n(L_1 + \mathcal{L}_1))(R_2 + j\varpi_n(L_2 + \mathcal{L}_2)) + \varpi_n^2(M + \mathcal{M})^2} \right), \quad (42)$$

$$i_2(t) = -\frac{2v_0}{P} \sum_{n=1}^{\infty} \operatorname{Re} \left( \frac{(M + \mathcal{M})e^{j\varpi_n t}}{(R_1 + j\varpi_n(L_1 + \mathcal{L}_1))(R_2 + j\varpi_n(L_2 + \mathcal{L}_2)) + \varpi_n^2(M + \mathcal{M})^2} \right), \quad (43)$$

where  $\mathcal{L}_1$ ,  $\mathcal{L}_2$  and  $\mathcal{M}$  need only be evaluated at  $\omega = \varpi_n$  for each  $n$ . Solutions (42) and (43) are rewritten in terms of trigonometric functions

$$i_1(t) = \frac{v_0}{2R_1} + \frac{2v_0}{P} \sum_{n=1}^{\infty} \left( \frac{\alpha_n \varpi_n (L_2 + \Re(\mathcal{L}_2)) - \beta_n (R_2 - \varpi_n \Im(\mathcal{L}_2))}{\varpi_n (\alpha_n^2 + \beta_n^2)} \cos(\varpi_n t) \right. \\ \left. + \sin(\varpi_n t) \frac{\beta_n \varpi_n (L_2 + \Re(\mathcal{L}_2)) + \alpha_n (R_2 - \varpi_n \Im(\mathcal{L}_2))}{\varpi_n (\alpha_n^2 + \beta_n^2)} \right), \quad (44)$$

$$i_2(t) = -\frac{2v_0}{P} \sum_{n=1}^{\infty} \left( \frac{\alpha_n (M + \Re(\mathcal{M})) + \beta_n \Im(\mathcal{M})}{\alpha_n^2 + \beta_n^2} \cos(\varpi_n t) \right. \\ \left. + \sin(\varpi_n t) \frac{\beta_n (M + \Re(\mathcal{M})) - \alpha_n \Im(\mathcal{M})}{\alpha_n^2 + \beta_n^2} \right), \quad (45)$$

where  $\alpha_n$  and  $\beta_n$  are defined in (35) and (36), and where  $\varpi_n$  is defined in (41). Equations (44) and (45) are re-expressed as summations of phase-shifted sine waves such that

$$i_1(t) = \frac{2v_0}{P} \sum_{n=1}^{\infty} \frac{1}{\varpi_n} \sqrt{\frac{\varpi_n^2 (L_2 + \Re(\mathcal{L}_2))^2 + (R_2 - \varpi_n \Im(\mathcal{L}_2))^2}{\alpha_n^2 + \beta_n^2}} \sin(\varpi_n t - \arctan\left(\frac{(R_2 - \varpi_n \Im(\mathcal{L}_2))\beta_n - \alpha_n \varpi_n (L_2 + \Re(\mathcal{L}_2))}{(L_2 + \Re(\mathcal{L}_2))\beta_n \varpi_n + \alpha_n (R_2 - \varpi_n \Im(\mathcal{L}_2))}\right)), \quad (46)$$

$$i_2(t) = \frac{2v_0}{P} \sum_{n=1}^{\infty} \sqrt{\frac{(M + \Re(\mathcal{M}))^2 + \Im(\mathcal{M})^2}{\alpha_n^2 + \beta_n^2}} \sin\left(\varpi t - \arctan\left(\frac{\Im(\mathcal{M})\beta_n + \alpha_n (M + \Re(\mathcal{M}))}{\Im(\mathcal{M})\alpha_n - \beta_n (M + \Re(\mathcal{M}))}\right)\right). \quad (47)$$

Equations (46) and (47) are the final solutions describing the resultant currents flowing through the driver and pickup coils, respectively, when coupled to a ferromagnetic conducting structure and driven by a square waveform voltage with amplitude  $v_0$  and period  $P$ .

### III. Experimental Results

A power supply with an internal resistance of  $2.46 \, \Omega$  was used to generate a  $4.53 \, \text{V}$  square pulse excitation. Coaxial cables with negligible losses route the pulse through a  $2.00 \, \Omega$  resistor to a  $80.8 \, \Omega$  driving coil. A  $47.6 \, \Omega$  pickup coil was connected in series with a  $50.0 \, \Omega$  termination resistor and to a National Instruments signal acquisition card (NI6211 USB DAQ board). Transient voltages were measured across the  $2.00 \, \Omega$  and  $50.0 \, \Omega$  resistors in the driver and receiver circuits, respectively, at  $2 \, \mu\text{s}$  intervals. The transient currents flowing through the circuits are related to the experimentally measured voltages in accordance with Ohm's Law (i.e.  $i_{1,\text{exp}} = v_{1,\text{exp}}/2.00\Omega$  and  $i_{2,\text{exp}} = v_{2,\text{exp}}/50.0\Omega$ ). The coupled inductor circuit is depicted in Figure 32.

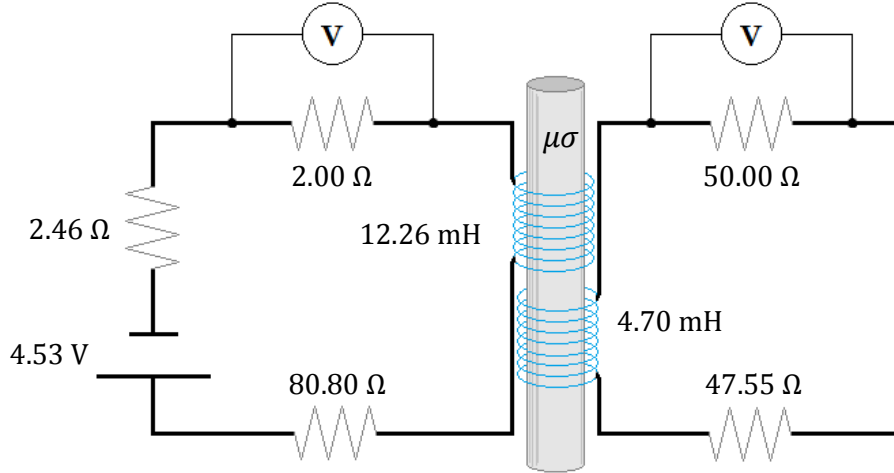


Figure 32: Experimental driver and pickup circuit diagram.

The coils were carefully wound with known number of turns, uniform turns density and windings exactly perpendicular to coil axes. The centers of the coaxial coils forming the probe are separated by a distance  $d$  of 0.025 mm along the axis. The characteristics of the experimental coils and rods are listed in Table XIII below.

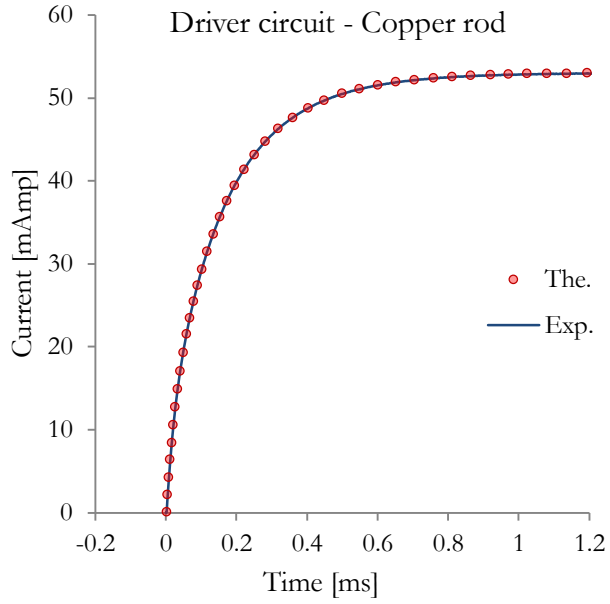
Table XIII: Experimental coil and rod characteristics.

<b>Coil:</b>	<b>Driver</b>	<b>Receiver</b>	<b>Rod :</b>	<b>Copper</b>	<b>Brass</b>	<b>Steel</b>
Number of turns :	991	787	Radius [mm] :	3.172	3.191	3.005
Wire gage [AWG] :	36	36	Conductivity [ $\text{MS}\cdot\text{m}^{-1}$ ] :	58.14	12.44	4.30
Length [mm] :	14.97	14.98	Relative Permeability :	1	1	97.2
Inner radius [mm] :	8.21	5.93				
Outer radius [mm] :	9.47	7.03				
Resistance [ $\Omega$ ] :	80.80	47.55				
Inductance [mH] :	12.26	4.70				

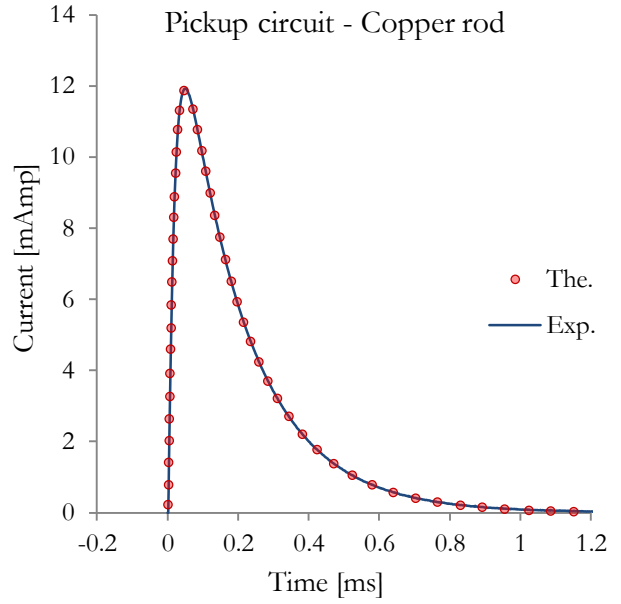
A comparison between experimental and theoretical values for the driver and pickup coil self-inductances has been performed in [1]. The theoretical values for  $L_1$  and  $L_2$ , calculated using

equations (13) and (14) and listed in table 1, are in good agreement with the experimentally measured values, 12.249 mH and 4.707 mH respectively. The conductivity of the rod was measured using the four-point method, and the relative magnetic permeability, calculated using an extension of the theory developed here and presented in [22], is typical of steels [23].

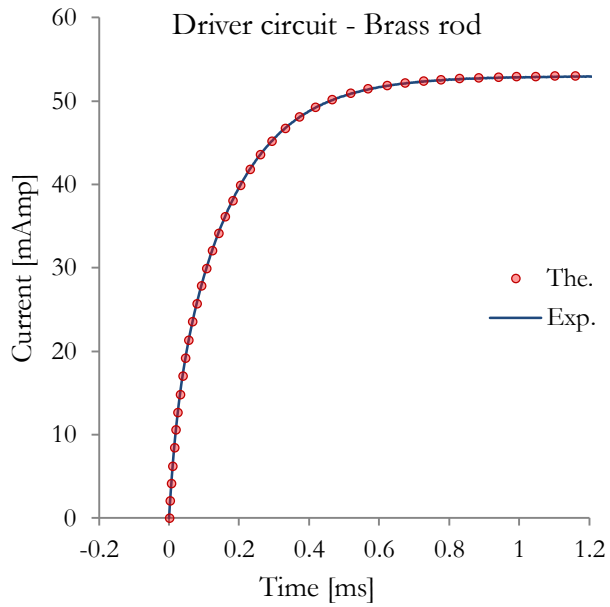
Solutions (46) and (47) are plotted, using the values listed in Table XIII, and compared with experimental results for rods, which are non-conducting and non-magnetic (air), conducting and non-magnetic (copper and brass), and conducting and magnetic (steel). Results were computed from the solutions using Maplesoft's *Maple 18* software. The frequency-dependent integral expressions  $\mathcal{L}_1$ ,  $\mathcal{L}_2$  and  $\mathcal{M}$  were calculated numerically with NAG method d01akc, which uses adaptive Gauss 30-point and Kronrod 61-point rules. In order to assure convergence, the summation was truncated at 300 terms for a 3 ms square wave pulse, which corresponds to a maximum frequency of 100 kHz. Each term required the evaluation of the real and imaginary parts of functions  $\mathcal{L}_1$ ,  $\mathcal{L}_2$  and  $\mathcal{M}$ , corresponding to six numerical integrations per term. On average, 22 minutes were required, using an Intel® Core™ i7-4820K CPU at 3.70 GHz, to compute both the driver and the pickup response.



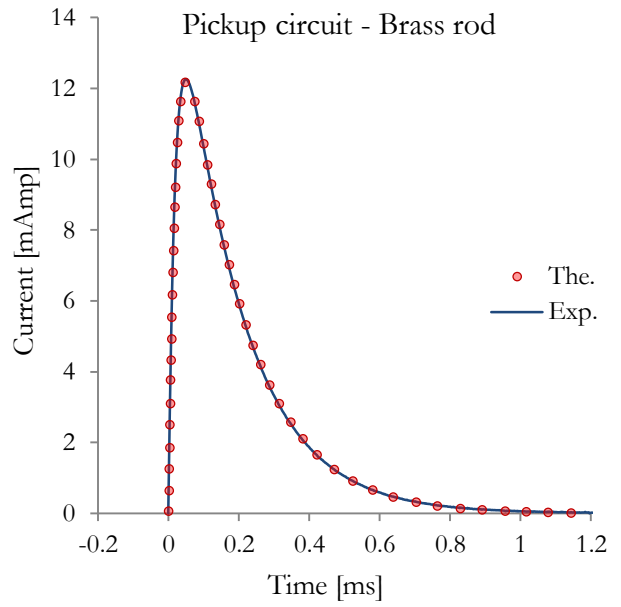
(a)



(b)



(c)



(d)

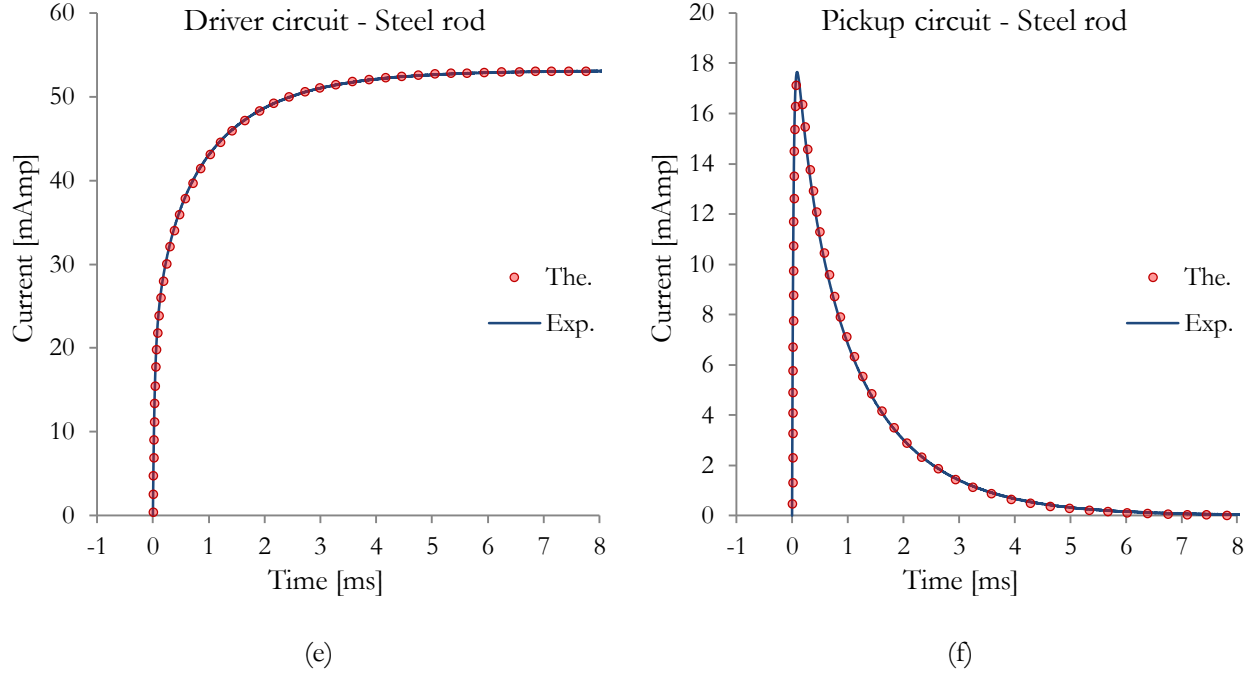


Figure 33: Experimental and theoretical results of the transient currents in the driver and pickup circuits, respectively, following the application of a square wave excitation. The coils are in a coaxial driver-pickup configuration and encircle a copper rod (a)(b), a brass rod (c)(d) and a steel rod (e)(f).

The experimental results are in excellent agreement with the theory. This confirms the validity of the solutions and of the complex-valued self- and mutual coupling coefficients,  $\mathcal{L}$  and  $\mathcal{M}$ , respectively. The theory, from which these experimentally validated solutions have emerged, sets the stage for the consideration of different conducting structure geometries, different probe configurations and arbitrary excitation waveforms.

## IV. Discussion

A novel approach for the calculation of induced electrical transients under voltage control, which was developed in [1] and applied for the case of a driver coil coupled to a ferromagnetic conducting structure [17], was extended here to consider a system including both a driver and a pickup coil. Additional complex frequency-dependent inductance effects, which describe the electromagnetic interactions between coils and ferromagnetic conducting structures, have emerged

from the theory. These quantities, denoted as  $\mathcal{L}_1$ ,  $\mathcal{L}_2$  and  $\mathcal{M}$  depend on the geometry and material characteristics of the conducting structure and on the interacting coils, as expected. Whereas  $L_1$  and  $L_2$  represent direct self-coupling of the driver and pickup coils, respectively,  $\mathcal{L}_1$  and  $\mathcal{L}_2$  are interpreted as the indirect self-coupling of the coils through the sample. In the same fashion,  $M$ , the mutual inductance coefficient, represents the direct coupling of the driver and the pickup coils. The complex mutual inductance coefficient,  $\mathcal{M}$ , represents the indirect coupling of the coils through the sample. These coupling effects are schematically represented in Figure 30 below.

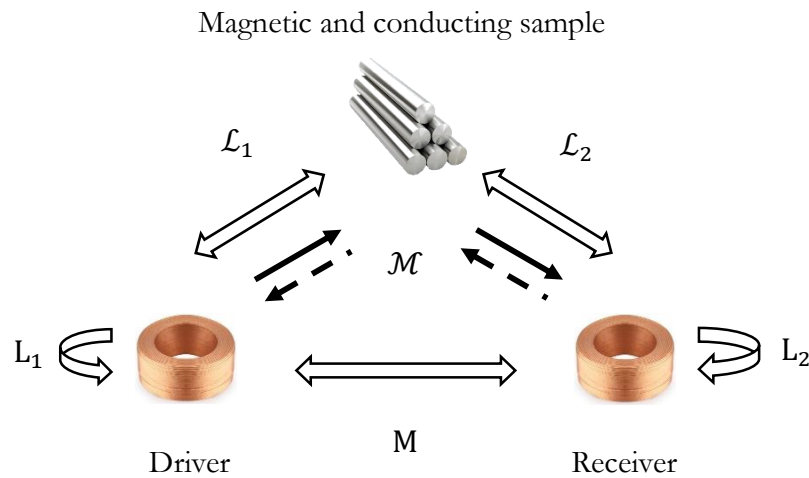


Figure 34: Schematic description of the coupling coefficients.

These complex coefficients account for real (inductive) and imaginary (resistive) elements associated with a conducting sample. As explained in [17], it may be more natural to consider the coupling effects of the material using complex inductances  $\mathcal{L}$  and  $\mathcal{M}$ , since they arise naturally from the theory, as opposed to the complex impedance  $Z$ , which is defined by convention as  $R + j\omega L$ .

In previous transient driver-pickup models [9]-[13], the pickup coil's self-inductance ( $L_2$ ) and self-coupling effects ( $\mathcal{L}_2$ ) have been neglected. Specifically in these works, the step-function response of a conducting sample was derived, convoluted with a fitted or measured driver signal using

Duhamel's Theorem, and integrated over the cross-section of a receiver coil. Therefore, this formulation only considers the fields associated with the driver coil, and is equivalent to considering only the first term on the right-hand-side of equation (23), such that

$$R_2 I_2(\omega) = -j\omega(M + \mathcal{M})I_1(\omega). \quad (48)$$

Note that equation 48 corresponds to the Dodd and Deeds formalism (Eqn. (94) on page 2837 in [15]). In reality, two fields exist in superposition; one arising from the driver coil, and another from the receiver coil. This was also noted by Burke et. al. [2]. The correction brought forth in this work incorporates the additional self-inductance and material coupling effects associated with the pickup. The correct formulation for the pickup signal is given in equation (23) of this work, and can be rearranged as

$$R_2 I_2(\omega) = \frac{-j\omega(M + \mathcal{M})}{1 + \frac{j\omega(L_2 + \mathcal{L}_2)}{R_2}} I_1(\omega). \quad (49)$$

Clearly, equation (49) reduces to the Dodd and Deeds formalism in cases where the effects of a pickup coil on a system can be neglected - i.e. when

$$\frac{j\omega(L_2 + \mathcal{L}_2)}{R_2} \ll 1. \quad (50)$$

At low frequencies, when small self-inductances and large resistances are present, very little current will flow in the pickup coil, thereby having a negligible effect on the system. However, since transient eddy currents encompass an infinite set of frequencies, the condition in (50) cannot be maintained and the Dodd and Deeds formalism, equation (48), breaks down. The approximation is made worse when ferromagnetic materials are considered, since they amplify the coupling of the pickup coil with the sample - i.e.  $\mathcal{L}_2$  is increased

The typical approach to circumvent feedback effects, and thereby justify the use of the Dodd and Deeds approximation, has been to consider open pickup circuits and to employ sophisticated, and often expensive, current control systems. The open-circuit requirement for the pick-up coil applies engineering limitations on the eddy current technology. Similarly, the requirement for an invariant current excitation, which could be achieved under current control, is also an engineering limit, particularly, since most measurements are done under voltage control. There are good examples for which such engineering limits would be undesirable. For example, in eddy current array probes, driver and pick-up coils may be alternated in order to maximize coverage and to minimize the number of coils. Switching large resistances in and out would be possible, but significantly more complicated. Signal-to-noise may also be compromised by the high impedance requirement, since maximum power transfer occurs when impedances are matched. Current control presents an ‘engineering limit’, since under large back-emf conditions, such as coils in the presence of ferromagnetic materials or transformers, the technology becomes more challenging to implement [24].

## V. Summary

An approach developed in [1], which has enabled the correct formulation of solutions to eddy-current induction problems under voltage control, was applied to the case of a coaxial driver-pickup probe encircling a long ferromagnetic conducting rod. Coupled circuit equations were formulated in terms of the rod’s impulse response using convolution theory. Analytical expressions for complex inductances in the circuit, which accounts for real (inductive) and imaginary (loss) elements associated with the rod, have arisen from the theory. Solutions describing the time-dependant currents flowing through the driver and pickup coils, for applications in both conventional and pulsed eddy current, were developed. The former are in closed-form and the latter in series-form.

The final solutions account for all electromagnetic coupling effects arising in the system, and are the first in the literature to provide correct voltage responses in driver-pickup configurations. Experimental results, obtained for the case of square wave excitation, were in excellent agreement with the analytical equations. Furthermore, the theory is valid for any ferromagnetic conducting structure provided that the complex coupling coefficients can be obtained by solving the corresponding boundary value problem. Thus, this theory can be straightforwardly extended to inductive circuit problems containing other geometries, such as half-spaces, plates, rods, tubes, spheres and right-angled wedges for instance. Ultimately, model-assisted analyses of experimental data may provide a direct method of extracting values such as liftoff, wall thickness, conductivity, permeability, and other parameters of interest. This is left as future work.

## VI. References

- [1] Bowler JR, Theodoulidis TP. Coil impedance variation due to induced current at the edge of a conductive plate. *J Phys D: Appl Phys* 2006;39:2862-2868.
- [2] Burke SK, Ibrahim ME. Mutual impedance of air-cored coils above a conductive plate. *J Phys D: Appl Phys* 2004;37:1857-1868.
- [3] Simm A, Theodoulidis T, Poulakis N, Tian GY. Investigation of the magnetic field response from eddy current inspection of defects. *Int J Adv Manuf Technol* 2011;54:223–230.
- [4] Harfield N, Bowler JR. Solution of the two-dimensional problem of a crack in a uniform field in eddy-current non-destructive testing. *J Phys D: Appl Phys* 1995;28:2197-2205.
- [5] Bowler JR, Theodoulidis T. Eddy currents induced in a conducting rod of finite length by a coaxial encircling coil. *J Phys D: Appl Phys* 2005;38:2861–2868
- [6] Bowler JR, Theodoulidis T, Xie H, Ji Y. Evaluation of eddy-current probe signals due to cracks in fastener holes. *IEEE Trans on Magn* 2012;48:1159-1170.

- [7] Burke SK, Theodoulidis T. Impedance of a horizontal coil in a borehole: a model for eddy current borehole probes. *J Phys D: Appl Phys* 2004;37:485-494.
- [8] Bowler JR. Thin-skin eddy-current inversion for the determination of crack shapes. *Inverse Problems* 2002;18:1891-1905.
- [9] Fan M, Huang P, Ye B, Hou D, Zhang G, Zhou Z. Analytical modeling for transient probe response in pulsed eddy current testing. *NDT & E Int* 2009;42:376-383.
- [10] Theodoulidis T. Developments in calculating the transient eddy-current response from a conductive plate. *IEEE Trans on Magn* 2008;44:1894-1896.
- [11] Morozova GM, Polygalov VF, Epov MI, Mogilatov VS. Transient electromagnetic field of a current loop centered on the axis of a hollow magnetic cylinder. *Russian Geo and Geophys* 2000;41:1435-1444.
- [12] Epov MI, Morazova GM, Yu Antonov E. Electromagnetic processes in a conducting magnetic casing string. *Russian Geo and Geophys* 2007;48:523-531.
- [13] Desjardins D, Krause TW, Gauthier N. Analytical modeling of the transient response of a coil encircling a ferromagnetic conducting rod in pulsed eddy current testing. *NDT&E Int* 2013;60:127-131.
- [14] S.K. Burke, G.R. Hugo and D.J Harrison, 1998, "Transient eddy-current NDE for hidden corrosion in multilayer structures," *Review of Progress in QNDE*, Vol. 17A, eds. D.O. Thompson and D.E. Chimenti, (Plenum, New York), pp. 307-314
- [15] Dodd CV, Deeds WE. Analytical solutions to eddy-current probe-coil problems. *J Appl Phys* 1968;39:2829-2838.
- [16] Desjardins DR, et al. Concerning the derivation of exact solutions to inductive circuit problems for eddy current testing. *NDT&E Int* (2014), <http://dx.doi.org/10.1016/j.ndteint.2014.07.008>.

- [17] Desjardins D, Krause TW, Clapham L. (2014) Transient Response of a Driver Coil in Pulsed Eddy Current Testing. Manuscript submitted for publication.
- [18] Moulder JC, Tai C, Larson BF, Rose JH. Inductance of a coil on a thick ferromagnetic plate. IEEE Trans on Magn 1999;34:505-514.
- [19] J.T. Cowway. Analytical solutions for the self- and mutual inductance of concentric coplanar disk coils. IEEE transactions on magnetics, Vol. 49, No. 3, March 2013, pp 1135-1142.
- [20] D.J. Harrison, L.D. Jones, S.K. Burke, Posada, "Benchmark problems for defect size and shape determination in eddy-current non-destructive evaluation", Journal of Non-destructive Evaluation, Vol.15, No.1, pp.21-34, 1996.
- [21] Kammler D. A First Course in Fourier Analysis. New York: University Press; 2000.
- [22] D.R. Desjardins, T.K. Krause, L. Clapham. Simultaneous evaluation of material parameters using transient eddy current models. Proceedings of the 19<sup>th</sup> International Workshop on Electromagnetic Nondestructive Evaluation, June 25-28, 2014, Xi'an. (submitted for publication)
- [23] Woolman J, Mottram RA. Mechanical and Physical Properties of the BS En Steels. Pergamon Press;1964.
- [24] S. White, L. Clapham and T.W. Krause, A multi-channel magnetic flux controller for periodic magnetizing conditions. IEEE Trans. Instr. and Meas. 61, no. 7, (2012) pp. 1896-1907.

**Manuscript 4:** “*Transient response of a driver-pickup probe encircling a ferromagnetic conducting tube*”. NDT&E Intl. In preparation for submission 25 May 2015.

Author contributions: D.R Desjardins (theory, experiment, primary writer), T.W. Krause (editor, literature survey suggestions), and L. Clapham.

# Transient response of a driver-pickup probe encircling a ferromagnetic conducting tube

D. Desjardins<sup>1\*</sup>, T.W. Krause<sup>2</sup> and L. Clapham<sup>1</sup>

1. *Department of Physics, Queen's University, Kingston, ON, Canada, K7L 3N6*

2. *Department of Physics, Royal Military College of Canada, Kingston, ON, Canada, K7K 7B4*

**Abstract** – Recent analytical solutions, that correctly describe transient eddy current signals in driver-pickup circuits, are applied for the case of a coaxial probe encircling a long ferromagnetic conducting tube. The differential circuit equations are formulated in terms of the complex self- and mutual inductance functions associated with the tube, and solved by Fourier transform. The solutions presented here are the first to account for feedback between a ferromagnetic conducting tube and the driver and pickup coils, providing correct signal response of the coils. Experimental results, obtained for the case of square wave excitation, are in excellent agreement with the analytical equations.

**Key Words**– Transient; Eddy Current; Analytical; Tube

## I. Introduction

Conventional eddy current inspection of equipment and infrastructure is a critical element in all industrial maintenance operations. Analytical models, built upon the original 1968 Dodd and Deeds formalism [15], have been used to enhance analysis and information, extracted from signals obtained using electromagnetic non-destructive evaluation technologies. However, in cases where two or more coils are involved, these models fail to yield results consistent with experimental observations [2]-[6]. Ferromagnetic conductors, which are commonly encountered in industry,

---

\* *Corresponding author:* dandesja@gmail.com

exhibit stronger and, therefore, more complicated feedback effects between driver, pickup and sample circuit elements. Since driver-pickup transient eddy current non-destructive testing is an increasingly popular technique for the inspection and characterization of metallic objects, solutions that correctly incorporate all inductive coupling interactions arising in inductively coupled circuits, are of significant interest. Exact mathematical models would facilitate the quantitative analysis and interpretation of experimental signals obtained from particular inspection geometries, thereby enhancing the potential applicability of transient eddy current non-destructive evaluation.

The Dodd and Deeds formalism does not account for the effects of the pickup coil on a system. Specifically, their model [15] does not include values for the pickup coil's resistance and self-inductance. Furthermore, currents induced in the pickup also modify and redistribute the eddy current density within the sample. These coupling effects are also neglected by this formalism. Recently, a complete analytical description of a driver-pickup circuit has been developed in [1]-[9] and applied for the case of a ferromagnetic conducting rod structure. The final solutions contain complex frequency-dependant self- and mutual induction coefficients that represent the direct and indirect coupling of the coils with the conducting structure [9]. Experimental results, obtained for the case of square wave excitation, are in excellent agreement with the analytical predictions, and validate the correction brought forth to the Dodd and Deeds formalism.

In this paper, this new formalism [9] is applied for the case of a driver-pickup probe encircling a conducting tube. The appropriate boundary value problem is solved in the same manner as in [8]. An encircling tandem driver-pickup probe was constructed and experimental results obtained for square waveforms. The complete agreement between theory and experiment further supports the solutions developed in [9].

## II. Forward Problem

A description of the model geometry is as follows. A pickup coil is centered about the axis of a larger encircling driver coil. These coaxial coils are centered about the axis of a long, ferromagnetic and conducting tube as shown in Figure 31.

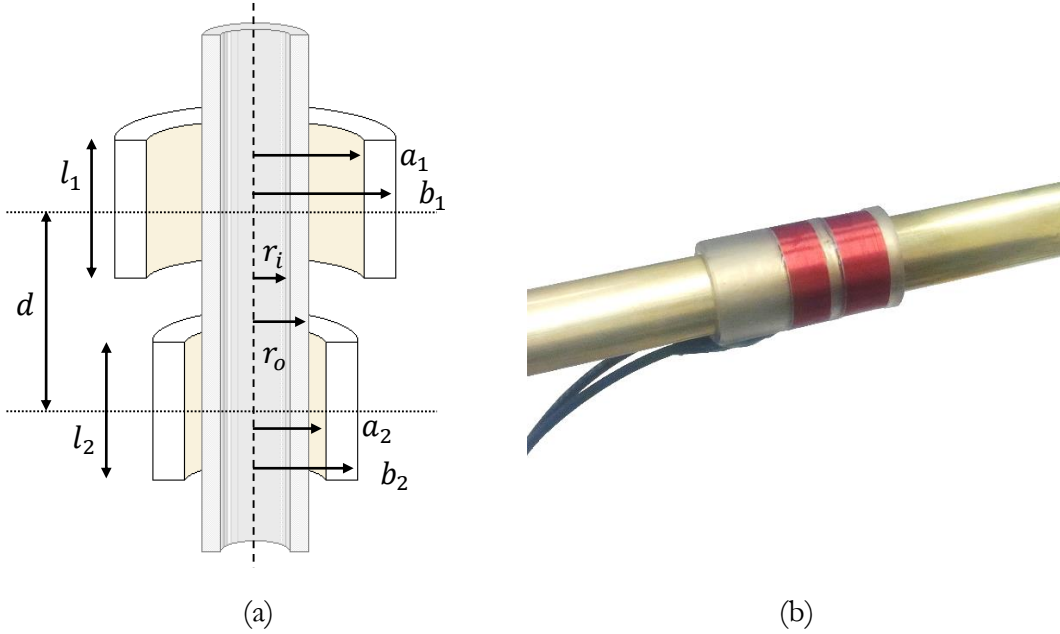


Figure 35: Coaxial driver coil, pickup coil and tube configuration; (a) diagram, (b) experiment.

Time-varying currents flowing in the driver and pickup coils will induce eddy currents within the volume of the tube. These eddy currents give rise to transient magnetic fields which, in turn, induce currents within the coils. The general solutions to the circuit equations describing time-dependent currents  $i_1(t)$  and  $i_2(t)$  flowing in the driver and pickup, respectively, have been developed in [9] and are written here as

$$i_1(t) = \frac{1}{2\pi} \int_{-\infty}^{\infty} \frac{V(\omega)(R_2 + j\omega(L_2 + \mathcal{L}_2))e^{j\omega t}}{(R_1 + j\omega(L_1 + \mathcal{L}_1))(R_2 + j\omega(L_2 + \mathcal{L}_2)) + \omega^2(M + \mathcal{M})^2} d\omega, \quad (1)$$

$$i_2(t) = \frac{1}{2\pi} \int_{-\infty}^{\infty} \frac{-j\omega V(\omega)(M + \mathcal{M})e^{j\omega t}}{(R_1 + j\omega(L_1 + \mathcal{L}_1))(R_2 + j\omega(L_2 + \mathcal{L}_2)) + \omega^2(M + \mathcal{M})^2} d\omega, \quad (2)$$

where  $V(\omega)$  is the Fourier transform of an arbitrary excitation function  $v(t)$  - step, harmonic, multi-frequency, ramp, saw-tooth, etc. -  $L_1$  and  $L_2$  are the coils' self-inductances,  $R_1$  and  $R_2$  are the total driver and pickup circuits' resistances, and  $M$  is a mutual inductance coefficient. Additionally,  $\mathcal{L}_1$  and  $\mathcal{L}_2$  are complex inductances arising from the self-coupling of the driver and pickup coils through the sample, and  $\mathcal{M}$  is a complex mutual inductance coefficient arising from cross-coupling between the coils through the sample. Mathematically, the effects of the conducting, and possibly ferromagnetic, structure on an eddy current signal are represented by these coupling coefficients. The different inductive coupling effects are schematically represented in Figure 30 below.

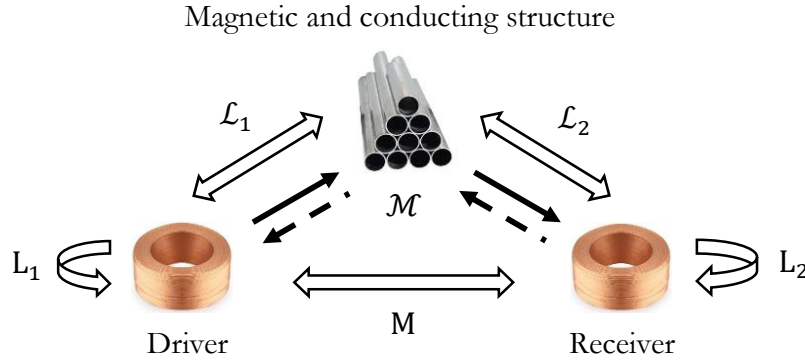


Figure 36: Schematic description of the coupling coefficients.

The coupling coefficients associated with a ferromagnetic conducting tube are obtained by solving the corresponding boundary value problem. They are summarily written here as

$$\mathcal{L}_1 = 8n_1^2\mu_0 \int_0^\infty \frac{\sin^2\left(\frac{\lambda L_1}{2}\right)}{\lambda^2} \left( \int_{a_1}^{b_1} r K_1(\lambda r) dr \right)^2 \Gamma(\mu_r, \sigma, c, d) d\lambda, \quad (3)$$

$$\mathcal{L}_2 = 8n_2^2\mu_0 \int_0^\infty \frac{\sin^2\left(\frac{\lambda l_2}{2}\right)}{\lambda^2} \left( \int_{a_2}^{b_2} rK_1(\lambda r) dr \right)^2 \Gamma(\mu_r, \sigma, c, d) d\lambda, \quad (4)$$

$$\mathcal{M} = 8n_1n_2\mu_0 \int_0^\infty \frac{\sin\left(\frac{\lambda l_1}{2}\right) \cos(\lambda d) \sin\left(\frac{\lambda l_2}{2}\right)}{\lambda^2} \left( \int_{a_1}^{b_1} rK_1(\lambda r) dr \right)^2 \Gamma(\mu_r, \sigma, c, d) d\lambda, \quad (5)$$

where  $n_1$  and  $n_2$  are the coil winding densities – the ratio of a coil's number of turns to its cross sectional area - of the driver and pickup coils, respectively, and  $\mu_0$  is the permeability of free space. Parameters  $l_1$  and  $l_2$  are the lengths of the driver and pickup coils, and  $d$  is the distance between their edges as illustrated in Figure 31 (a). The geometry and material-dependent tube function  $\Gamma(\mu_r, \sigma, r_i, r_o)$  is written as

$$\Gamma(\mu_r, \sigma, r_i, r_o) = \frac{\mu_r I_0(\lambda r_o) \Theta + I_1(\lambda r_o) Y}{\mu_r K_0(\lambda r_o) \Theta - K_1(\lambda r_o) Y}, \quad (6)$$

where functions  $\Theta_1$  and  $\Theta_2$  are given by

$$\begin{aligned} \Theta \equiv & \mu_r \lambda^2 I_0(\lambda r_i) (I_1(\Lambda r_i) K_1(\Lambda r_o) - K_1(\Lambda r_i) I_1(\Lambda r_o)) \\ & - \lambda \Lambda I_1(\lambda r_i) (I_0(\Lambda r_i) K_1(\Lambda r_o) + K_0(\Lambda r_i) I_1(\Lambda r_o)), \end{aligned} \quad (7)$$

$$\begin{aligned} Y \equiv & \mu_r \lambda \Lambda I_0(\lambda r_i) (I_1(\Lambda r_i) K_0(\Lambda r_o) + K_1(\Lambda r_i) I_0(\Lambda r_o)) \\ & - \Lambda^2 I_1(\lambda r_i) (I_0(\Lambda r_i) K_0(\Lambda r_o) - K_0(\Lambda r_i) I_0(\Lambda r_o)), \end{aligned}$$

with

$$\Lambda \equiv \sqrt{\lambda^2 + j\omega\mu_0\mu_r\sigma}. \quad (8)$$

In equations (6)-(8),  $\mu_r$  is the tube's relative magnetic permeability,  $\sigma$  is its conductivity and  $r_i$  and  $r_o$  are its inner and outer radii, respectively

Consider an arbitrary excitation waveform  $v(t)$  expressed as a Fourier series. Its Fourier transform,  $V(\omega)$ , will always consist of a weighted sum of Dirac delta functions whose effect, under the integrals in equations (26) and (27), is to select out a set of particular frequencies in accordance with the sampling theorem. Thus, frequency-dependent functions  $\mathcal{L}_1$ ,  $\mathcal{L}_2$  and  $\mathcal{M}$  need only be evaluated at specific frequencies, and the integral becomes a summation of trigonometric functions. Consider a square-wave excitation for applications in transient eddy current testing. The Fourier series representation of a square wave with period  $P$  and amplitude  $v_0$  is given as

$$v(t) = \frac{v_0}{2} + \frac{2v_0}{P} \sum_{n=1}^{\infty} \frac{\sin(\varpi_n t)}{\varpi_n}, \quad \varpi_n \equiv \frac{(2n-1)\pi}{P}. \quad (9)$$

The Fourier transform of equation (9) is substituted into equations (26) and (27), and the resulting expressions are recast as series expansions of phase-shifted sinusoids with frequencies  $\varpi_n$ . The final solutions are written as

$$i_1(t) = \frac{v_0}{2R_1} + \frac{2v_0}{P} \sum_{n=1}^{\infty} \frac{1}{\varpi_n} \sqrt{\frac{(\varpi_n(L_2 + \text{Re}(\mathcal{L}_2)))^2 + (R_2 - \varpi_n \text{Im}(\mathcal{L}_2))^2}{\alpha_n^2 + \beta_n^2}} \times \sin\left(\varpi_n t - \arctan\left(\frac{(R_2 - \varpi_n \text{Im}(\mathcal{L}_2))\beta_n - \varpi_n(L_2 + \text{Re}(\mathcal{L}_2))\alpha_n}{(R_2 - \varpi_n \text{Im}(\mathcal{L}_2))\alpha_n + \varpi_n(L_2 + \text{Re}(\mathcal{L}_2))\beta_n}\right)\right), \quad (10)$$

$$i_2(t) = \frac{2v_0}{P} \sum_{n=1}^{\infty} \sqrt{\frac{(\text{M} + \text{Re}(\mathcal{M}))^2 + \text{Im}(\mathcal{M})^2}{\alpha_n^2 + \beta_n^2}} \times \sin\left(\varpi_n t - \arctan\left(\frac{\text{Im}(\mathcal{M})\beta_n + (\text{M} + \text{Re}(\mathcal{M}))\alpha_n}{\text{Im}(\mathcal{M})\alpha_n - (\text{M} + \text{Re}(\mathcal{M}))\beta_n}\right)\right) \quad (11)$$

where the coefficients  $\alpha_n$  and  $\beta_n$  are defined as

$$\alpha_n \equiv (R_1 - \varpi_n \text{Im}(\mathcal{L}_1))(R_2 - \varpi_n \text{Im}(\mathcal{L}_2)) - \varpi_n^2 (L_1 + \text{Re}(\mathcal{L}_1))(L_2 + \text{Re}(\mathcal{L}_2)) + \varpi_n^2 ((M + \text{Re}(\mathcal{M}))^2 - \text{Im}(\mathcal{M})^2), \quad (12)$$

$$\beta_n \equiv \varpi_n (R_1 - \varpi_n \text{Im}(\mathcal{L}_1))(L_2 + \text{Re}(\mathcal{L}_2)) + \varpi_n (R_2 - \varpi_n \text{Im}(\mathcal{L}_2))(L_1 + \text{Re}(\mathcal{L}_1)) + 2\varpi_n^2 (M + \text{Re}(\mathcal{M}))\text{Im}(\mathcal{M}), \quad (13)$$

and where the expressions  $\mathcal{L}_1$ ,  $\mathcal{L}_2$  and  $\mathcal{M}$  need only be evaluated at  $\omega = \varpi_n$  for each  $n$ . Final solutions (10) and (11), together with the coupling coefficients from (3), (4) and (5), describe the transient currents flowing through the driver and pickup coils, respectively, when coupled to a conducting and ferromagnetic tube and driven by a square waveform voltage with amplitude  $v_0$  and period  $P$ .

### III. Experimental Results

A power supply with an internal resistance of  $0.46 \, \Omega$  was used to generate  $1.75 \, \text{V}$  and  $0.60 \, \text{V}$  square pulse excitations for the brass and steel tube experiments, respectively. Coaxial cables with negligible losses route the pulse through a  $2.00 \, \Omega$  resistor to a  $87.5 \, \Omega$  driving coil. A  $92.4 \, \Omega$  pickup coil was connected in series with two  $26.7 \, \Omega$  termination resistors and to a National Instruments signal acquisition card (NI6211 USB DAQ board). In the driver circuit, the transient voltage is measured across  $2.00 \, \Omega$  and  $26.7 \, \Omega$  resistors in parallel. In the pickup circuit, the voltage is measured across two  $26.7 \, \Omega$  resistors in series. The voltage measurements were taken at  $4 \, \mu\text{s}$  intervals. The transient currents flowing through the circuits are related to the experimentally measured voltages in accordance with Ohm's Law (i.e.  $v_{1,\text{exp}} = i_1(t) * (2.00^{-1} + 26.7^{-1})^{-1}$  and  $v_{2,\text{exp}} = i_2(t) * (26.7 + 26.7)$ ). The coupled inductor circuit is depicted in Figure 32.

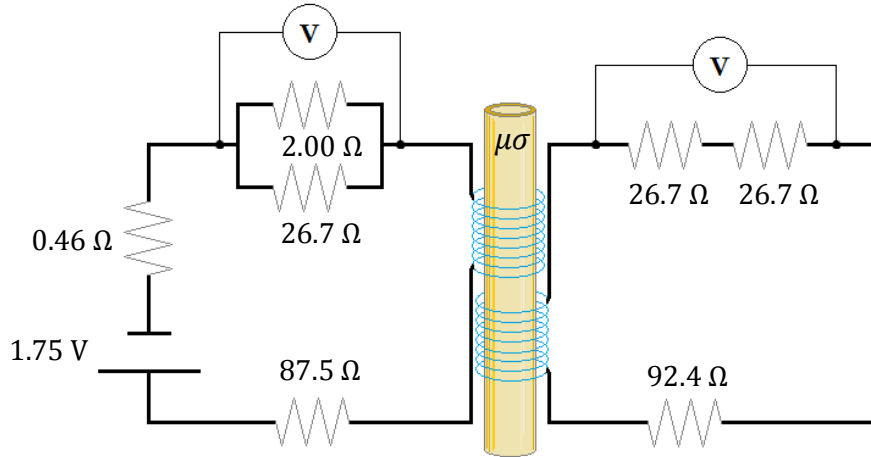


Figure 37: Experimental driver and pickup circuit diagram.

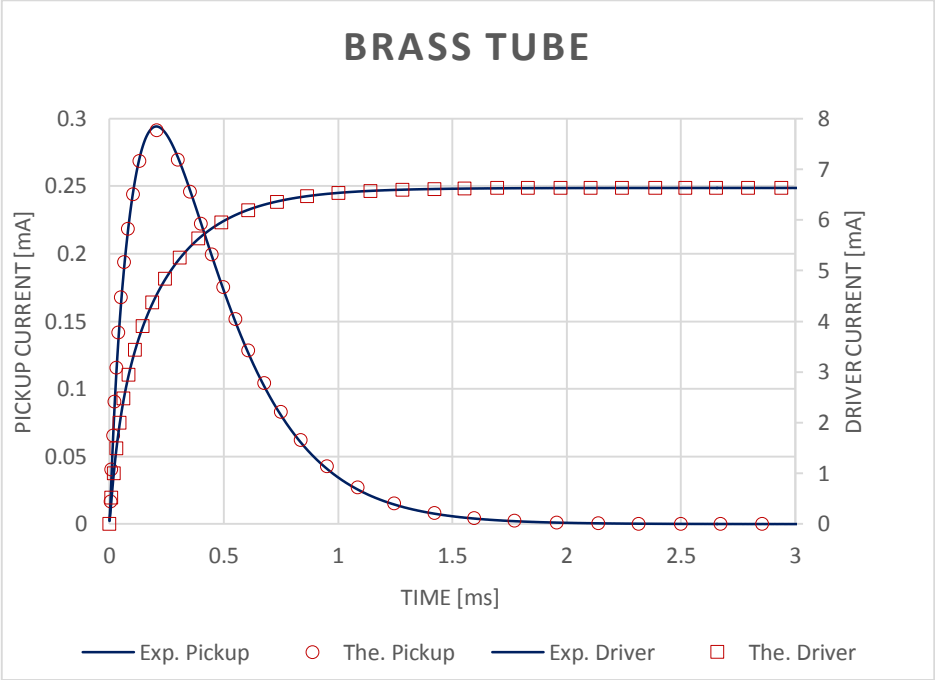
The coils were carefully wound with known number of turns, uniform turns density and windings exactly perpendicular to coil axes. The centers of the coaxial coils forming the probe are separated by a distance  $d$  of 3.78 mm along the axis. The characteristics of the experimental coils and tubes are listed in Table XIII below.

Table XIV: Experimental coil and tube characteristics.

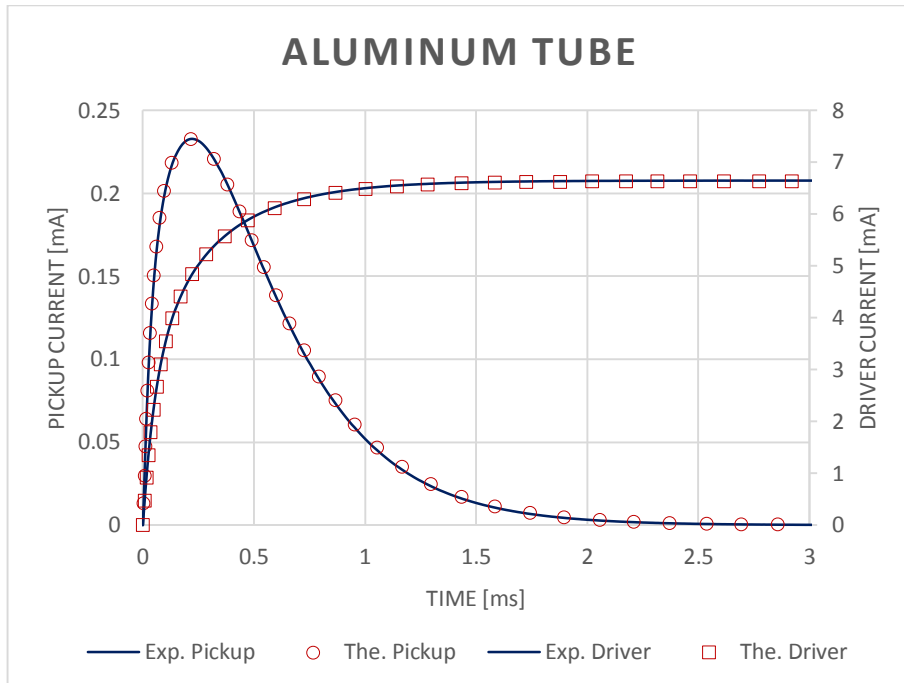
Coil:	Driver	Receiver	Tube :	Brass	Aluminum	Steel
Number of turns :	838	887	Wall thickness [inch] :	.065	.065	.065
Wire gage [AWG] :	36	36	Outer diameter [inch] :	$\frac{3}{4}$	$\frac{3}{4}$	$\frac{3}{4}$
Length [mm] :	9.01	11.09	Conductivity [ $\text{MS}\cdot\text{m}^{-1}$ ] :	15.7	28.1	7.79
Inner radius [mm] :	10.73	10.71	Relative Permeability :	1.013	1	154
Outer radius [mm] :	12.54	12.26				
Resistance [ $\Omega$ ] :	87.5	92.4				
Self-Induct. [mH] :	17.4	17.6				
Mut. Induct. [mH]:		3.73				

Solutions (10) and (11) are plotted, using the values listed in Table XIII, and compared with experimental results for conducting and non-magnetic (brass and aluminum), and conducting and

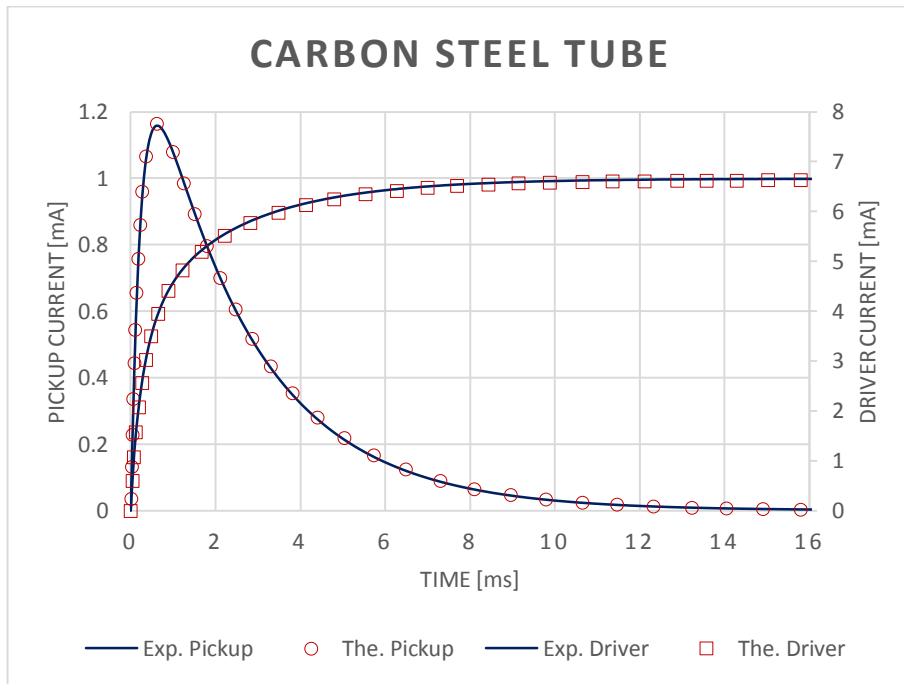
ferromagnetic (carbon steel) tubes. The transient pickup and driver signal amplitudes are measured in milliamps by the primary (left) and secondary (right) vertical axes, respectively. The sign of the pickup signal, required by Lenz's law to be opposite in sign to that of the driver signal, has been inverted for the purpose of displaying both signals on the same graph.



(a)



(b)



(c)

Figure 38: Experimental and theoretical results of the transient currents in the driver (squares) and pickup (circles) circuits, respectively, resulting from the application of a square wave excitation. The coils are in a coaxial driver-pickup configuration and encircle a brass (a), and aluminum (b) and a carbon steel (c) tube.

The experimental results are in excellent agreement with the analytical predictions. The general solutions developed, and validated for the case of rod structures, in [9] has been successfully applied to tubular structures. Multi-layer tubular structures will be considered in subsequent work.

#### **IV. Discussion & Future Work**

The correct approach to obtain driver-pickup probe response in voltage-controlled eddy current systems, developed in [1]-[9], was applied here to ferromagnetic conducting tubular structures. Complex frequency-dependent self- and mutual inductance coefficients, that describe the electromagnetic interactions between the coils and a ferromagnetic conducting tube, are given. These quantities, denoted as  $\mathcal{L}_1$ ,  $\mathcal{L}_2$  and  $\mathcal{M}$  depend upon the geometry and material characteristics of the conducting structure, and upon the interacting coils, as expected.

Final solutions (10) and (11) describe the transient current responses of a driver coil and a pickup coil in the vicinity of any ferromagnetic conducting structure, provided that the corresponding expressions for the complex inductance coefficients can be obtained. Furthermore, the series form of the solutions provides exact expressions for the amplitudes and phase shifts associated with each sinusoid. Thus, frequency analysis of transient inspection data, interpreted with the aid of analytical solutions, offers more information than conventional single eddy current systems. Since each frequency has an associated skin depth, solutions (10) and (11) may be used, for example, to reconstruct volumetric profiles of a material's characteristics. Work in this area is currently underway.

In the forward problem, the material parameters, such as conductivity, magnetic permeability and wall thickness, appear in the mathematical solutions in distinct ways and, therefore, have different measurable effects on the amplitudes and phases of a signal. Novel algorithms enabling the simultaneous determination of these characteristics may be developed from these forward

solutions. Algorithms that exploit the theory would be probe-specific and application specific, and would enable precise interpretation of measured eddy current signals. For example, multiple material characteristics could be calculated simultaneously and unambiguously, as opposed to present conventional eddy current practices, that rely on calibration standards and trained technicians for the interpretation of multivariate inspection data. Detailed maps of a component's thickness, conductivity and permeability would provide valuable information about the component's state and structural integrity.

## V. Summary

The circuit approach developed in [1], which has enabled the correct formulation of solutions to eddy-current induction problems under voltage control, was applied to the case of a coaxial driver-pickup probe encircling a long ferromagnetic conducting tube. Coupled circuit equations were formulated in terms of the tube's impulse response using convolution theory. Analytical expressions for complex inductances in the circuit, which accounts for real (inductive) and imaginary (loss) elements associated with the tube, have arisen from the theory. As a result, electromagnetic field theory and circuit theory have been intuitively combined to provide a complete model of eddy current induction phenomena. Solutions describing the time-dependant currents flowing through the driver and pickup coils, for applications in both conventional and pulsed eddy current, were developed. The former are in closed-form and the latter in series-form. The final solutions account for all electromagnetic coupling effects arising in the system, and are the first in the literature to provide correct voltage responses in driver-pickup configurations. Experimental results, obtained for the case of square wave excitation, were in excellent agreement with the analytical equations. Furthermore, the theory valid for any ferromagnetic conducting structure provided that the complex coupling coefficients can be obtained by solving the corresponding boundary value problem. Thus,

this theory can be straightforwardly extended to inductive circuit problems containing other geometries, such as half-spaces, plates, tubes, tubes, spheres and right-angled wedges for instance. Ultimately, model-assisted analyses of experimental data may provide a direct method of extracting values such as liftoff, wall thickness, conductivity, permeability, and other parameters of interest. This is left as future work.

## VI. References

- [1] Dodd CV, Deeds WE. Analytical solutions to eddy-current probe-coil problems. *J Appl Phys* 1968;39:2829-2838.
- [2] Bowler JR, Fu F. Transient Eddy-current driver pickup probe response due to a conductive plate. *IEEE transactions on magnetics*, Vol. 42, NO. 8, August 2006. pp. 2029-2037.
- [3] Theodoulidis T. Developments in calculating the transient eddy-current response from a conductive plate. *IEEE Trans on Magn* 2008;44:1894-1896.
- [4] Desjardins D, Krause TW, Gauthier N. Analytical modeling of the transient response of a coil encircling a ferromagnetic conducting tube in pulsed eddy current testing. *NDT&E Int* 2013;60:127-131.
- [5] Morazova GM, Polygalov VF, Epov MI, Mogilatov VS. Transient electromagnetic field of a current loop centered on the axis of a hollow magnetic cylinder. *Russian Geo and Geophys* 2000;41:1435-1444.
- [6] Xiao Chun-Yanm Zhang Jun. Analytical solutions of transient pulsed eddy current problem due to elliptical electromagnetic concentrative coils. *Chin.Phys.B*; Vol.19, No.12 (2010)
- [7] Desjardins D, Krause TW. Concerning the Derivation of Exact Solutions to Inductive Circuit Problems for Eddy Current Testing. *NDT&E Int.* 68 (2014) 128–135.

- [8] Desjardins D, Krause TW. Transient Response of a Driver Coil in Pulsed Eddy Current Testing. *NDT&E Int.* 73 (2015) 22–27.
- [9] Desjardins D, Krause TW. Transient response of a driver-pickup coil probe in pulsed eddy current testing. *NDT&E Int.* Accepted 28 Apr 2015.
- [10] Moulder JC, Tai C, Larson BF, Rose JH. Inductance of a coil on a thick ferromagnetic plate. *IEEE Trans on Magn* 1999;34:505-514.

**Manuscript 5:** “*Simultaneous evaluation of material parameters using analytical transient eddy current models*”.

Proc. of 19th Intl. Workshop on ENDE. Submitted 24 Aug 2014.

Author contributions: D.R Desjardins (theory, experiment, primary writer), T.W. Krause (editor, literature survey suggestions), and L. Clapham.

# Simultaneous Evaluation of Material Parameters Using Analytical Transient Eddy Current Models

D.R. Desjardins<sup>1\*</sup>, T.W. Krause<sup>2</sup> and L. Clapham<sup>1</sup>

1. Department of Physics, Queen's University, Kingston, ON, Canada, K7L 3N6

2. Department of Physics, Royal Military College of Canada, Kingston, ON, Canada, K7K 7B4

**Abstract** – Recently, analytical transient eddy current models, which correctly account for each of the electromagnetic coupling effects arising in inductive circuits containing a conducting and ferromagnetic sample, have been developed. This work extends the model results with the development of algorithms for the simultaneous evaluation of material parameters. In particular, geometrical and material characteristics, such as probe lift-off, wall thickness, electrical conductivity and magnetic permeability can be extracted from a single transient eddy current signal. Simple Laplace and Fourier transform rules are used to generate independent equations relating experimental data and theory. These equations are simultaneously solved for the material parameters of interest. Furthermore, results computed from these equations can be tabulated and implemented in a lookup-table scheme for an ultra-fast multi-parameter characterization of materials.

## I. Introduction

Pulsed eddy current (PEC) is being developed to inspect at depth within multilayered structures [1]-[4] and rods [5]. Unlike sinusoidal excitation of conventional eddy current, PEC utilizes a square pulse, which carries a spectrum of discrete frequencies and, for long time pulse excitation, generates magnetization at depth within ferromagnetic materials. For aerospace applications in the

---

\* Corresponding author: dandesja@gmail.com

presence of ferrous fasteners, the fastener is used as a conduit for the magnetic flux created by the driving coil, allowing for deeper penetration of eddy currents into multilayer aluminum structures [5]-[7]. The separate effects of conductivity and permeability on PEC signals have also recently been investigated [8]. PEC signal analysis often includes examination of rise time, peak height and zero-crossing time. However, when changes in these features are subtle, it becomes increasingly difficult to distinguish between signals. A statistical technique, principal components analysis (PCA), has been used to re-express multivariate data in order to extract key signal features [9]. A comparative process has been used to show that PCA performs better than traditional methods in the classification of defects [10]. Recently, PCA has been used to successfully detect stress corrosion cracking in the inner wing spars of F/A-18 aircraft without skin removal [11]. These analysis techniques are largely empirical however, and the development of analytical models that describe transient signal generation in these materials could be used to extract other material parameters and properties.

Analytical solutions to eddy current problems involving relatively simple geometries, such as layered planar and tubular structures [12][13], have been known for quite some time now. The complexity and range of solutions have also been extended to consider geometries containing corners and edges [14][15]. In each case, good agreement between theory and experiment is demonstrated for impedance-type calculations and measurements. Progress in transient eddy current (TEC) models for applications in pulsed eddy current testing, however, have not advanced at the same rate [16][17]. Recently analytical solutions, which completely describe driver and pickup probe transient responses, have been developed [18][19]. In the present work, these solutions are used to develop a strategy to address the inverse problem; that of extracting information about a test material using pulsed eddy current signals. Eddy current material characterization techniques have

been, and are still, of great interest [20][21][22]. The generally applicable inverse problem algorithms presented in this work are applied to the case of a coaxial driver-pickup probe encircling a ferromagnetic conducting tube. Additional geometries will be considered in future work. In an example that will follow, tube wall thickness and relative permeability are extracted from a single transient pickup signal using this algorithm.

## II. Forward problem

Consider the magnetically coupled driver-pickup circuit presented in Figure 39.

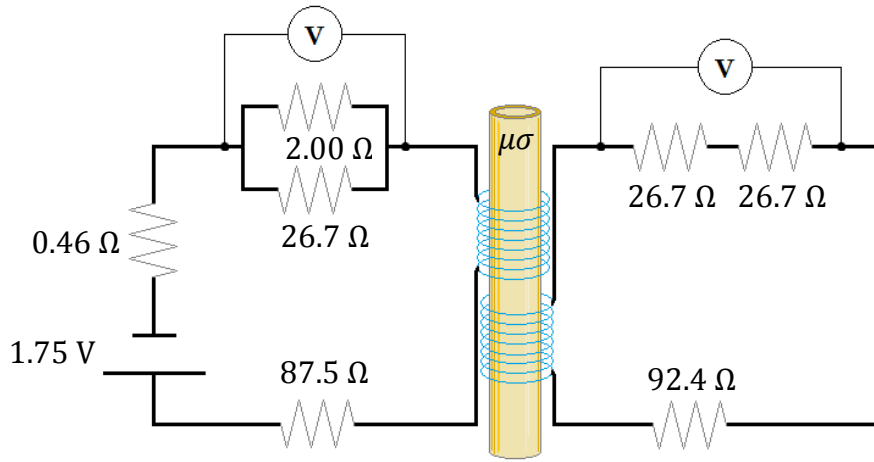


Figure 39: Eddy current driver (left) and pickup (right) circuit.

The Laplace-space solution [18] for the transient current,  $i(t)$ , flowing in the pickup coil is

$$\int_0^{\infty} i(t)e^{-st} dt = v_0 \frac{M + \mathcal{M}}{(R_1 + s(L_1 + \mathcal{L}_1))(R_2 + s(L_2 + \mathcal{L}_2)) - s^2(M + \mathcal{M})^2}, \quad (1)$$

where  $L_1$  and  $L_2$  are the driver and pickup coils' self-inductances, respectively,  $R_1$  and  $R_2$  are the total driver and pickup circuit resistances,  $v_0$  is the amplitude of the applied voltage step and  $M$  is a mutual inductance coefficient.  $\mathcal{L}_1$  and  $\mathcal{L}_2$  are complex inductances arising from the self-coupling of the driver and pickup coils through the sample, and  $\mathcal{M}$  is a complex mutual inductance coefficient

arising from cross-coupling of the coils through the sample. These coupling effects, obtained by solving the relevant boundary value problem, are schematically represented in Figure 40 below.

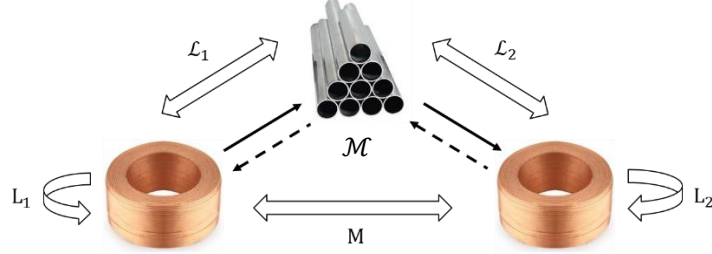


Figure 40: Schematic of coupling coefficients.

The complex self- and mutual inductance coefficients, in the case of a coaxial driver-pickup probe encircling a tube, are given as [19]

$$\mathcal{L}_{1,2} = 8n_{1,2}^2\mu_0 \int_0^\infty \frac{\sin^2\left(\frac{\lambda l_{1,2}}{2}\right)}{\lambda^2} \left( \int_{a_{1,2}}^{b_{1,2}} rK_1(\lambda r) dr \right)^2 \Gamma(s, \lambda) d\lambda, \quad (2)$$

$$\mathcal{M} = 8n_1 n_2 \mu_0 \int_0^\infty \frac{\sin\left(\frac{\lambda l_1}{2}\right) \cos(\lambda d) \sin\left(\frac{\lambda l_2}{2}\right)}{\lambda^2} \left( \int_{a_1}^{b_1} rK_1(\lambda r) dr \right) \left( \int_{a_2}^{b_2} rK_1(\lambda r) dr \right) \Gamma(s, \lambda) d\lambda, \quad (3)$$

where the tube function is written as

$$\Gamma(s, \lambda) \equiv \frac{\mu_r I_0(\lambda c_2) \Theta + I_1(\lambda c_2) Y}{\mu_r K_0(\lambda c_2) \Theta - K_1(\lambda c_2) Y}, \quad (4)$$

with the following function definitions

$$\begin{aligned} \Theta \equiv & \mu_r \lambda^2 I_0(\lambda c_1) (I_1(\Lambda c_1) K_1(\Lambda c_2) - K_1(\Lambda c_1) I_1(\Lambda c_2)) \\ & - \lambda \Lambda I_1(\lambda c_1) (I_0(\Lambda c_1) K_1(\Lambda c_2) + K_0(\Lambda c_1) I_1(\Lambda c_2)), \end{aligned} \quad (5)$$

$$\begin{aligned} Y \equiv & \mu_r \lambda \Lambda I_0(\lambda c_1) (I_1(\Lambda c_1) K_0(\Lambda c_2) + K_1(\Lambda c_1) I_0(\Lambda c_2)) \\ & - \Lambda^2 I_1(\lambda c_1) (I_0(\Lambda c_1) K_0(\Lambda c_2) - K_0(\Lambda c_1) I_0(\Lambda c_2)), \end{aligned} \quad (6)$$

$$\Lambda \equiv \sqrt{\lambda^2 + s\mu_0\mu_r\sigma}. \quad (7)$$

In equations (2)-(7), values  $n$ ,  $a$ ,  $b$  and  $l$  are coil turn density, inner radius, outer radius and length, and subscripts 1 and 2 denote the driver and pickup coils, respectively.  $d$  is the distance along the axis separating the centers of the coils. Finally,  $c_1$  and  $c_2$  are the inner and outer radii of the tube,  $\mu_r$  is its relative permeability and  $\sigma$  is its conductivity.

Thus, all quantities are described and the solution may be reconstructed in the time domain by Fourier superposition as was done in [19]. The response of the probe may then be plotted as a function of various tube conductivities, permeabilities and wall thicknesses. This work, however, focusses on the inverse problem.

### III. Inverse Problem

The frequency domain differentiation property of the Laplace transform [24], written as

$$\int_0^{\infty} t^n i(t) e^{-st} dt = (-1)^n \frac{d^n}{ds^n} F(s), \quad (8)$$

provides a simple method for the generation of linearly independent correspondences between theory and experiment. In effect, the Laplace transform of a measured signal  $i(t)$  scaled by  $t^n$ , where  $t$  is time and  $n$  is an integer, corresponds to the  $n^{\text{th}}$  derivative of the Laplace-space solution. Therefore, by applying the frequency domain differentiation property to equation (1), multiple linearly independent relationships between experimental measurement and theory can be drawn from *a single measured TEC signal*. Two unknowns, permeability and conductivity for example, require two equations ( $n = 0$  and  $n = 1$ ). In general,  $k$  unknowns will require  $k$  relationships.

For the purposes of describing this method, only two unknowns are considered, since illustrating a 3D matrix would be impractical. However, the theory is straightforwardly extendable to consider additional unknown material parameters.

Application of the frequency domain differentiation property to equation (1) with  $n = 0$  returns the equation unchanged, where  $i(t)$  is the experimentally measured pickup signal. Equation (1), evaluated at  $s = 0$ , is of particular physical significance; it corresponds to the area under the transient pickup signal. This is immediately apparent from the left-hand-side of the equation. The experimental value for this area is henceforth denoted by  $A_0$ . The analytical solution, which describes the area under a transient pickup signal, is then written as

$$A_0 \equiv \int_0^{\infty} i(t)dt = v_0 \frac{M + \mathcal{M}}{R_1 R_2} \Big|_{s=0}, \quad (9)$$

where the complex mutual inductance coefficient  $\mathcal{M}$  (evaluated at  $s = 0$ ) is a function which depends on the geometrical and material properties of the test object. Following inspection of equation (7), evaluated at  $s = 0$ , substituted into equations (5) and (6), then into (4), then into (3) and finally into (9), it becomes apparent that the area under a transient pickup signal is independent of a test piece's conductivity, an interesting theoretical prediction. Furthermore, equation (9) is generally valid, provided that  $\mathcal{M}$  can be obtained by solving the appropriate boundary value problem.

In order to uniquely determine the value of two unknowns, an additional equation is required. The frequency domain differentiation property of the Laplace transform is applied for  $n = 1$  to the Laplace-space solution in (1) such that

$$\int_0^{\infty} t \cdot i(t)e^{-st} dt = -\frac{d}{ds} \frac{v_0(M + \mathcal{M})}{(R_1 + s(L_1 + \mathcal{L}_1))(R_2 + s(L_2 + \mathcal{L}_2)) - s^2(M + \mathcal{M})^2}, \quad (10)$$

Again, the point  $s = 0$  is of special significance; it corresponds to the area under the transient signal scaled by  $t$ , henceforth denoted by  $A_1$ , such that

$$A_1 \equiv \int_0^\infty t \cdot i(t) dt = v_0 \left( \left( \frac{L_1 + \mathcal{L}_1}{R_1} + \frac{L_2 + \mathcal{L}_2}{R_2} \right) \frac{M + \mathcal{M}}{R_1 R_2} - \frac{\mathcal{M}'}{R_1 R_2} \right) \Big|_{s=0}, \quad (11)$$

where the prime denotes differentiation with respect to complex frequency  $s$ . This second general expression, which provides an analytical description of the measurable quantity  $A_1$ , is used in conjunction with equation (9) to uniquely quantify two unknowns.

Unfortunately, these equations cannot, in general, be algebraically solved due to the complexity of functions  $\mathcal{L}_1$ ,  $\mathcal{L}_2$  and  $\mathcal{M}$ . Therefore, analytical solutions for the unknown material characteristics cannot often be easily achieved. In order to circumvent this problem, solutions (9) and (11) are pre-computed over a range of relative permeability and wall thickness values,  $\mu_r$  and  $w$ , and the resulting values  $A_0$  and  $A_1$  are stored in an array as shown in Table XV.

Table XV: Pre-computed array of values  $A_0$  and  $A_1$  as a function of  $\mu_r$  and  $w$ .

$\mu_r / w$	$w_1$	$w_2$	...
$\mu_{r_1}$	$A_0(\mu_{r_1}, w_1), A_1(\mu_{r_1}, w_1)$	$A_0(\mu_{r_1}, w_2), A_1(\mu_{r_1}, w_2)$	...
$\mu_{r_2}$	$A_0(\mu_{r_2}, w_1), A_1(\mu_{r_2}, w_1)$	$A_0(\mu_{r_2}, w_2), A_1(\mu_{r_2}, w_2)$	...
$\vdots$	$\vdots$	$\vdots$	$\ddots$

The array is then inverted in order to obtain tabulated values of relative permeability and wall thickness as a function of measurable values  $A_0$  and  $A_1$  as shown in Table XVI.

Table XVI: Inverted array;  $\mu_r$  and  $w$  as a function of pre-computed values  $A_0$  and  $A_1$ .

$A_0 / A_1$	$A_{11}$	$A_{12}$	...
$A_{01}$	$\mu_r(A_{01}, A_{11}), w(A_{01}, A_{11})$	$\mu_r(A_{01}, A_{12}), w(A_{01}, A_{12})$	...
$A_{02}$	$\mu_r(A_{02}, A_{11}), w(A_{02}, A_{11})$	$\mu_r(A_{02}, A_{12}), w(A_{02}, A_{12})$	...
$\vdots$	$\vdots$	$\vdots$	$\ddots$

Finally, following a transient eddy current measurement, the array is searched for computed values that coincide with measured values  $A_0$  and  $A_1$  (interpolating as required) to yield the unique pair of  $\mu_r$  and  $w$  corresponding to that measurement.

#### IV. Array computation

Consider a carbon steel tube [23] with an outer diameter of  $\frac{3}{4}$ ", conductivity of 7.86 MSm/m, but with unknown thickness and relative permeability. The values  $L_1$ ,  $L_2$ ,  $R_1$ ,  $R_2$  and  $M$  for a particular driver-pickup probe configuration are listed in Table XVII.

Table XVII:  $L_1$  and  $L_2$  are the self-inductances of the driver and pickup coils, respectively,  $R_1$  and  $R_2$  are their resistances and  $M$  is the mutual inductance coefficient.

$L_1$	$L_2$	$R_1$	$R_2$	$M$
17.41 mH	17.63 mH	87.5 $\Omega$	92.4 $\Omega$	3.729 mH

Equations (2)-(7) are substituted into equations (9) and (11), and an array of values  $A_0$  and  $A_1$  is computed as a function of  $\mu_r$  and  $w$ . For illustration purposes, Table XVIII contains only a sample of the array computed with Maplesoft's Maple 18 computational software [25]; a complete array would ideally have a finer mesh and span a larger set of values  $\mu_r$  and  $w$ . Thickness values  $w$  are expressed in thousandths of an inch (0.025 mm).

Table XVIII: Example 2D array of observables  $A_0$  and  $A_1$  as functions of  $\mu_r$  and  $w$ .

$\mu_r / w$	40	45	50	55
100	[.497e-1, .802e-4]	[.532e-1, .920e-4]	[.565e-1, .104e-3]	[.595e-1, .116e-3]
110	[.528e-1, .890e-4]	[.565e-1, .102e-3]	[.599e-1, .115e-3]	[.631e-1, .129e-3]
120	[.557e-1, .979e-4]	[.595e-1, .112e-3]	[.631e-1, .127e-3]	[.664e-1, .142e-3]
130	[.585e-1, .106e-3]	[.624e-1, .122e-3]	[.661e-1, .138e-3]	[.696e-1, .155e-3]
140	[.612e-1, .115e-3]	[.653e-1, .132e-3]	[.691e-1, .150e-3]	[.726e-1, .167e-3]

The 2D matrix above, whose first row and column specify tube wall thickness and relative magnetic permeability, contains sets of  $A_0$  and  $A_1$  as matrix elements. For illustration purposes, 3D surface plots of  $A_0$  and  $A_1$ - the first and second terms, respectively, of each matrix element -are generated as a function of thickness  $w$  and permeability  $\mu_r$  - specified by the first row and column, respectively - and presented in Figure 41 below.

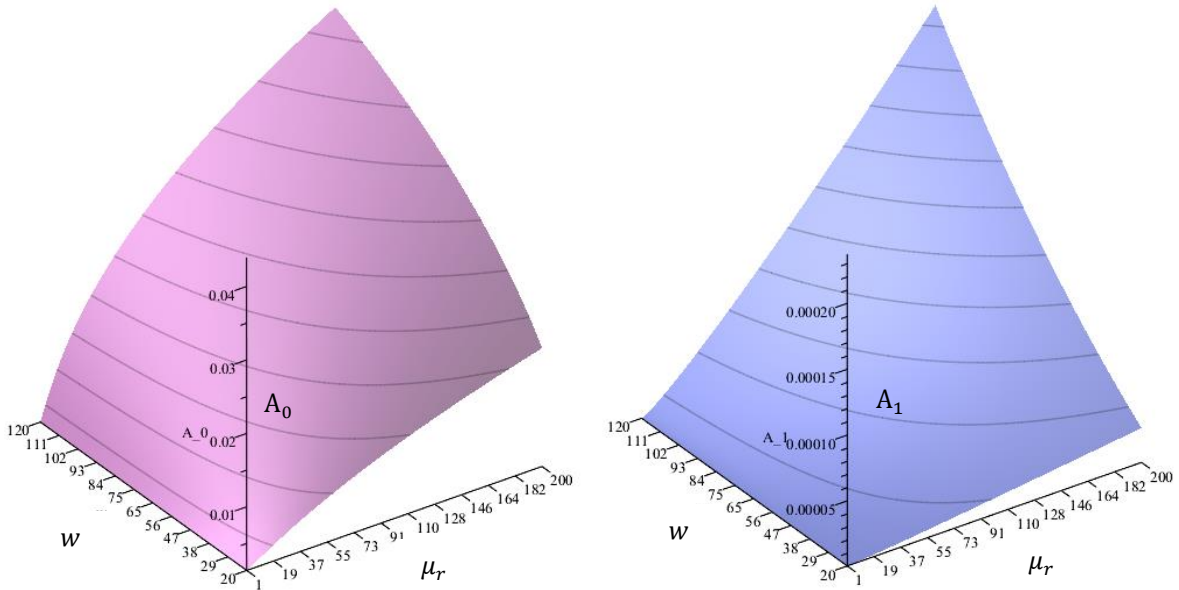


Figure 41: Surface plots of  $A_0$  and  $A_1$  as functions of  $\mu_r$  and  $w$ .

For inversion, values  $A_0$  and  $A_1$  become the axes, whereas permeability and thickness become the array elements. 3D surface plots of permeability and thickness are displayed, in Figure 42, as functions of  $A_0$  and  $A_1$ .

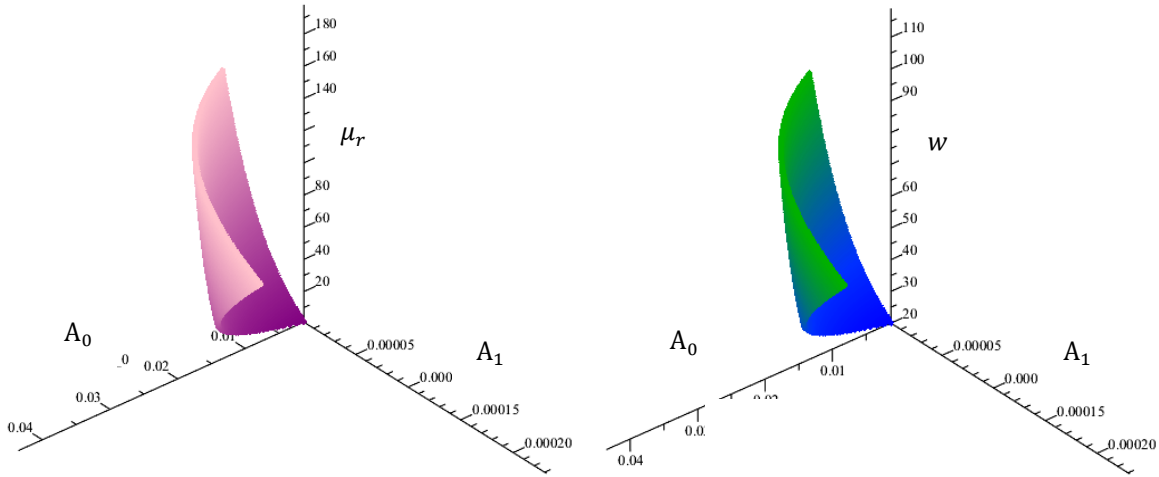


Figure 42: Surface plots of  $\mu_r$  and  $w$  as functions of values  $A_0$  and  $A_1$ .

Finally, experimentally measured values  $A_0$  and  $A_1$  can be used to enter the inverted matrix, and the corresponding values of  $\mu_r$  and  $w$  are identified.

## V. Example application

A power supply with an internal resistance of  $0.46 \Omega$  was used to generate a  $0.60 \text{ V}$  square pulse excitation for a transient eddy current steel tube experiment. Coaxial cables with negligible losses route the pulse through a  $2.00 \Omega$  resistor to a  $87.5 \Omega$  driving coil (further details were listed in Table XVII). A  $92.4 \Omega$  pickup coil was connected in series with two  $26.7 \Omega$  termination resistors and to a National Instruments signal acquisition card (NI6211 USB DAQ board). In the driver circuit, the transient voltage is measured across  $2.00 \Omega$  and  $26.7 \Omega$  resistors in parallel. In the pickup circuit, the voltage is measured across two  $26.7 \Omega$  resistors in series. The voltage measurements were taken at  $4 \mu\text{s}$  intervals. The transient current flowing through the pickup circuit is related to the

experimentally measured transient voltage in accordance with Ohm's Law i.e.  $i(t) = v_{\text{exp}}/(2 \times 26.7\Omega)$ . The coupled inductor circuit is depicted in Figure 39.

The coaxial driver-pickup probe encircles a carbon steel tube (vendor specifications listed in [23]) with an outer diameter of 19 mm ( $\frac{3}{4}$ "') and a conductivity of 7.86 MSm/m. It's wall thickness and relative magnetic permeability are considered to be unknown. The transient pickup signal  $i(t)$  and the scaled pickup signal  $t \cdot i(t)$  are plotted in Figure 43.

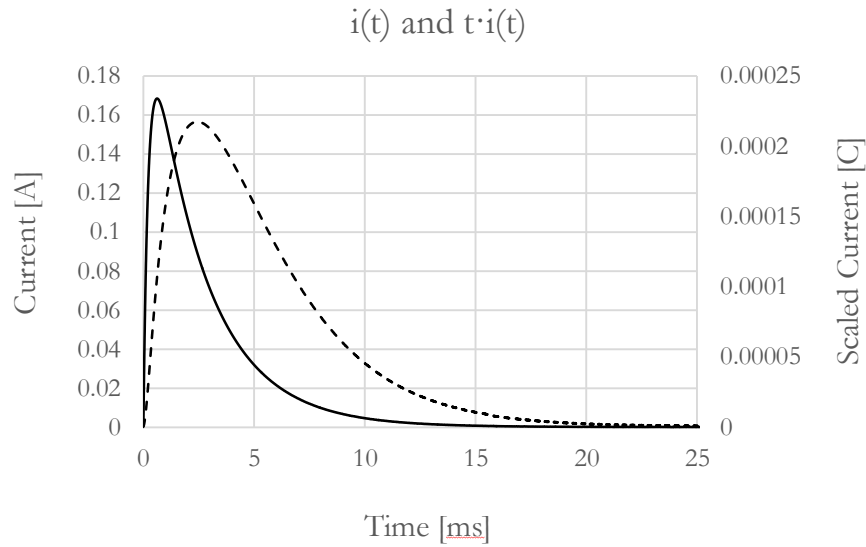


Figure 43: Transient voltage signal measured by a pickup coil encircling a carbon steel tube (solid curve) and transient pickup signal scaled by time  $t$  (dashed curve).

The area under the pickup signal  $i(t)$  (solid curve) is measured and found to be

$$A_0 = 2.878 \cdot 10^{-2} \quad (12)$$

The pickup signal is then scaled by time  $t$ , such that  $t \cdot i(t)$  (dashed curve). The area under this curve is found to be

$$A_1 = 7.957 \cdot 10^{-5} \quad (13)$$

Finally, the inverted matrix (or equivalently the 3D surface plots) are entered with the measured values of  $A_0$  and  $A_1$  from equations (12) and (13) in order to uniquely determine the values of  $\mu_r$  and  $w$  corresponding to measurement.

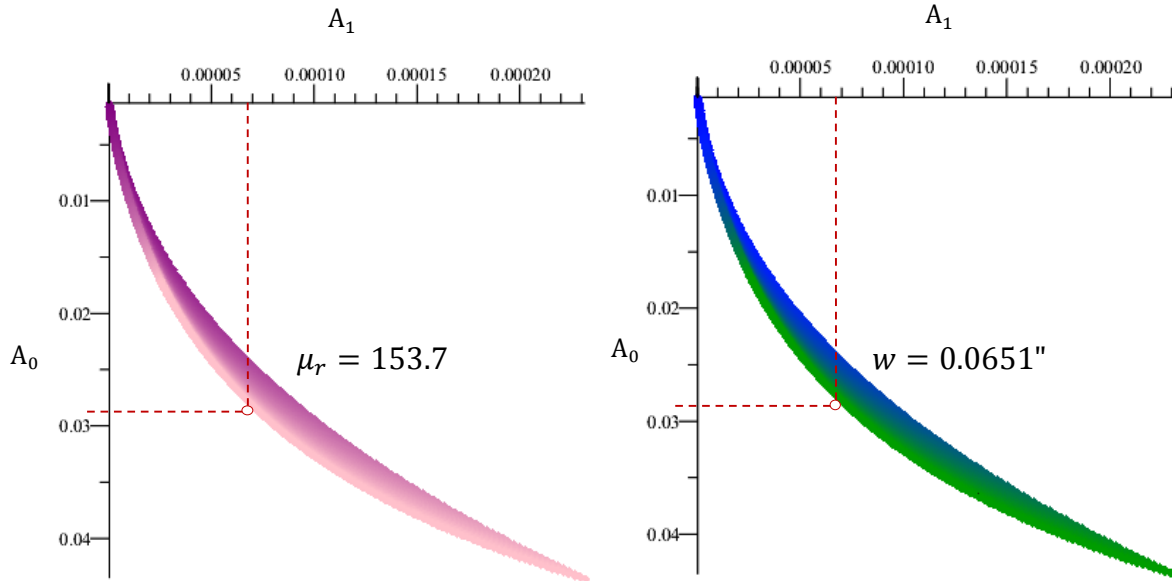


Figure 44: Top view of  $\mu_r(A_0, A_1)$  and  $w(A_0, A_1)$  surface plots.

Therefore, the tube's relative magnetic permeability is 153.7 and its wall thickness is 1.6535 mm (0.0651"). Whereas the magnetic permeability cannot be precisely corroborated by an alternate method, the nominal tube wall thickness is indeed 1.651 mm (0.065"). A relative permeability value of 150 is reasonable for carbon steel [26].

## VI. Discussion

The method presented in this work may be straightforwardly extended to consider additional unknowns (number of unknowns coincides with the dimension of the array required). Clearly, the required computational time increases exponentially with the dimension of the array. However, once the array is computed, a simple look-up scheme may be implemented for the simultaneous and ultra-fast characterization of material parameters.

Care must be taken when performing the numerical integration of the differentiated complex mutual inductance coefficient  $\mathcal{M}'$ . Integration was performed with Maple 18 using the NAG method d01akc, which uses adaptive Gauss 30-point and Kronrod 61-point rules. In particular, it was noted that software-induced numerical instability occurred about the origin  $\lambda = 0$ . Mathematically, the limit  $\lim_{\lambda \rightarrow 0} \mathcal{M}'$  is well-defined and finite. The instability was remedied by performing a Taylor series expansion about the origin.

Only areas under pickup signal transients and their scaled counterparts are considered in this work. However, additional schemes may rely on other distinctive measurable features such as signal peak heights, zero-crossing time, phase angles, or PCA scores, for example.

## VII. Conclusion

In summary, novel algorithms, developed from analytical transient eddy current models, enable multi-parameter characterization. The method was demonstrated on a tube with unknown magnetic permeability and unknown wall thickness, but is scalable in order to consider additional unknown parameters such as conductivity, diameter and eccentricity. Also, the method is applicable to different geometries such as multilayer tubular or plate structures, provided that the expressions for the complex self- and mutual inductances can be obtained. A model-based approach, such as this, is useful for the interpretation of multivariate transient eddy current inspection data.

## VIII. References

- [1] Y. He, F. Luo, M. Pan, F. Weng, X. Hu, J. Gao and B. Liu, "Pulsed eddy current technique for defect detection in aircraft riveted structures," *NDT&E International*, vol. 43, pp. 176-181, 2009.
- [2] I. Z. Abidin, C. Mandache, G. Y. Tian and M. Morozov, "Pulsed eddy current testing with variable duty cycle on rivet joints," *NDT&E International*, vol. 42, no. 7, pp. 599-605, October 2009.

- [3] T. W. Krause, C. Mandache and J. H. Lefebvre, "Diffusion of Pulsed Eddy Currents in Thin Conducting Plates," in AIP Conf, 2008.
- [4] R. A. Smith and G. R. Hugo, "Deep Corrosion and Crack Detection in Aging Aircraft Using Transient Eddy Current NDE," in 5th Joint NASA/FAA/DoD Aging Aircraft Conference, 2001.
- [5] D. Desjardins, T. W. Krause and N. Gauthier, "Analytical modeling of the transient response of a coil encircling a ferromagnetic conducting rod in pulsed eddy current testing," NDT&E International, vol. 60, pp. 127-131, March 2013.
- [6] R. A. Smith and G. R. Hugo, "Deep corrosion and crack detection in aging aircraft using transient eddy current NDE," in 5th Joint NASA/FAA/DoD Aging Aircraft Conference, 2001.
- [7] D. R. Desjardins, G. Vallieres, P. P. Whalen and T. W. Krause, "Advances in Transient (Pulsed) Eddy Current For Inspection of Multi-Layer Aluminum Structures in the Presence of Ferrous Fasteners," Review of Progress in Quantitative Nondestructive Evaluation, pp. 400-407, 2012.
- [8] I.D. Adewale and G.Y. Tian. Decoupling the influence of permeability and conductivity in pulsed eddy-current measurements, IEEE Transactions on Magnetics. 49, 1119 (2013); doi: 10.1109/TMAG.2012.2225634.
- [9] J. Lattin, J. D. Carroll and P. E. Green, Analyzing Multivariate Data, Pacific Grove: Brooks/Cole, 2003, pp. 4, 264-275.
- [10] A. Sophian, G. Y. Tian, D. Taylor and J. Rudlin, "A Feature Extraction Technique Based in Pricipal Component Analysis for Pulsed Eddy Current NDT," NDT&E International, vol. 36, pp. 37-41, 2003.
- [11] P. Horan, P. Underhill and T. W. Krause, "Pulsed Eddy Current Detection of Cracks in F/A-18 Inner Wing Spar Without Wing Skin Removal Using Modified Principal Components Analysis," NDT&E International, vol. 55, pp. 21-27, 2013.

- [12] C.V. Dodd, C.C. Cheng, and W.E. Deeds. Induction Coils coaxial with an Arbitrary Number of Cylindrical Conductors, *Int. J. Nondestructive Test.* 3(2) (1971) 109-130.
- [13] C.V. Dodd, J.W. Luquire, W.G. Spoeri, and W.E. Deeds. Some eddy current problems and their integral solutions.(1969).
- [14] T.P. Theodoulidis and J.R. Bowler. Impedance of an induction coil at the opening of a borehole in a conductor. *Journal of Applied Physics* 103, 024905 (2008); doi: 10.1063/1.2827459.
- [15] T.P. Theodoulidis and J.R. Bowler. Eddy current coil interaction with a right-angled conductive wedge. *Proc. R. Soc. A*, doi:10.1098/rspa.2005.1509.
- [16] Smith RA, Hugo GR. Transient eddy current NDE for ageing aircraft - capabilities and limitations. *Insight* 2001;43:14-25.
- [17] Ward WW, Moulder JC. Low frequency, pulsed eddy currents for deep penetration. *Rev. of Prog. in QNDE.* 1998;17A:291-298.
- [18] D.R. Desjardins, T.W. Krause and L. Clapham. Transient response of a driver-pickup coil probe in pulsed eddy current testing. (2014) Manuscript submitted for publication.
- [19] D.R. Desjardins, T.W. Krause and L. Clapham. Transient eddy current response of a driver-pickup coil probe encircling a ferromagnetic conducting tube. (2014) Manuscript submitted for publication.
- [20] R.C. Callarotti and M. Alfonzo. Measurement of the conductivity of metallic cylinders by means of an inductive method. *Journal of Applied Physics* 43, 3040 (1972); doi: 10.1063/1.1661656
- [21] R.C. Callarotti, P. Schmidt, and H. Arqué. Theory of the measurement of thickness and conductivity of cylindrical shells by an inductive method. *Journal of Applied Physics* 43, 3952 (1972); doi: 10.1063/1.1660855.
- [22] J. Íñiguez, V. Raposo, and M. Zazo. Measurement of electrical conductivity in nonferromagnetic tubes and rods at low frequencies. *American Journal of Physics* 77, 949 (2009); doi: 10.1119/1.3184154.

- [23] DOM Steel Tube. (2013). Retrieved May 15, 2014, from <http://www.speedymetals.com/information/material17.html>.
- [24] R.J. Beerends, H.G. terMorche, J.C. van den Berg and E.M. van de Vrie. Fourier and Laplace transforms. Cambridge University Press, Cambridge (2003).
- [25] Maple 18. (2014). Retrieved May 26, 2014, from <http://www.maplesoft.com/products/Maple/>.
- [26] W.F. Brown. Magnetic Materials, Ch 8 in the Handbook of Chemistry and Physics, Condon and Odishaw, eds., McGraw-Hill, 1958.

## CHAPTER 5 – DISCUSSION

The analytical harmonic solutions for a single coil interacting with a conducting specimen, developed in the celebrated Dodd and Deeds paper [1], are complete in that they account for feedback between a single coil and a metallic specimen. However, their description of the voltage induced in a pickup coil is incomplete. Section 7 on page 2837 in [1] reads:

“The voltage generated in a “pickup” coil with dimensions  $r_2'$ ,  $r_1'$ ,  $l_2'$ ,  $l_1'$  by a current  $I$  flowing in a “driver” coil with dimensions  $r_2$ ,  $r_1$ ,  $l_2$ ,  $l_1$  is:”

$$V = M dI/dt = j\omega MI, \quad (72)$$

where  $M$  “is the mutual inductance between the driver coil and the pickup coil in the presence of a clad conductor.”

Upon inspection of equation (72), Dodd and Deeds’ formulation [1] for the pickup signal accounts for mutual inductance effects, but ignores the pickup coil’s self-inductance (direct self-coupling, and indirect self-coupling through the sample). In effect, this formulation ignores the effects of the pickup coil on the system. The correct method of obtaining the induced pickup voltage, which accounts for *all* inductive coupling effects, was developed in manuscripts I and III as presented in Chapter 4. The voltage induced in the pickup should, instead, be written as

$$V_p(t) = R_p i_p(t) = -(L_p + \mathcal{L}_p) * \frac{d}{dt} i_p(t) - (M + \mathcal{M}) * \frac{d}{dt} i_d(t), \quad (73)$$

where  $R_p$  is the resistance of the pickup circuit,  $(L_p + \mathcal{L}_p)$  is the total self-inductance of the pickup coil,  $(M + \mathcal{M})$  is the total mutual inductance – equivalent to  $M$  in the Dodd and Deeds formalism – and  $i_d$  and  $i_p$  are the currents flowing in the driver and pickup circuits, respectively. The Fourier transform of equation (73) yields

$$V_p(\omega) = R_p I_p(\omega) = -j\omega(L_p + \mathcal{L}_p)I_p(\omega) - j\omega(M + \mathcal{M})I_d(\omega). \quad (74)$$

This expression differs from equation (72) by the addition of the term  $j\omega(L_p + \mathcal{L}_p)I_p(\omega)$ , which corresponds to a back-emf arising from self-inductance effects associated with the pickup coil. On a less important note, Dodd and Deeds [1] have omitted the negative sign required by Lenz's Law. Solution of equation (74) yields the voltage response of a pickup coil as a function of the current flowing in the driver coil. Thus, the corrected formulation for the induced voltage is

$$V_p(\omega) = \frac{-j\omega(M + \mathcal{M})}{1 + \frac{j\omega(L_p + \mathcal{L}_p)}{R_p}} I_d(\omega). \quad (75)$$

Clearly, equation (75) reduces to the Dodd and Deeds formalism in cases where the effects of a pickup coil on a system can be neglected - i.e. when

$$\frac{j\omega(L_p + \mathcal{L}_p)}{R_p} \ll 1. \quad (76)$$

This appears intuitive, since at low frequencies, small self-inductances and large resistances, very little current will flow in the pickup coil, thereby having a negligible effect on the system. However, since transient eddy currents encompass an extended set of frequencies, the condition in (76) cannot be maintained and the Dodd and Deeds formalism, equation (72), breaks down. The approximation is made worse when ferromagnetic materials are considered, since they amplify the coupling of the pickup coil with the sample - i.e.  $\mathcal{L}_p$  is increased.

On a more important note, the Dodd and Deeds formalism [1] - the foundation upon which the majority of driver-pickup models reported in the literature are based - expresses the induced pickup voltage as a function of an applied current. This is problematic, since the magnetic field

arising from the eddy currents modifies the excitation current. The correct method of addressing feedback effects is to solve the coupled circuit equations in terms of an applied *voltage*. The differential equation developed in this thesis, which governs the current in the driver circuit, is written as

$$R_d i_d(t) = v(t) - (L_d + \mathcal{L}_d) * \frac{d}{dt} i_d(t) - (M + \mathcal{M}) * \frac{d}{dt} i_p(t), \quad (77)$$

where  $v(t)$  is the time-dependent voltage applied to the driver coil. Coupled equations (73) and (77), which correctly account for all electromagnetic coupling effects, must be solved simultaneously. The final and complete Fourier domain solutions for the driver and the pickup responses, developed in manuscript III of this thesis, are written as

$$I_d(\omega) = \frac{V(\omega) (R_p + j\omega(L_p + \mathcal{L}_p))}{(R_d + j\omega(L_d + \mathcal{L}_d)) (R_p + j\omega(L_p + \mathcal{L}_p)) + \omega^2 (M + \mathcal{M})^2}, \quad (78)$$

$$I_p(\omega) = \frac{-j\omega V(\omega) (M + \mathcal{M})}{(R_d + j\omega(L_d + \mathcal{L}_d)) (R_p + j\omega(L_p + \mathcal{L}_p)) + \omega^2 (M + \mathcal{M})^2}. \quad (79)$$

where  $V(\omega)$  is the Fourier transform of an arbitrary voltage waveform applied to the driver coil. Equations (78) and (79) are, therefore, the first in the literature to completely and correctly describe the currents arising in inductively coupled driver-pickup circuits in the presence of a metallic conductor.

Unfortunately, the Dodd and Deeds formalism [1] has persisted for four decades and is widely present in the literature today (equation (1) in [26], (1) in [13], eqn. (35) in [11], section 3.6 in [14]). The persistent disagreement [6][12] between theory and experiment may well be attributed to this. The correction brought forth by this doctoral research completes the theory.

## CHAPTER 6 – CONCLUSION

A novel approach for the formulation of solutions to eddy-current induction problems has been developed. Electromagnetic field theory and circuit theory have been intuitively combined to provide a complete model of eddy current induction phenomena in which all feedback effects have been addressed. Analytical expressions for complex inductances, which accounts for real (inductive) and imaginary (resistive) elements associated with a metallic test piece, have arisen from the theory. The final solutions, which predict time-dependant currents flowing in the driving and sensing coils, have been generalized to consider arbitrary voltage excitations. Furthermore, the solutions are also valid for arbitrary probe and metallic structure configurations, provided that the corresponding boundary value problems can be solved. Thus, the theory developed in this thesis is compatible with all existing electromagnetic field solutions, which address geometries such as half-spaces, plates, rods, tubes, spheres and right-angled wedges for instance. Experimental results, obtained for the case of square wave excitation for pulsed eddy current applications, are in excellent agreement with the analytical equations.

The forward solutions were extended with the development of algorithms for the simultaneous evaluation of material parameters, which is of significant interest to industry. In particular, geometrical and material characteristics, such as probe lift-off, wall thickness, electrical conductivity and magnetic permeability were extracted from a single transient eddy current signal. Simple Laplace and Fourier transform rules were used to generate independent equations relating experimental data and theory. These equations were simultaneously solved for the material parameters of interest. Furthermore, results computed from these equations can be tabulated and implemented in a lookup-table scheme for an ultra-fast multi-parameter characterization of materials.

A general mathematical formalism for the treatment of transient eddy current phenomena has been developed. The developed theory correctly addresses feedback effects in inductively coupled circuits, and completes the original Dodd and Deeds formalism. The theory is in excellent agreement with a number of experimental measurements in driver-pickup configurations for rod and tube geometries under conditions of variable conductivity and permeability.

## CHAPTER 7 – FUTURE WORK

Subsequent work will consider more complicated geometries. Layered structures, such as multi-layer planar or tubular structures will be considered. Subsequently, forward solutions involving structures with edges, such as quarter spaces and bored plates, will be developed and validated by experiment. Such geometries will require use of the Truncated Region Eigenfunction Expansion (TREE) method. Finally, more complex geometries, such as tube support plates in nuclear power facilities, will be investigated.

The ability to calculate the response of a coil, or probe, to an arbitrary voltage excitation function, and to model any configuration of inductors and capacitors, opens a realm of interesting possibilities. Band-pass and band-stop circuits may be constructed and tuned for the precise measurement of selected frequency bands. Such a capability would be useful in targeting specific features of a test piece. Controlling the excitation signal would also enable feature specific targeting, but with even greater flexibility. An attractive capability would be the creation of constructive and destructive interference waves within a conductor, using multiple coils and specific driving signals, such that induced eddy current densities could be focused and even displaced.

Solutions to the inverse characterization problems are also of significant interest to industry. Despite the pioneering work of Dodd and Deeds [1] and of the many works that followed, calibration standards are still required today when performing material inspections. This thesis provides a novel and direct method of extracting values such as liftoff, wall thickness, conductivity, permeability, and other characteristics that relate to the structural integrity of a specimen. However, in future work, the method will be extended in order to be able to simultaneously determine four,

five and six parameters. In a specific example, the model is currently being adapted in order to obtain the liftoff, thickness, conductivity and magnetic permeability of a metal plate.

A thorough sensitivity analysis will be conducted. Specifically, the effects of various probe and material parameters on a measured signal will be quantified. This study will be useful for probe optimization, with the goal of increasing sensitivity to material features, and for determining the dominant sources of uncertainty in the analytical models. The findings will help identify strategies for mitigating these sources of uncertainty and increasing signal-to-noise ratio.

## REFERENCES

- [1] C.V. Dodd, W.E. Deeds, Analytical solutions to eddy current probe-coil problems, *J. of Appl. Phys.* 39 (1968) 2829-2838.
- [2] V.S. Cecco, G. Van Drunen, F.L. Sharp, Eddy current testing manual on eddy current method, Chalk River Nuclear Laboratories, 1 (1981)
- [3] Olympus: Introduction to Eddy Current Testing. (2014). Retrieved 27 Oct 2014, from <http://www.olympus-ims.com/en/eddycurrenttesting/>
- [4] H. Sun, J.R. Bowler, T. Theodoulidis, Eddy currents induced in a finite length layered rod by a coaxial coil, *IEEE Trans. on Magn.* 41 (2005) 2455-2461.
- [5] P. Horan, P.R. Underhill, T.W. Krause, Real time pulsed eddy current detection of cracks in F/A-18 inner wing spar using discriminant separation of Modified Principal Component Analysis scores, *IEEE Sensors J.* 14 (2014) 171-177.
- [6] D. Desjardins, G. Vallières, P.P. Whalen, T.W. Krause, Advances in transient (pulsed) eddy current for inspection of multi-layered aluminum structures in the presence of ferrous fasteners, *Review of Progress in Quantitative Nondestructive Evaluation*, 31, Edited by: D.E. Chimenti, Melville, New York (2012 American Institute of Physics) 440-407.
- [7] P. Hammond, The calculation of the magnetic field of rotating machines, *IEEE* 514S (1962): 508-515.
- [8] T.W. Krause, V.K. Babbar, P.R. Underhill, A pulsed eddy current probe for inspection of support plates from within alloy-800 steam generator tubes, *Review of Progress in Quantitative Nondestructive Evaluation*, Vol. 33, edited by: D.E. Chimenti, Melville, New York (2014 American Institute of Physics) 1352-1358.
- [9] V.K. Babbar, P.R. Underhill, C. Stott, T.W. Krause, Finite element modeling of second layer crack detection in aircraft boltholes with ferrous fasteners present, *NDT&E Int.* 65 (2014) 64-71.

- [10] Y. Yoshida, J.R. Bowler, Vector potential integral formulation for eddy-current probe response to cracks, *IEEE Trans. on Magn.* 36 (2000) 461-469.
- [11] D. Desjardins, T.W. Krause, N. Gauthier, Analytical modeling of the transient response of a coil encircling a ferromagnetic conducting rod in pulsed eddy current testing, *NDT&E Int.* 60 (2013) 127-131.
- [12] G.M. Morozova, V.F. Polygalo, M.I. Epov, V.S. Mogilatov, Transient electromagnetic field of a current loop centered on the axis of a hollow magnetic cylinder, *Russian Geo and Geophys.* 41 (2000) 1435-1444.
- [13] T. Theodoulidis, Developments in calculating the transient eddy-current response from a conductive plate, *IEEE Trans. on Magn.* 44 (2008) 1894-1896.
- [14] X. Chun-Yanm, Z. Jun, Analytical solutions of transient pulsed eddy current problem due to elliptical electromagnetic concentrative coils, *Chin. Phys. B* 19 (2010) 120302.
- [15] D. Desjardins, Analytical modeling for transient probe response in eddy current testing. MSc Thesis, Royal Military College, 2011.
- [16] V.B. Wwedensky, Concerning the eddy currents generated by a spontaneous change of magnetization (Translated - Jan. 2008), *Annalen der Physik* 64 (1921) 609-620.
- [17] C.P. Bean, R.W. DeBlois, L.B. Nesbitt, Eddy-current method for measuring the resistivity of metals, *J. of Appl. Phys.* (1959) 1976-1980.
- [18] R.C. Callarotti, M. Alfonzo, Measurement of the conductivity of metallic cylinders by means of an inductive method, *J. of Appl. Phys.* 43 (1972) 3040-3046.
- [19] <http://www.google.com/patents/US3234458>.
- [20] C.C. Cheng, C.V. Dood, W.E. Deeds, General analysis of probe coils near stratified conductors, *Int. J. Nondestr. Test* 3 (1971) 109-130.

- [21] C.V. Dodd, C.C. Cheng, W.E. Deeds, Induction coils with an arbitrary number of cylindrical conductors, *J. Appl. Phys.* 45 (1974) 638-647.
- [22] T. Theodoulidis, E. Kriezis, Series expansion in eddy current non-destructive evaluation models, *J. Mater. Process. Tech.* 161 (2005) 343-347.
- [23] M. Fan, P. Huang, B. Ye, D. Hou, G. Zhang, Z. Zhou, Analytical modeling for transient probe response in pulsed eddy current testing, *NDT&E Int.* 42 (2009) 376-383.
- [24] J.R. Bowler, T. Theodoulidis, Coil impedance variation due to induced current at the edge of a conductive plate. *J. Phys. D: Appl. Phys.* 39 (2006) 2862-2868.
- [25] J.R. Bowler, T. Theodoulidis, Eddy currents induced in a conducting rod of finite length by a coaxial encircling coil. *J. Phys. D: Appl. Phys.* 38 (2005) 2861–2868.
- [26] J.R. Bowler, F. Fu, Transient eddy-current driver pickup probe response due to a conductive plate, *IEEE Trans. on Magn.* 42 (2006) 2029-2037.
- [27] T. Theodoulidis, J.R. Bowler, Eddy current coil interaction with a right-angled conductive wedge, *Proc. R. Soc. A* 461 (2005) 3123-3139.
- [28] T. Theodoulidis, J.R. Bowler, The truncated region eigenfunction expansion method for the solution of boundary value problems in eddy current nondestructive Evaluation, *AIP Conference Proceedings*, 760 (2005) 403-408.
- [29] J.R. Bowler, T. Theodoulidis, H. Xie, Y. Ji, Evaluation of eddy-current probe signals due to cracks in fastener holes, *IEEE Trans. on Magn.* 48 (2012) 1159-1170.
- [30] G. Micolau, G. Pichenot, D. Premel, D. Lesselier, M. Lambert, Dyad-based model of the electric field in a conductive cylinder at eddy-current frequencies, *IEEE Trans. Magn.* 40 (2004) 400-409.
- [31] T. Theodoulidis, Analytical model for tilted coils in eddy-current nondestructive inspection, *IEEE Trans. on Magn.* 41 (2005) 2447-2454.

- [32] S.K. Burke, T. Theodoulidis, Impedance of a horizontal coil in a borehole: a model for eddy-current borehole probes, *J. Phys. D: Appl. Phys.* 37 (2007) 485-494.
- [33] T. Theodoulidis, A. Skarlatos, Eddy current interaction of an arbitrarily positioned probe coil with a conductive cylinder, *IEEE Trans. on Magn.* 48 (2012) 2392-2394.
- [34] C. Tai, J.H. Rose, J.C. Moulder, Thickness and conductivity of metallic layers from pulsed eddy-current measurements, *Review of Scientific Instruments* 67 (1996) 3965.
- [35] R.F. Jardim, B. Laks, C. Santos, Eddy current decay method applied to a new geometry, *J. Appl. Phys.*, 61(12), pp.5237-5242, 1987.
- [36] I.D. Adewale, G.Y. Tian, Decoupling the Influence of Permeability and Conductivity in Pulsed Eddy-Current Measurements, *IEEE Trans. on Magn.*, Vol. 49, NO. 3, Mar 2013.
- [37] J.D. Jackson, *Classical electrodynamics*, 3rd Ed. New York: John Wiley & Sons, Inc., 1999.
- [38] H.E. Knoepfel, *Magnetic fields: a comprehensive theoretical treatise for practical use*. New York: John Wiley & Sons, 2000.
- [39] E.W. Weisstein, Vector Laplacian, From MathWorld--A Wolfram Web Resource.  
<http://mathworld.wolfram.com/VectorLaplacian.html>
- [40] M.A. Plonus, *Applied Electro-Magnetics*, (McGraw-Hill, New York, 1978), pp. 356.
- [41] R.M. Bozorth, *Ferromagnetism*, IEEE Press, Piscataway, NJ, 1993.
- [42] Magnetic properties of materials, Kaye&Laby Tables of Physical & Chemical Constants, National Physical Laboratory. [http://www.kayelaby.npl.co.uk/general\\_physics/2\\_6/2\\_6\\_6.html](http://www.kayelaby.npl.co.uk/general_physics/2_6/2_6_6.html). Accessed October 2014.
- [43] E. Gumlich, Dependence of magnetic properties, specific resistance and density of Fe alloys on chemical composition and heat treatment, *Wiss. Abhandl. physico-techn. Reichsanstalt.* 4, 267-410. 68, 76, 79, 83, 217, 234, 235, 367, 369.

- [44] T.D. Yensen, Magnetic properties of Ternary Fe-Si-C alloys, Trans. Am. Inst. Elec. Engrs. 43, 145-75. 68, 75, 83, 84, 87, 367.
- [45] J.D. Gaskill, Linear systems, Fourier transforms and optics. New York: John Wiley & Sons; 1978.
- [46] E.W. Weisstein, Fourier Cosine Transform, From MathWorld--A Wolfram Web Resource. Retrieved Oct 28, 2014, from <http://mathworld.wolfram.com/FourierCosineTransform.html>
- [47] Larry C. Andrews, Bhimsen K. Shivamoggi, Integral Transforms for Engineers, Bellingham Washington: SPIE Press, 1988.
- [48] E.W. Weisstein, Bessel Function of the First Kind, From MathWorld--A Wolfram Web Resource. Retrieved Nov 1, 2014, from <http://mathworld.wolfram.com/BesselFunctionoftheFirstKind.html>
- [49] D. Kammler, A first course in Fourier analysis. New York: Cambridge University Press; 2000.
- [50] R.L. Liboff, Introductory quantum mechanics. 2<sup>nd</sup> ed. Reading; Addison-Wesley; 1992.
- [51] M.N.O. Sadiku, Elements of Electromagnetics, 3rd Ed. New York: Oxford University Press, 2001.
- [52] Maple 18. (2014). Retrieved May 26, 2014, from <http://www.maplesoft.com/products/Maple/>
- [53] Maple online help: Numerical Integration. (2014). Retrieved June 26, 2014, from <http://www.maplesoft.com/support/help/Maple/view.aspx?path=evalf/Int&term=evalf/int>
- [54] Four Point Probes: Four Point Probe Theory. (2013). Retrieved October 8, 2014, from <http://four-point-probes.com/four-point-probe-theory/>
- [55] F. Kojima, T. Takagi, S.S. Udpa, Electromagnetic nondestructive evaluation, 6th Ed. IOS Press, 2002.

## ANNEX A

Sample code for transient response of a driver coil to a rod.

## ANNEX B

Magnetic vector potential boundary conditions for axisymmetric systems

$$\frac{\mathbf{B}_{1,\parallel}}{\mu_1} = \frac{\mathbf{B}_{2,\parallel}}{\mu_2} \quad (\text{B.1})$$

$$\frac{\mathbf{B}_1}{\mu_1} \cdot \hat{\mathbf{z}} = \frac{\mathbf{B}_2}{\mu_2} \cdot \hat{\mathbf{z}} \quad (\text{B.2})$$

$$\frac{\nabla \times \mathbf{A}_1}{\mu_1} \cdot \hat{\mathbf{z}} = \frac{\nabla \times \mathbf{A}_2}{\mu_2} \cdot \hat{\mathbf{z}} \quad (\text{B.3})$$

$$\frac{1}{\mu_1} \frac{\partial}{\partial r} (rA_1) = \frac{1}{\mu_2} \frac{\partial}{\partial r} (rA_2) \quad (\text{B.4})$$

$$\frac{A_1}{r} + \frac{\partial A_1}{\partial r} = \frac{A_2}{r} + \frac{\partial A_2}{\partial r} \quad (\text{B.5})$$

$$\frac{A_1 + r \frac{\partial A_1}{\partial r}}{\mu_1} = \frac{A_2 + r \frac{\partial A_2}{\partial r}}{\mu_2} \quad (\text{B.6})$$

$$\mathbf{B}_{1,\perp} = \mathbf{B}_{2,\perp} \quad (\text{B.7})$$

$$\mathbf{B}_1 \cdot \hat{\mathbf{r}} = \mathbf{B}_2 \cdot \hat{\mathbf{r}} \quad (\text{B.8})$$

$$\nabla \times \mathbf{A}_1 \cdot \hat{\mathbf{r}} = \nabla \times \mathbf{A}_2 \cdot \hat{\mathbf{r}} \quad (\text{B.9})$$

$$-\frac{\partial A_1}{\partial z} = -\frac{\partial A_2}{\partial z} \quad (\text{B.10})$$

$$\frac{\partial A_1}{\partial z} = \frac{\partial A_2}{\partial z} \quad (\text{B.11})$$